Astronomy & Astrophysics manuscript no. main_archive_final
September 25, 2024

Binarity at LOw Metallicity (BLOeM)*,†

I. A spectroscopic VLT monitoring survey of massive stars in the SMC

T. Shenar[1], J. Bodensteiner[2], H. Sana[3], P. A. Crowther[4], D. J. Lennon[5,6], M. Abdul-Masih[5,6], L. A. Almeida[7], F. Backs[3], S. R. Berlanas[5,6], M. Bernini-Peron[8], J. M. Bestenlehner[4], D. M. Bowman[9,3], V. A. Bronner[10,11], N. Britavskiy[12], A. de Koter[13,3], S. E. de Mink[14], K. Deshmukh[3], C. J. Evans[15], M. Fabry[3], M. Gieles[16,17], A. Gilkis[18], G. González-Torà[8], G. Gräfener[19], Y. Götberg[20], C. Hawcroft[21], V. Hénault-Brunet[22], A. Herrero[5,6], G. Holgado[5,6], S. Janssens[3], C. Johnston[14,3], J. Josiek[8], S. Justham[14], V. M. Kalari[23], Z. Z. Katabi[1], Z. Keszthelyi[24], J. Klencki[2], J. Kubát[25], B. Kubátová[25], N. Langer[19], R. R. Lefever[8], B. Ludwig[26], J. Mackey[27], L. Mahy[12], J. Maíz Apellániz[28], I. Mandel[29,30], G. Maravelias[31,32], P. Marchant[3], A. Menon[5,6], F. Najarro[33], L. M. Oskinova[34], A. J. G. O'Grady[35], R. Ovadia[1], L. R. Patrick[33], D. Pauli[34], M. Pawlak[36], V. Ramachandran[8], M. Renzo[37], D. F. Rocha[38], A. A. C. Sander[8], T. Sayada[1], F. R. N. Schneider[10,8], A. Schootemeijer[19], E. C. Schösser[8], C. Schürmann[19], K. Sen[39], S. Shahaf[40], S. Simón-Díaz[5,6], M. Stoop[13], S. Toonen[13], F. Tramper[33], J. Th. van Loon[41], R. Valli[14], L. A. C. van Son[42], A. Vigna-Gómez[14], J. I. Villaseñor[43], J. S. Vink[44], C. Wang[14], and R. Willcox[3]

(Affiliations can be found after the references)

Received -; accepted -

ABSTRACT

Surveys in the Milky Way and Large Magellanic Cloud have revealed that the majority of massive stars will interact with companions during their lives. However, knowledge of the binary properties of massive stars at low metallicity, and therefore in conditions approaching those of the Early Universe, remain sparse. We present the Binarity at LOw Metallicity (BLOeM) campaign, an ESO large programme designed to obtain 25 epochs of spectroscopy for 929 massive stars in the Small Magellanic Cloud, allowing us to probe multiplicity in the lowest-metallicity conditions to date ($Z = 0.2\,Z_\odot$). BLOeM will provide (i) the binary fraction, (ii) the orbital configurations of systems with periods of $P \lesssim 3$ yr, (iii) dormant black-hole binary candidates (OB+BH), and (iv) a legacy database of physical parameters of massive stars at low metallicity.

Main sequence (OB-type) and evolved (OBAF-type) massive stars are observed with the LR02 setup of the GIRAFFE instrument of the Very Large Telescope (3960 – 4570Å resolving power $R = 6200$; typical signal-to-noise ratio(S/N) $\approx 70-100$) . This paper utilises the first nine epochs obtained over a three-month time period. We describe the survey and data reduction, perform a spectral classification of the stacked spectra, and construct a Hertzsprung-Russell diagram of the sample via spectral-type and photometric calibrations.

Our detailed classification reveals that the sample covers spectral types from O4 to F5, spanning the effective temperature and luminosity ranges $6.5 \lesssim T_{\rm eff}/{\rm kK} \lesssim 45$ and $3.7 < \log L/L_\odot < 6.1$ and initial masses of $8 \lesssim M_{\rm ini} \lesssim 80\,M_\odot$. The sample comprises 159 O-type stars, 331 early B-type (B0–3) dwarfs and giants (luminosity classes V–III), 303 early B-type supergiants (II–I), and 136 late-type BAF supergiants. At least 82 stars are OBe stars: 20 O-type and 62 B-type (13% and 11% of the respective samples). In addition, the sample includes 4 high-mass X-ray binaries, 3 stars resembling luminous blue variables, 2 bloated stripped-star candidates, 2 candidate magnetic stars, and 74 eclipsing binaries.

Key words. stars: massive – binaries: close – binaries: spectroscopic – Magellanic Clouds

1. Introduction

Massive stars ($M_{\rm ini} \gtrsim 8\,M_\odot$), typically classified as OB-type stars on the main sequence, play an increasingly important role in modern astrophysics, with direct links to stellar dynamics, stellar transients, and gravitational-wave (GW) astrophysics (Portegies Zwart & Verbunt 1996; Langer 2012; Woosley 2017; Wang et al. 2020; Marchant & Bodensteiner 2023). Spectroscopic and interferometric surveys in the Milky Way (MW) and the Large Magellanic Cloud (LMC) have shown that stellar multiplicity is common among massive stars (e.g. Abt 1983; Kobulnicky & Fryer 2007; Mason et al. 2009; Sana et al. 2012; Sana et al. 2014; Bordier et al. 2024); over 50% of massive stars are expected to interact with a companion during their lifetime (Sana et al. 2012; Sana et al. 2013; Stegmann et al. 2022; Offner et al. 2023; Kummer et al. 2023). Such interactions dramatically alter the evolutionary paths and final fates of massive stars, resulting in a plethora of astronomical phenomena such as stripped helium stars and Wolf-Rayet (WR) stars (Paczyński 1967; Shenar et al. 2016; Götberg et al. 2018; Pauli et al. 2022a; Drout et al. 2023), rapidly rotating stars with decretion disks (OBe stars; Pols et al. 1991; Rivinius et al. 2013; de Mink et al. 2013; Wang et al. 2017; Bodensteiner et al. 2020; Britavskiy et al. 2023; Renzo & Götberg 2021), stellar mergers and magnetic stars (Ferrario et al. 2009; de Mink et al. 2014; Schneider et al. 2019; Shenar et al. 2023; Frost et al. 2024), single-degenerate binaries and high-mass X-ray binaries (Corral-Santana et al. 2016; Shenar et al. 2022a; Mahy et al. 2022), and GW sources (de Mink & Man-

* Based on observations collected at the European Southern Observatory under ESO program ID 112.25W2.

† Table A.2 is available in electronic form at the CDS via anonymous ftp to cdsarc.u-strasbg.fr (130.79.128.5) or via `http://cdsweb.u-strasbg.fr/cgi-bin/qcat?J/A+A/`.

del 2016; Marchant et al. 2016; Tauris et al. 2017; Mandel & Broekgaarden 2022; Mandel & Farmer 2022).

Of special interest is massive-star research in low-metallicity (low Z) environments, which reflect the conditions prevalent in the distant Universe. An increasing number of transients, such as long-duration γ-ray bursts (LGRBs; Yoon & Langer 2005; Woosley & Heger 2006), superluminous supernovae (SNe; Quimby et al. 2011; Gal-Yam 2012), broad-lined type Ic supernovae (Modjaz et al. 2008), and pair-instability SNe (Barkat et al. 1967; Fryer et al. 2001; Langer et al. 2007; Woosley 2017; Farmer et al. 2019), are thought to be associated mainly or exclusively with low-Z conditions. Similarly, the bulk of black-hole (BH) mergers observed with the LIGO-Virgo-KAGRA collaboration are thought to originate in low-metallicity conditions (Abbott et al. 2016; Giacobbo et al. 2018; Klencki et al. 2018).

Modern investigations expose deficiencies in our understanding of massive stars at low Z. For example, the rates and mass distribution of BH mergers defy original expectations (Broekgaarden et al. 2021; Mandel & Broekgaarden 2022; van Son et al. 2022), and observables such as the rate of LGRBs (Graham & Fruchter 2017; Chen et al. 2017) and the fraction of OBe stars and Be X-ray binaries (Haberl & Sturm 2016; Schootemeijer et al. 2022) as a function of Z are not reproduced by contemporary models (Graham & Fruchter 2017; Chen et al. 2017; Hastings et al. 2021). Such discrepancies are likely related to insufficient knowledge of massive-star evolution at low Z, or to a false extrapolation of the initial conditions of massive stars (e.g. binary fraction, orbital configurations) to low Z. The recent detection of a 33 $M_\odot$ BH with a low-metallicity companion through *Gaia* astrometry provides additional evidence suggesting that low-Z environments are crucial for the formation of massive BHs (Gaia Collaboration et al. 2024).

While it has been shown that the binary properties of solar-type stars can depend on natal metallicity, this remains a prediction for massive stars (Kroupa 2001; Saigo et al. 2004; Machida 2008; Marks et al. 2012; Moe et al. 2019; Price-Whelan et al. 2020). To mitigate this, we need spectroscopic monitoring surveys of massive-star populations at different Z environments sensitive to the regime of binary interactions (i.e. orbital periods $0 \lesssim \log_{10}(P/\mathrm{d}) \lesssim 3$). A notable spectroscopic campaign in this context was the VLT-FLAMES Tarantula Survey (VFTS; PI: Evans), which monitored about 1000 massive stars in the Tarantula nebula of the LMC (Evans et al. 2011), which has a metallicity of $\approx 0.5 Z_\odot$. The VFTS survey yielded a comparable intrinsic binary fraction for OB-type stars in the LMC (50-60%; Sana et al. 2013; Dunstall et al. 2015) to that observed in different Galactic environments (50-70%, e.g. Sana et al. 2012; Kiminki & Kobulnicky 2012; Banyard et al. 2022; Guo et al. 2022). The follow-up Tarantula Massive Binary Monitoring (TMBM; PI: Sana) and B-type Binary Characterisation (BBC; PI: Taylor) programmes also revealed an overall similar distribution of orbital parameters and mass ratios to Galactic samples (Almeida et al. 2017; Villaseñor et al. 2021; Shenar et al. 2022b; Mahy et al. 2020b). However, the LMC metallicity only differs by a factor of ≈ 2 from that of the MW.

The Small Magellanic Cloud (SMC) is a neighbouring dwarf galaxy with $Z \approx 0.2 Z_\odot$ (Hunter et al. 2007) located about 62 kpc from Earth (Graczyk et al. 2020), hosting thousands of massive stars (Humphreys & McElroy 1984). It had a star-formation peak 10 – 40 Myr ago (Antoniou et al. 2010; Rubele et al. 2015; Schootemeijer et al. 2021), potentially triggered by a collision with the LMC about 100-150 Myr ago (e.g. Zivick et al. 2018). While galaxies of lower metal content exist in the Local Group (e.g. Sextans A, Skillman et al. 1989; Lorenzo et al. 2022; Leo P, McQuinn et al. 2015; Evans et al. 2019; Telford et al. 2023), the SMC is the only galaxy in which a large sample of massive stars at low Z can currently be resolved and spectroscopically monitored with sufficient spectral resolution and signal-to-noise ratio (S/N). Previous or ongoing surveys addressed aspects related to the SMC massive-star contents (Humphreys & McElroy 1984; Evans et al. 2006; Martayan et al. 2007; Evans et al. 2004; Schootemeijer et al. 2021), stellar winds and mass-loss (Ramachandran et al. 2019; Vink et al. 2023), and runaway status (RIOTS4, Lamb et al. 2016), but multiplicity has been largely neglected beyond analyses of selected eclipsing binaries (Hilditch et al. 2005), clusters (Dufton et al. 2019; Bodensteiner et al. 2021), and individual objects of interest (e.g. Pauli et al. 2022b). Moe & Di Stefano (2013) investigated the frequency of eclipsing massive binaries among B-type stars in the SMC, LMC, and MW, and found no significant differences between the populations. However, their study was limited to the period range $P \lesssim 20$ d, and is generally bias-dominated given the small fraction of eclipsing binaries. There is no further information available regarding multiplicity in the SMC.

The need to establish the multiplicity of massive stars at low Z is not the only reason to monitor massive stars in the SMC. Recent spectroscopic monitoring of massive stars in the MW (Mahy et al. 2022) and the LMC (Shenar et al. 2022b,a) uncovered the 'tip of the iceberg' of a new population of massive single-degenerate binaries: X-ray dormant OB+BH binaries (e.g. Giesers et al. 2018). Such binaries yield precious constraints on core-collapse mechanisms and the presence of SN explosions and possible natal kicks during the collapse into BHs (Mirabel & Rodrigues 2003; Renzo et al. 2019; Atri et al. 2019; Langer et al. 2020; Banagiri et al. 2023). For example, Vigna-Gómez et al. (2024) recently used the dormant OB+BH binary VFTS 243 to derive a natal kick of 4 km s^{-1} and an ejection of 0.3 $M_\odot$ neutrino mass during the collapse of the progenitor. The *Gaia* mission will likely uncover dozens more OB+BH binaries in the MW via high-precision astrometry (Mashian & Loeb 2017; Breivik et al. 2017; Janssens et al. 2022, 2023), though so far only low-mass stars with BH companions have been discovered (El-Badry et al. 2023b; Chakrabarti et al. 2023; El-Badry et al. 2023a; Shahaf et al. 2023; Gaia Collaboration et al. 2024). The formation scenarios of these objects are still debated, and it is possible that they originate from dynamical captures, making them less useful for constraints on SN physics (Rastello et al. 2023; El-Badry 2024; Marín Pina et al. 2024). In any case, *Gaia* will not uncover extragalactic OB+BH binaries. Finding the first dormant OB+BH binaries in the SMC via spectroscopic monitoring of massive stars has the potential to yield unprecedented constraints on BH formation at low Z.

Finally, binary monitoring provides a crucial testbed for single-star models. Eclipsing binaries enable the determination of accurate stellar masses and radii (Hilditch et al. 2005; Torres et al. 2010; Mahy et al. 2020a). Moreover, well-separated binaries are less likely to have been affected by binary interaction, and hence provide a more solid basis for benchmarking endeavours of single-star models (de Mink et al. 2014).

Motivated by these objectives, we initiated a novel spectroscopic monitoring survey of a large population of massive stars in the SMC. The Binarity at LOw Metallicity (BLOeM) campaign is a European Southern Observatory (ESO) Large Programme (PI: Shenar, dPI: Bodensteiner; ID: 112.25R7) scheduled for 2023 – 2025. Relying on 116 hr of observing time with the Fibre Large Array Multi Element Spectrograph (FLAMES; Pasquini et al. 2002) of the Very Large Telescope (VLT), the survey is underway and assembling 25 epochs of spectroscopy

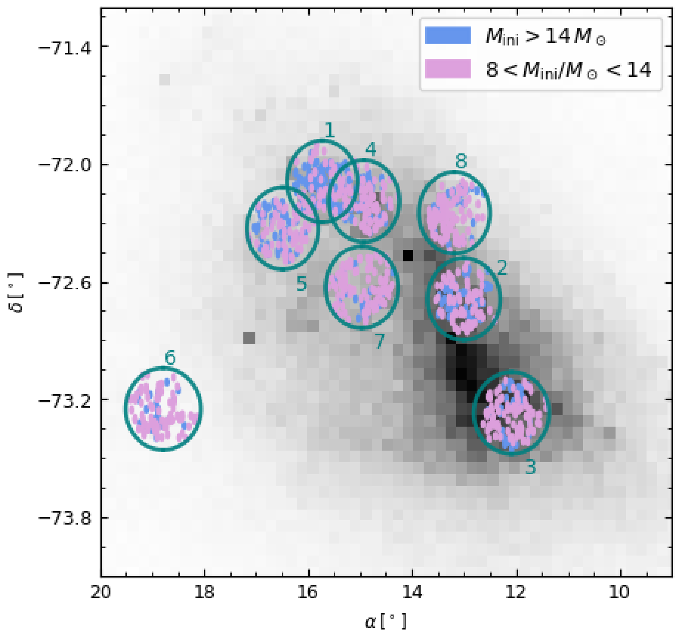

Fig. 1: The eight FLAMES pointings marked on a density map of the underlying *Gaia* source catalogue of the SMC (with $G < 19$ mag) as a function of right ascension (α) and declination (δ) (darkest pixels correspond to $\approx$ 900 stars). The green rings correspond to the FLAMES FoVs, which are 25' in diameter. The 929 targets are shown as blue and pink dots based on their estimated initial masses (see legend and text). We note that the regions most densely populated with stars in the SMC (e.g. the bar) are not rich in massive stars, and hence only a few fields were allocated there.

for 929 massive stars for a total baseline of two years (four semesters). The survey will enable a full characterisation of the binary fraction and the orbital parameters of stars with orbital periods of up to a few years and with mass ratios of as low as $M_2/M_1 \approx 1/10$; the discovery of dormant OB+BH binaries; and a complete analysis of the binary and single-star content of the sample.

This first paper in the series provides an overview of the sample and sample selection (Sect. 2), a description of the data reduction and quality (Sect. 3), a detailed spectral classification (Sect. 4), and a first characterisation of the physical mass range and evolutionary status of the sample stars (Sect. 5), followed by our main conclusions (Sect. 6).

2. Sample selection

The BLOeM sample (see Fig. 1) was selected from the third *Gaia* data release catalogue (*Gaia* DR3, Gaia Collaboration et al. 2023). The catalogue was retrieved from the *Gaia* database using a search radius of 2.6° around the SMC centre (α[hrs], δ[deg] = 00:52:38, -72:48:01; epoch J2000). To achieve S/N $\gtrsim$ 20 per pixel (0.2 Å spectral bin), only stars with $G < 16.5$ mag were retrieved. Foreground objects were filtered via two constraints. First, the parallax π was required to be consistent with zero[1] within 5σ, that is $\pi/\sigma_\pi < 5$. Second, the proper motions of the stars were required to be consistent within 15σ with the SMC proper motion ($\mu_\alpha = 0.695 \pm 0.240\,\mathrm{mas\,yr^{-1}}$ and $\mu_\delta = -1.206 \pm 0.140\,\mathrm{mas\,yr^{-1}}$) following Yang et al. (2019) and Schootemeijer et al. (2021).

We omitted the 12 known SMC Wolf-Rayet (WR) stars (Neugent et al. 2018) from the sample, because they have been previously monitored (Foellmi et al. 2003; Hainich et al. 2015; Shenar et al. 2016; Schootemeijer et al. 2024). Finally, we omitted potential red supergiants (RSGs) from the sample by imposing $G_{\rm BP} - G_{\rm RP} < 1$ mag: due to the large radii of RSGs, RSG binaries have periods that exceed a few years (e.g. Patrick et al. 2019; Neugent et al. 2020) and hence exceed the two-year baseline of our programme.

To avoid crowding, we removed objects that have a *Gaia* source brighter than $G = 19$ mag closer than 1.2", which corresponds to the FLAMES fibre size. We also explicitly excluded stars within 30" of the centres of the dense SMC clusters NGC 330 and NGC 346.

we made use of an evolutionary track of a $M_{\rm ini} = 8\,M_\odot$ star (see Sect 5.4) computed by Schootemeijer et al. (2019) and Hastings et al. (2021) with

In an attempt to select only massive stars, we made use of an evolutionary track of a $M_{\rm ini} = 8\,M_\odot$ star (see Sect. 5.4) computed by Schootemeijer et al. (2019) and Hastings et al. (2021) with the Modules for Experiments in Stellar Astrophysics (MESA) stellar evolution code (Paxton et al. 2011, 2013, 2015, 2018, 2019; Jermyn et al. 2023). We converted the physical parameters along the track to a G-band magnitude and $G_{\rm BP} - G_{\rm RP}$ colours using bolometric corrections taken from the MIST webpage[2] (Dotter 2016; Choi et al. 2016). We adjusted the track on the colour–magnitude diagram (CMD) by adopting a distance of 62 kpc (Graczyk et al. 2020), and assuming an average value for the reddening of $E_{\rm BP-RP} = 0.14$ mag and extinction of $A_G = 0.28$ mag (Schootemeijer et al. 2021). We then only selected targets whose CMD positions lie above this track before becoming a RSG (effective temperature $T_{\rm eff} > 6$ kK; see Fig. 2). This resulted in a massive-star catalogue of 5576 stars subject to the criteria above. We also made use of a MESA track computed for $M_{\rm ini} = 14\,M_\odot$ by Schootemeijer et al. (2019) to divide the sample into stars with $M_{\rm ini} \gtrsim 14\,M_\odot$ (born as O-type stars) and $M_{\rm ini} \lesssim 14\,M_\odot$ (born as B-type stars)[3]. While massive stars are typically born as OB-type on the main sequence, they can appear as OBAF blue/yellow supergiants after leaving the main sequence (in addition to Wolf-Rayet stars and GMK red supergiants, which were omitted from our survey, as described above). Hence, we can expect the spectral types of the sample stars to span the entire OBAF range.

Our programme includes a total of eight FLAMES plate configurations, each with a field-of-view (FoV) of 25' in diameter, although the instrument setup ensures visibility of targets only within a 20' diameter (Fig. 1). For each FLAMES plate configuration, 130 GIRAFFE fibres are available. We allocated 14 fibres for sky, leaving each field with 116 science targets. The only exception is field 8, for which 13 sky fibres and 117 science targets are available. This makes a total of $7 \times 116 + 117 = 929$ science targets.

To obtain a balanced sample of 929 science targets out of the 5576 available targets, we aimed to achieve a G–band magni-

[1] *Gaia* is not sensitive enough to measure non-vanishing parallaxes within errors at the SMC distance.

[2] http://waps.cfa.harvard.edu/MIST/model_grids.html; the bolometric corrections were retrieved by fitting a fifth-order polynomial to MIST values for $\log g = 3\,\mathrm{cm\,s^{-2}}$ and $Z = 0.18\,Z_\odot$.

[3] The threshold mass for O-type stars is typically taken as $15\,M_\odot$ for the Galaxy (e.g. Martins et al. 2005). However, stars in the SMC are more compact and hot at a fixed mass (e.g. Georgy et al. 2013), such that this threshold is likely lower at low Z.

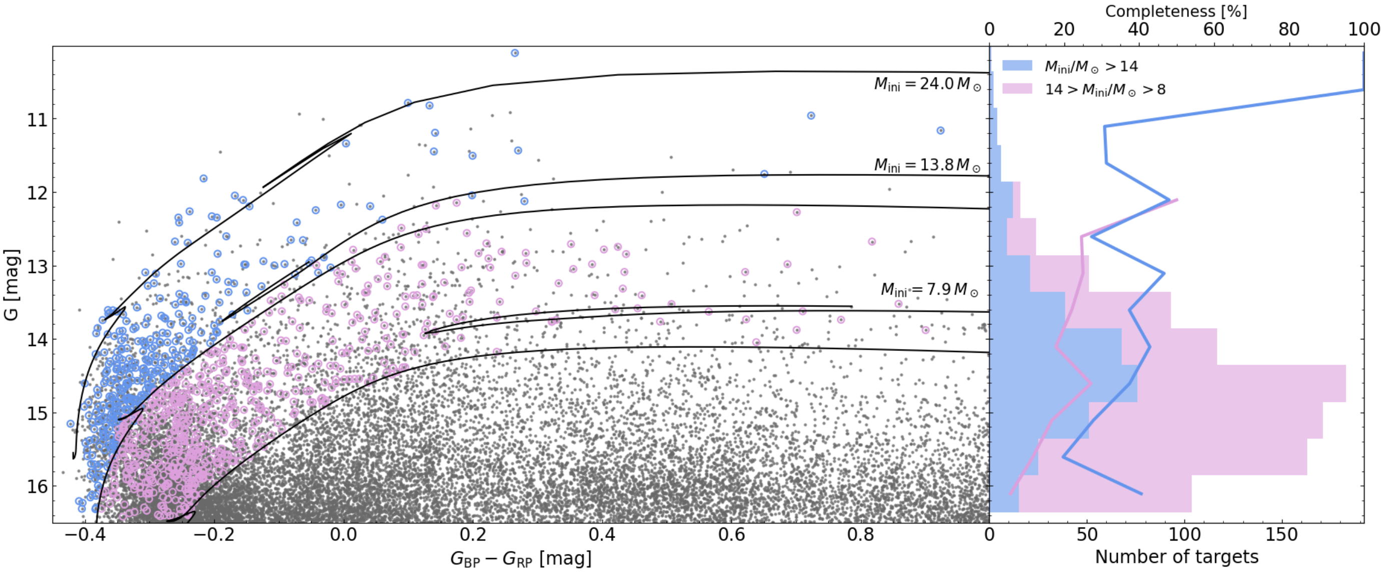

Fig. 2: Completeness of the BLOeM dataset with respect to the underlying *Gaia* catalogue. *Left:* CMD showing the underlying *Gaia* catalogue used to choose the BLOeM sample (black dots). Three evolution tracks computed by Schootemeijer et al. (2019) and Hastings et al. (2021) with the MESA stellar evolution code (see Sect. 5.4) for $M_{\rm ini} = 7.9, 13.8$, and $24\,M_\odot$ are plotted. The tracks were adjusted to the SMC distance and an average reddening and extinction (see text for details). BLOeM targets are encircled with blue ($M_{\rm ini}/M_\odot \gtrsim 14$; born as O-type stars) and pink ($8 \lesssim M_{\rm ini}/M_\odot \lesssim 14$; born as B-type stars) circles. *Right:* Magnitude distribution of the subsamples, along with completeness fractions for the two subsamples with respect to the underlying *Gaia* SMC catalogue.

tude distribution that is as homogeneous as possible, while prioritising the brightest and hence most massive stars, which are rarer. The target allocation was then followed via the two steps described below.

First, the centre of a FLAMES pointing was chosen. The choice of field centre followed automatically by identifying the coordinate that encloses as many massive and bright stars as possible within a circle of 25' in diameter centred on that coordinate, after removing stars which were already allocated in previous field allocations. Specifically, the pointings were selected by identifying the centre coordinates that result in the largest number of stars with $M_{\rm ini} \gtrsim 14\,M_\odot$ (see above) and $G < 14.7$ mag. This resulted in fields 1 – 8 shown in Fig. 1, which provide a good coverage of the massive-star content of the SMC. We note that while some of the fields overlap (e.g. 1 and 4), there is no overlap between the allocated stars within each field.

As a second step, for each plate configuration, targets within a circle of 20' in diameter were allocated to the available fibres, starting from the brightest ones, while aiming to achieve a homogeneous sampling across the G-band. Specifically, we divided the magnitude range 10 – 16.5 mag into 15 bins, and aimed to achieve homogeneous coverage across these bins, resulting in 7 – 8 stars per magnitude bin, per field. This was not always possible, given the rarity of bright stars, and the smaller parameter range of massive stars at lower magnitudes. As the final fibre allocation depends on limitations related to the FLAMES fibre positioner, the remaining massive stars in each field within a circle of 25' in diameter were taken as backup targets, with their priority sorted by brightness.

The final fibre allocation was then performed using ESO's Fibre Positioner Observation Support Software (FPOSS). The majority of our input targets made it to the final allocation, but the final sample includes a few dozen backup targets. Sky fibres were allocated to 14 fibres in each field (13 for field 8) selected from concentric rings around the field centre where no known *Gaia* source is located. Finally, guide stars were selected following requirements in the ESO FLAMES manual for cycle P112.

The final sample of 929 targets is shown on a CMD in Fig. 2, along with a magnitude histogram. We also show the completeness fraction with respect to the underlying SMC *Gaia* catalogue as a function of G-band magnitude. Of the 929 stars, and based on the single-star tracks in Fig. 2, 323 have initial masses of above $\approx 14\,M_\odot$ ("born as O-type stars") and 606 are below this mass ('born as B-type stars'). Evidently, the sample reaches a completeness fraction of $\gtrsim 40\%$ for the $M_{\rm ini} \gtrsim 14\,M_\odot$ subsample, and $\gtrsim 20\%$ for the $8\,M_\odot \lesssim M_{\rm ini} \lesssim 14\,M_\odot$ sample.

The naming convention for the sample stars follows the format F-NNN, where F is the field number (1 – 8), and NNN is the target number (001 – 117), sorted by ascending right ascension per field.

3. Observations and data reduction

At the time of writing, 9 out of 25 epochs were obtained during the first semester and were processed in the framework of the BLOeM survey. The field centres, along with the MJD values of the epochs acquired so far, are provided in Table A.1 of Appendix A.

The data reduction was performed with the GIRAFFE pipeline v. 2.16.11 under the ESO CPL environment (v. 3.13.5). Each exposure was split into two subexposures for a robust removal of cosmic rays (cosmics, Sect. 3.5). The data reduction itself consisted of four steps: bias and dark subtraction, flatfield correction, and wavelength calibration. All spectra were resampled by the ESO CPL pipeline to a constant wavelength step of 0.2Å (see also Sect. 3.2) and science spectra were then sky-subtracted and corrected for the barycentric motion. As a final step, we resampled the individual spectra to a common wavelength grid and co-added the spectra of individual targets to boost S/N in order to improve spectral typing. The spectra have a spectral resolving power of $R \approx 6200$ and cover the spectral range 3960 – 4570 Å, with a median S/N of 70 – 100 per pixel and epoch; details are provided below. We provide further details below on specific aspects of the data reduction process[4].

3.1. Temporal sampling

The temporal sampling of the epochs is not strictly defined a priori in order to allow for sufficient scheduling flexibility. We insist on a minimum separation between each epoch of 1 d, and a maximum of 20 d to ensure that all epochs are acquired within a semester. The typical separations between the epochs used here, acquired during September 2023 through December 2023, are days to weeks (see Table A.1), for a total time baseline of 50 – 70 d, depending on the field. The fact that the acquisition will take place across four semesters ensures that both short-scale and long-scale variability will be covered by the survey. As a multiplicity analysis is beyond the scope of the present paper, we refrain from a complete characterisation and Fourier mapping of the temporal sampling here.

3.2. Wavelength calibration

We paid particular attention to the quality of the wavelength solution. For FLAMES GIRAFFE, a reference ThAr calibration frame in the LR02 setup is obtained at the end of an observing night by illuminating each fibre on a given plate with the light of a ThAr lamp. As a result, each fibre of each epoch has its own calibration ThAr spectrum, which is used by the CPL pipeline to produce a 2D polynomial dispersion solution. The wavelength calibration solution was performed in two steps. First we used the instrument model provided by the pipeline static calibration v2.16.11 to compute a first-guess solution and run a first iteration of the `giwavecalibration` CPL recipe. We modified the standard options to allow for a large detection window of 20 pixels at first, for five iterations, and then progressively reduced it to 15 and ultimately 10 in the remaining five iterations. We decreased the rejection threshold from 1.2 to 3σ, allowing us to retain a greater number of lines and provide a first wavelength solution with a root mean square (rms) residual of 0.45-0.56 pixels. By comparing ThAr spectra of different nights we noticed a slight drift in the wavelength solution in various parts of the ThAr spectrum, with a higher stability in the centre of the wavelength range and a larger epoch-to-epoch variation in the blue and red parts of the wavelength solution. We estimated the internal consistency to be no better than a few km s^{-1}. To improve on this, we performed a second iteration using the first solution as a new input guess-solution and reiterating the `giwavecalibration` recipe. This yields a final dispersion solution, characterised with a rms residual in the range of 0.22 to 0.25 pixels.

Three epochs of field 1 were observed with the SIMCAL lamp on at the beginning of the survey. The SIMCAL lamp yields a set of five ThAr spectra spread across the detector and acquired simultaneously with the science observations. This setup was discontinued because the glow of the strongest ThAr lines impacted the signals of the adjacent fibres, leaving a noticeable imprint of ThAr on nearby sky and weak objects. Yet, we noticed no difference in the quality of the wavelength solution with or without the SIMCAL lamp.

[4] The reduced data and co-added spectra will be made available via ESO phase 3 upon termination of propriety time; they are currently available on http://www.astro.tau.ac.il/~tshenar/DR3/; please contact T. Shenar or J. Bodensteiner for credentials.

We experimented with the pipeline rebin pixel size (`-rbin-lstep`) but did not find this to yield any significant improvement and we decided to resort to the default resampling of 0.2 Å. The average spectral resolving power measured on the ThAr lines across all epochs is $R = 6224 \pm 90$.

Finally, we investigated the stability and consistency of the individual dispersion solutions across the BLOeM dataset. We specifically investigated the inter-epoch stability for given fibres as well as the intra-epoch consistency across all fibres of a given epoch. For the first one, which informs us about the temporal stability of the data, we cross-correlated the wavelength-calibrated ThAr spectra of a given fibre and field with that of the same fibre and field across all the epochs obtained so far. We found maximum peak-to-peak differences to be of 130 m s^{-1}, with a standard deviation of below 50 m s^{-1}. For the latter, which informs us about the consistency of the dispersion solution across the BLOeM data sets, we cross-correlated the ThAr spectra of all fibres for a given epoch and field with one arbitrary ThAr spectrum (fibre #10) for the epoch under consideration. While the peak-to-peak and rms variations are slightly larger (750 and 150 m s^{-1} in the worse case), they remain well within the specifications of the instrument. For a few nights, no ThAr calibration frame could be obtained in the morning following the observations. In such cases, we use the frame closest in time, typically the one from the morning before. However, in eight cases we had to resort to ThAr calibration frames taken 30 to 40 h before of after observations of our targets. Nevertheless, no noticeable difference in the quality of the calibration could be found, again suggesting that temporal drifts are limited.

3.3. Sky subtraction

Sky spectra were obtained simultaneously with the science integration through a set of fibres allocated to empty patches of sky. These are dubbed `SKY` fibres and record all background signal, including the moon and nebular and sky emission spectra depending on the wavelength regime. Hence, not all signal recorded by `SKY` fibres is from the 'sky' itself, but we nonetheless adopt the generic denomination here.

As described earlier, we typically used 14 `SKY` fibres in each field and kept the location constant across all epochs of a given field. We visually inspected the `SKY` spectra from each field and each epoch and flagged spectra that seemed to be significantly higher than the median of the epoch and field. These are possibly contaminated by faint objects and therefore not representative of the true background signal. Once a sky location has been flagged as contaminated in any of the epochs of a given field, it is rejected from all epochs so that the median sky is always computed with the same set of input locations. In this process, we rejected 4, 3, 1, and 2 sky fibres for fields 1, 2, 5, and 6, respectively. The sky correction was finally performed by subtracting the median spectra of the 'valid' `SKY` fibres at the corresponding field and epoch. The error sky spectrum was computed as the rms around the median sky at each pixel after masking sky pixels affected by cosmic rays through a $\kappa-\sigma$ iterative filtering. The error sky spectrum was added quadratically to the error science non-sky-subtracted spectrum produced by the pipeline in order to compute the error spectrum of the sky-subtracted science data.

Of importance, any nebular component in the sky spectra is obtained at the position of the `SKY` fibres. In our adopted observational setup, these are located tens of arcsecs to several arcminutes away from any science spectra and hence they do not reflect the local nebular conditions of any science targets. The process of taking the median across 10 to 14 sky positions ensures that any local nebulosity in the SKY fibres is averaged out. As a corollary, the sky-subtracted science spectra are not corrected for nebulosity and therefore retain their nebular component.

3.4. Normalisation

The sky-subtracted spectra of each subexposure were individually and automatically normalised using a designated Python script to remove the underlying continuum, which is a combination of the stellar continuum, reddening, and instrumental response. Overall, the non-normalised spectra are well-behaved and have a smooth, typically monotonically decreasing behaviour across the spectral range. The normalisation was performed by fitting a polynomial to automatically identified continuum points along the spectrum. Following several independent attempts, we found that a polynomial of degree eight provided the best results in terms of robust normalisation; lower polynomial degrees resulted at times in underfit regions, while higher degrees introduced wavy patterns in the spectra, which can impact subsequent analysis.

The continuum points were automatically selected in an iterative manner. For this purpose, we computed an average spectrum with a small 3-pixel window and a median spectrum with a large 250-pixel window, which is a first approximation for the continuum. A first batch of continuum points was defined as the set of points whose average flux is 2σ above the median flux, with σ originating in the error spectrum. To ensure that the edges of the spectra are included, we always include the first and last 10 pixels not affected by cosmics in this set. We then fit a polynomial of degree eight through these points to obtain an approximation for the continuum. This process is then repeated three times, with the polynomial fit for the continuum replacing the role of the median spectrum of the original iteration.

3.5. Cosmic correction and combination of subexposures

To boost the S/N, the two subexposures of each epoch and star were combined into one exposure. Moreover, we used the availability of two subexposures for a robust cosmic correction using a designated Python script. The process is as follows. First, positive flux outliers are identified in each of the two subexposures via the condition $f_{1,2}(\lambda) > \min\{f_1(\lambda), f_2(\lambda)\} + 6\sigma$, where $\sigma(\lambda)$ is the minimum of the error spectra of both subexposures. Cosmics are identified as points flagged as such in one spectrum but not in the other – this ensures that intrinsic emission features (e.g. disc features, wind features, nebular lines) are not removed via this process. In principle, cosmics may be present in the same pixels in both subexposures, but such cases occur so rarely that this does not warrant further consideration. The cosmics are then removed by replacing each pixel identified as cosmic in one subexposure with the flux value of the same pixel in the second subexposure. The flux of the remaining pixels is formed by quadratically adding the two subexposures. The S/N per pixel ranges between 20 and 300, with a median value of between 70 and 120, depending on the field (Fig. 3).

3.6. Co-added spectra

For a more robust spectral classification, we produced high-S/N spectra by stacking the nine available epochs for each target. To achieve this, the cross-correlation occurred in two steps. First, the spectra were shifted to the rest frame by cross-correlating them with a spectral model and then co-added, which enabled us to generate a first co-added spectrum. In this step, the entire spectral range was considered, which is dominated by the Balmer lines Hδ and Hγ. As a second step, we cross-correlated all the epochs against the co-added spectrum formed in the previous step, which is calibrated to the rest frame. However, this time we used a narrow spectral window around He I λ4471 (namely 4460–4485 Å), which is present in almost all objects[5]. This allows a more accurate radial-velocity (RV) measurement that is tuned to the spectral morphology of the individual star. For the first step, we used a precomputed model from the TLUSTY O-star model atmosphere grid (Hubeny & Lanz 1995; Lanz & Hubeny 2003) for $Z = 0.1\,Z_\odot$[6], an effective temperature of $T_{\rm eff} = 30\,$kK, and a surface gravity of $\log g = 4.0\,[{\rm cm\,s^{-2}}]$. The exact choice of the model can impact the absolute RV calibration, but has no impact on the process of spectral classification, which is the focus of this paper.

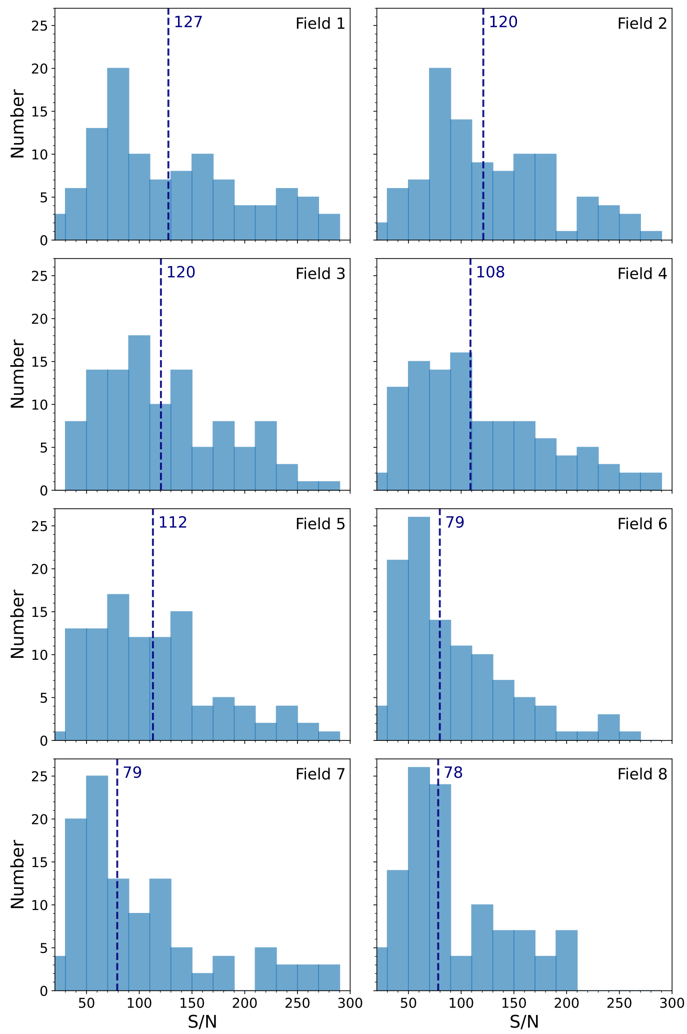

Fig. 3: Histograms of the median S/N per physical 0.2 Å pixel across the nine available epochs, for each of the eight fields of the sample. Red dashed lines and labels denote the median of all median S/N values per field.

[5] For AF supergiants, this range is rich in other spectral lines, such as Mg II λ4481, making the cross-correlation in this range equally possible.
[6] This is the closest available metallicity to that of the SMC. In any case, the impact of the metallicity on RV measurements is negligible

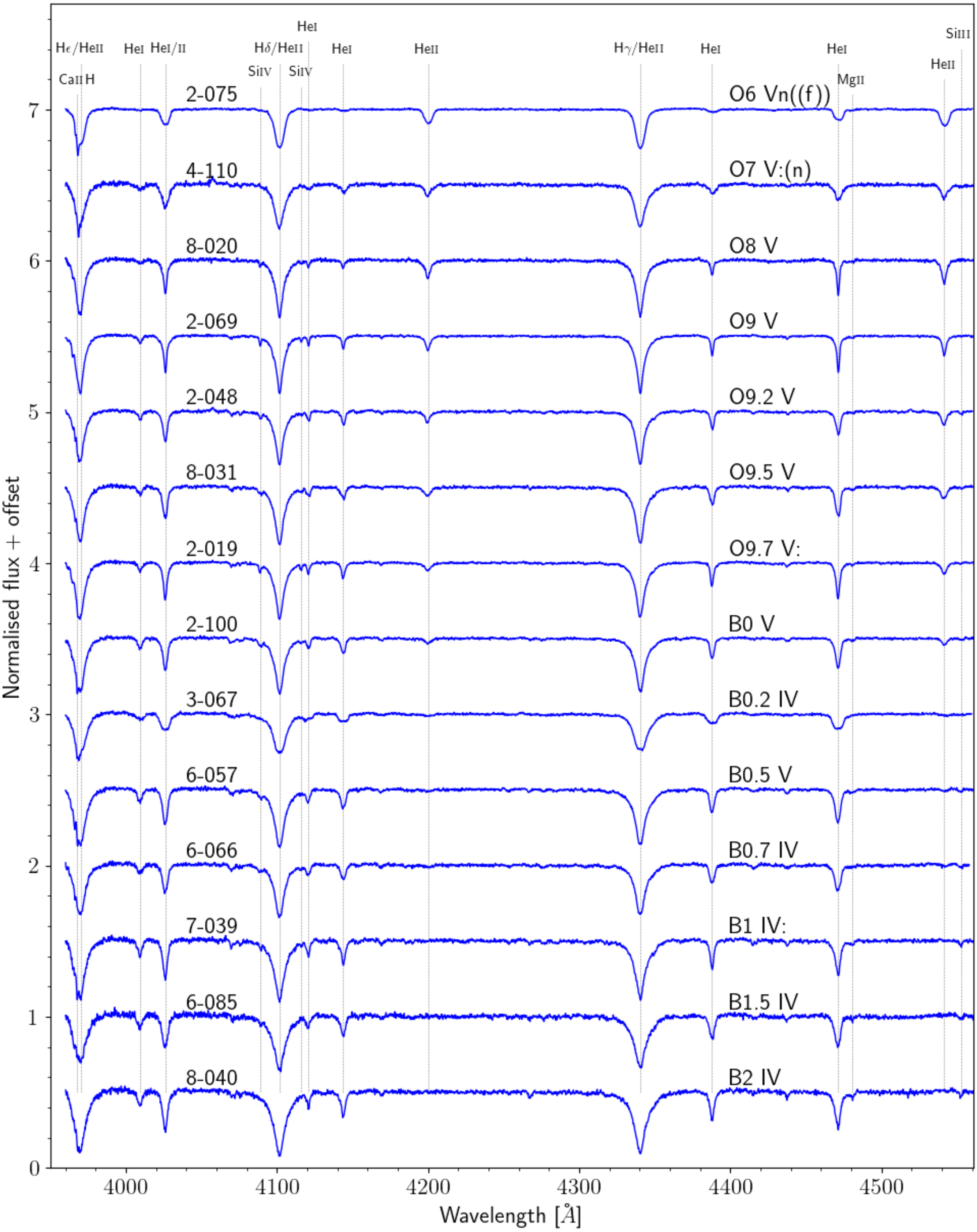

Fig. 4: Montage of the normalised co-added spectra formed from the nine available epochs for selected OB stars classified as dwarfs (luminosity class V) or sub-giants (IV). The spectra are shifted by a constant for clarity. BLOeM IDs and spectral types are noted above each spectrum, and diagnostic lines are identified.

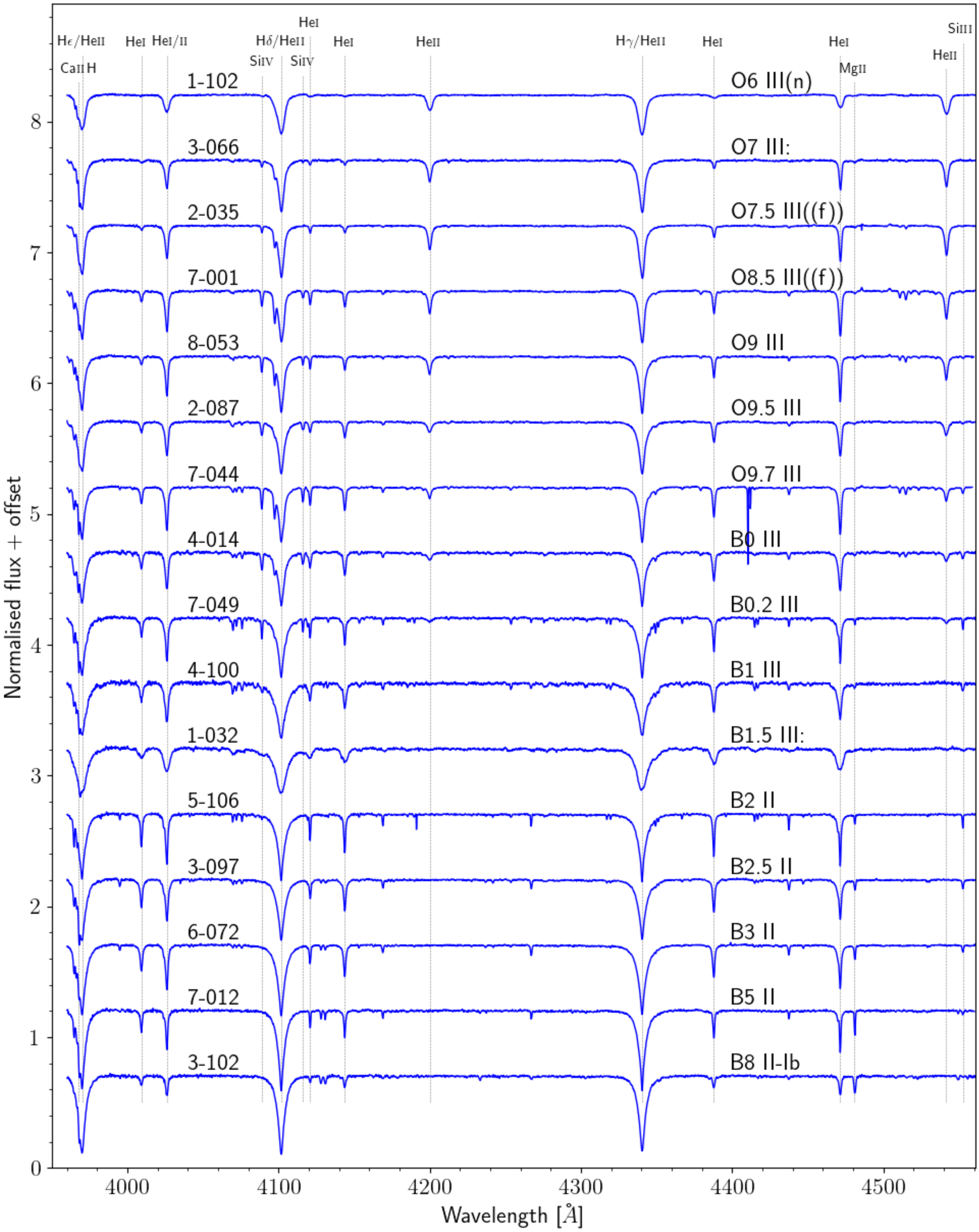

Fig. 5: Montage of a selection of giant (luminosity class III) and bright giant (II) OB stars in the BLOeM sample, ordered from early (top) to late (bottom) type. BLOeM IDs and spectral types are noted above each spectrum. Diagnostic lines are identified.

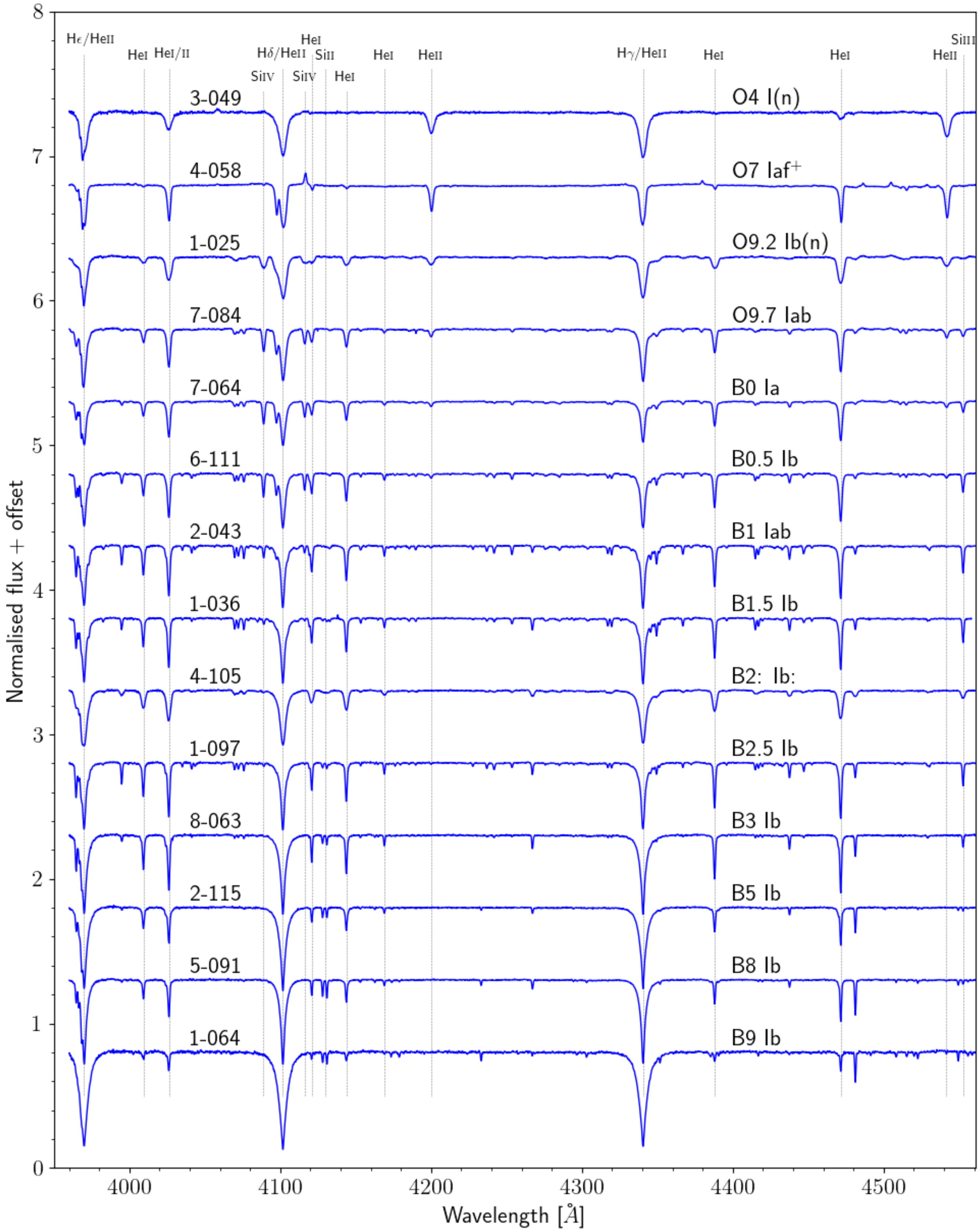

Fig. 6: Montage of a selection of supergiant OB stars in the BLOeM sample, ordered from early (top) to late (bottom) type. BLOeM IDs and spectral types are noted above each spectrum. Diagnostic lines are identified.

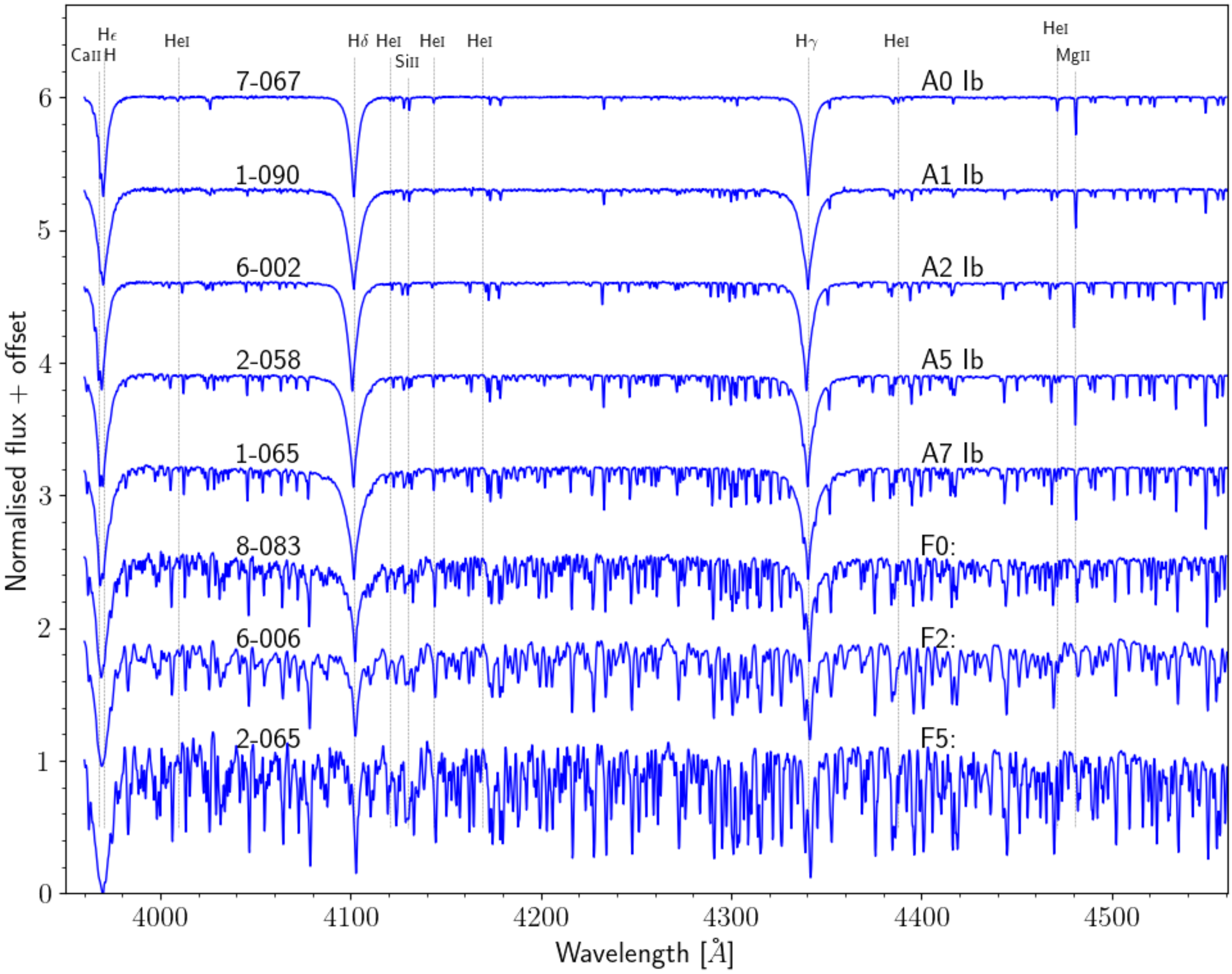

Fig. 7: Montage of a selection of AF supergiants in the BLOeM sample, ordered from early (top) to late (bottom) type. BLOeM IDs and spectral types are noted above each spectrum. Diagnostic lines are identified.

We note that for double-lined spectroscopic binaries (SB2), the process of co-adding the data will smear the spectral features of the two components and result in an average spectrum, which may well contaminate the classification. Clear cases of SB2s (40/929 in total) were identified via visual inspection of the available epochs (see also Sect. 4). A montage of the co-added spectra of selected stars ordered by descending spectral type (Sect. 4) is shown in Figs. 4 – 7.

4. Spectral classification

We established SMC reference OB stars from comparison with Galactic O star templates from Sota et al. (2011) and Maíz Apellániz et al. (2016) or Galactic B star templates from Negueruela et al. (2024). These stars are drawn from BLOeM datasets, supplemented by archival VLT/FLAMES (Evans et al. 2006; Dufton et al. 2019) or VLT/X-Shooter (Vink et al. 2023) datasets. Reference stars are ideally sharp-lined, permitting rotational broadening to be applied for comparison with fast rotators. We assign e, e+, and pe for stars exhibiting (i) H I, (ii) H I and Fe II, and (iii) H I and He I emission, respectively. Objects whose spectra are contaminated by nebular emission are designated 'neb'. In some cases, it was difficult to discern between intrinsic source emission and nebular contamination. To distinguish between these cases, we made use of images acquired with the wide-field Digitized Sky Survey (DSS) 2-red to identify objects that are embedded within nebulous regions. More details are given in Appendix B. The qualifier ':' deems the classification uncertain. We note that the BLOeM spectral range includes most diagnostic lines, but misses a few lines that can help refine the classification, such as N III $\lambda\lambda$4634, 4042, He II λ4686, Hβ, and Hα.

Spectral types of O stars are determined following the Galactic O star scheme of Sota et al. (2011) and Maíz Apellániz et al. (2016), which utilises the ratio of He II λ4542 to He I λ4471 or λ4388 for late subtypes (O8.5+). Luminosity classes are usually assigned courtesy of He II λ4686. As this line is not available for the BLOeM dataset, luminosity classes for O4–7 stars are estimated from the detection of N IV λ4058 and Si IV $\lambda\lambda$4088-4116 emission lines. For late O subtypes, we use a combination of Hγ and Hδ line profile morphologies supplemented by the ratio of Si IV λ4088, λ4116 to He I λ4121, λ4144 lines, following Walborn & Fitzpatrick (1990). It is well known that incorrect luminosity classes would be assigned for silicon-poor SMC stars based on Galactic templates (Walborn 1983). For example, Walborn et al. (2014) showed that using Si-He criteria results in luminosity classes that are different from those resulting from the use of He-line criteria alone. Hence, SMC reference stars are essential for this approach. Nomenclature linked to the region of He II λ4686 —such as f and (f), which reflect the presence of emission in the line— is not possible, but we are able to flag potential rapidly rotating O stars via (n), n, nn, and so on, on the basis of the FWHM of He II λ4542 (early and mid O-types) and He I λ4471 (late O-types). For a few O-type stars, spectral types (mostly luminosity classes) were adjusted based on previous literature, given the lack of diagnostics such as He II λ4686 and Hβ in the BLOeM dataset. These cases are documented in the comments in Table A.2.

We follow the SMC B-type scheme of Lennon (1997), supplemented by early B templates from Negueruela et al. (2024), in assigning spectral types from Si IV λ4088, Si III λ4553, and Si II $\lambda\lambda$4128–32, plus the ratio of He I λ4471 to Mg II λ4481 at late subtypes. Secondary criteria for B0–0.7 stars (Sota et al. 2011), involving the ratio of He I λ4388 to He II λ4541 or He I λ4144 to He II λ4200, are used for stars with extremely weak Si diagnostics. Luminosity classes are obtained from line morphologies of Hγ and Hδ with respect to reference stars. Unusual B-type systems with Balmer emission lines and forbidden [Fe II] lines are classified as supergiant B[e] (sgB[e]) following Lamers et al. (1998) and Kraus (2019).

For A and F supergiants, we are unable to follow the Ca II H+K criteria of Evans & Howarth (2003), because our dataset excludes the Fraunhofer K line, and so again we selected SMC reference A0–5 supergiants from archival VLT/FLAMES spectroscopy, with luminosity classes assigned from the equivalent width of Hγ from comparison with Millward & Walker (1985). Spectral types assigned to late A and F stars are relatively coarse, and are primarily based on the strength of the CH G-band in BLOeM datasets spectrally degraded to the resolution of SMC AF supergiants presented by Evans & Howarth (2003). All F stars have luminosity class II–I owing to the strength of their metallic features (Gray & Corbally 2009), even at the low metallicity of the SMC.

The derived spectral types are compiled in Table A.2 for each of our targets. While a multiplicity analysis is beyond the scope of this paper, a few dozen ($\approx$ 40/929) already portray clear evidence for the presence of at least two stellar components in their spectra. These are visually identified and, when possible, a preliminary spectral type for the companion(s) is provided.

5. Results

5.1. Census

A histogram of the spectral-type distribution across the range O4 to F5, subdivided into dwarfs and giants in one group and supergiants in the other, is shown in Fig. 8. The BLOeM sample includes the complete spectral range from the earliest stars in the SMC (excluding Wolf-Rayet stars) to yellow supergiants. Overall, the sample includes 159 O-type stars, 331 early B-type dwarfs and giants (B0 – B3 V–III), 303 early B-type supergiants (B0 – B3 II–I), and 136 late-type supergiants (B4 and later). Of these, 82 objects are classified as OBe stars, portraying characteristic emission in their Balmer lines: 20 Oe stars (including four uncertain cases, marked 'e?'), and 62 are Be stars (Sect. 5.2).

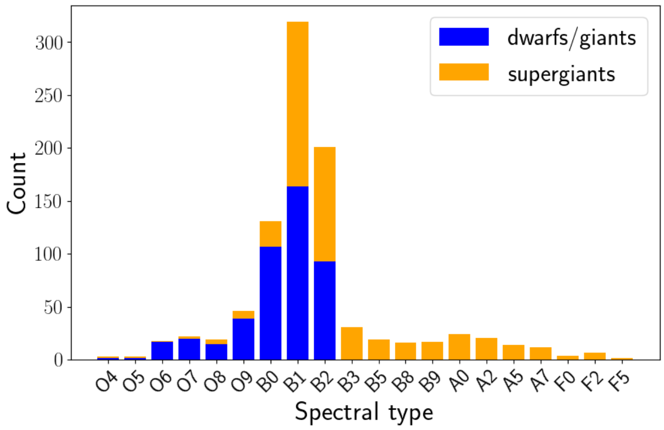

Fig. 8: Spectral-type histogram of the BLOeM sample. Fractional spectral types are rounded off. The sample is subdivided into dwarfs and giants (luminosity classes V-III), which are thought to be primarily core H-burning, and supergiants (luminosity classes I or II) thought to be mainly post main sequence.

The number of dwarfs and giants (generally interpreted as main sequence objects) steeply decreases around a spectral type of B2, which roughly corresponds to 8 $M_\odot$ (Harmanec 1988). Among the B1-B2 dwarfs and giants, the vast majority are giants, bright enough to have been included in our survey. These are likely evolved main sequence stars. In the O-star regime, we are sensitive to the full extent of the main sequence down to the youngest stars, assuming those are not dust-enshrouded.

5.2. OBe fraction: Complementary *Gaia* low-resolution spectra

As noted in Sect. 5.1, 82 targets have been identified as OBe stars in our sample. However, the BLOeM dataset does not cover the Hα line, which is the most sensitive line for circumstellar material in the visual range. For this reason, it is likely that we have missed OBe stars in the sample. To mark additional OBe candidates, we make use of *Gaia* XP low-resolution flux-calibrated spectra (De Angeli et al. 2023), which exist for all sources except BLOeM 4-041, 6-044, 7-012, and 8-033. While these data are of very low resolution ($R \approx 50$), and some are affected by problematic wiggles in the data, they may be used to detect the presence of strong emission, or candidate OBe stars in our case. To be pragmatic, we adopt a straightforward approach of measuring the Hα equivalent width (EW) in the XP 'sampled' data, using broad windows on both sides of the line to define a local continuum. While more complex approaches are possible (e.g. Weiler et al. 2023), our method should be adequate for detecting strong Hα emission. Candidate OBe stars are then flagged as 1σ outliers in the distribution of EW as a function of magnitude. As verification of this approach, a visual inspection of all spectra was also performed to define a second category of 'by-eye' OBe candidates. Both samples are illustrated in Fig. 9. The two methods agree for most targets, although given the contamination induced by the spectral wiggles on the EWs, we favour the by-eye classification of Hα emitters.

Overall, in addition to the 82OBe stars classified using the BLOeM dataset, we identify 16 additional Hα emitters. However, half of these are supergiants according to our classification from the BLOeM dataset, which, by definition, are not OBe

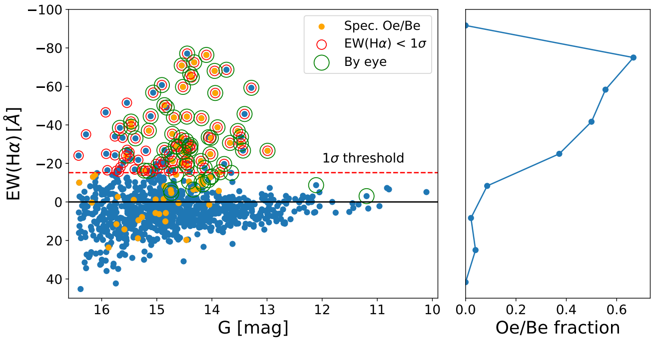

Fig. 9: Selection of OBe stars with *Gaia* data. Hα equivalent widths of the BLOeM targets measured from *Gaia* low-resolution spectra. Spectroscopically classified OBe stars are marked in orange. All targets with emission exceeding 1σ are circled in red, and by-eye identifications of Hα emitters are marked with green circles. *Right:* Fraction of spectroscopically classified OBe stars using the BLOeM dataset, versus Hα EW.

stars. Only eight targets are potential Be stars that have not been classified as such: BLOeM 4-046, 4-096, 5-096, 5-107, 7-008, 7-094, 7-099, and 8-078. Adding those, the total number of OBe stars in our sample is 90, amounting to a fraction among the non-supergiant OB stars of 11%. This fraction is much lower than the fraction of ≈30% that has been found in previous work (Bonanos et al. 2010; Schootemeijer et al. 2022). The difference can be explained by the diagonal CMD cut that we use to select our sample, which favours blue stars and hence disfavours OBe stars, which are about 0.3 magnitudes redder than OB stars (Schootemeijer et al. 2022, their figure A.5). The bias mentioned above likely does not impact the Oe fraction derived here, which is 20/159 = 13%, comparable to the 10% fraction reported by Bonanos et al. (2010).

5.3. Notable targets

We highlight a few unique objects in our sample. BLOeM 2-116, BLOeM 3-012, and BLOeM 4-055 are classified as sgB[e] stars. BLOeM 2-116 (alias LHA 115-S 18) has been the subject of several studies (e.g. Shore et al. 1987; Clark et al. 2013; Maravelias et al. 2014), as has BLOeM 3-012 (alias RMC 4; Zickgraf et al. 1996; Graus et al. 2012; Pasquali et al. 2000; Wu et al. 2020). Such objects are thought to represent a brief evolutionary phase of massive stars. Their spectra resemble those of luminous blue variables (LBVs), and their origin is debated in the literature (e.g. Podsiadlowski et al. 2006; Clark et al. 2013). The spectra of all these objects indicate variability. Whether or not this variability stems from binary motion is not yet clear, though BLOeM 3-012 has previously been reported to be a binary (Zickgraf et al. 1996) and seems well explained as the product of a binary merger in a triple system (Pasquali et al. 2000; Podsiadlowski et al. 2006; Wu et al. 2020).

BLOeM 3-031 and BLOeM 5-071 show spectra that resemble those of Be + bloated stripped-star binaries such as LB-1 (Irrgang et al. 2020; Abdul-Masih et al. 2020; Shenar et al. 2020; El-Badry & Quataert 2021) and HR 6819 (Bodensteiner et al. 2020; Frost et al. 2022). Such objects feature strong Balmer emission characteristic of Be stars, in combination with narrow and RV variable absorption features that stem from a putative bloated stripped-star companion.

BLOeM 2-104 and BLOeM 4-039 were classified as Of?p stars by Evans et al. (2004), which refers to the presence of emission lines associated with N III and C III in the range 4630–4660Å (Walborn 1972). We cannot independently verify this, because the BLOeM data lack this range, though we do confirm the presence of emission in the Balmer lines characteristic of such stars, and so we adopt this classification. All known Galactic Of?p stars possess strong global magnetic fields (Grunhut et al. 2017). It is therefore plausible that BLOeM 2-104 and BLOeM 4-039 are magnetic as well, although spectropolarimetric data are needed to verify this.

Nine targets are identified as significant X-ray emitters from a cross-match with various X-ray catalogues described in Appendix C, one of which may be a spurious X-ray detection (BLOeM 6-116). Four of those have been classified as high-mass X-ray binaries (HMXBs) in the past: BLOeM 2-055, 2-82, BLOeM 2-116, BLOeM 4-026 and BLOeM 4-113. BLOeM 3-042 may be a colliding-wind binary (CWB) given its classification (O6 III + O7.5). The origin of X-rays in BLOeM 8-029 (B1 IV:) and BLOeM 1-102 (O6 III(n)) is not yet clear. Further details regarding the cross-match process and X-ray luminosities of the objects can be found in Appendix C.

Finally, cross-matching with the OGLE catalogue of photometrically variable stars in the SMC (Pawlak et al. 2016), 74 (i.e. 8%) of the 929 BLOeM targets are found to be eclipsing binaries, while 8 are classified as ellipsoidal variables (Sect. C.4).

5.4. Hertzsprung–Russell diagram

Spectral classification of the BLOeM sample permits coarse estimates of surface temperatures of normal OBAF stars presented in Table 1. These are adapted from the SMC spectral type-temperature calibration of Dufton et al. (2019), incorporating results for SMC O stars from Bouret et al. (2013), Bouret et al. (2021) and SMC late B and AF supergiants from Evans & Howarth (2003).

Bolometric luminosities are estimated from K_s band point spread function (PSF) photometry fitting from VISTA/VMC (Cioni et al. 2011), a distance modulus of 18.95 mag for the SMC (Hilditch et al. 2005; Graczyk et al. 2020), intrinsic V-K_s colours from Martins & Plez (2006), Cox (2000), and Koornneef (1983), plus V-band bolometric corrections drawn from Bouret et al. (2013) and Bouret et al. (2021) for O stars, Lanz & Hubeny (2007) for B stars with effective temperatures $T_{\rm eff}$ ≥ 15kK, Kudritzki et al. (2008) for late B and A supergiants (8kK ≤ T ≤ 12kK), and Cox (2000) otherwise. The use of K_s band photometry avoids the need to correct for interstellar extinction, which is significantly smaller at the K_s band than at the G band. Given this and the typically negligible extinction towards SMC sightlines (see e.g. Schootemeijer et al. 2021), we assume $A_{\rm K}$ = 0 here; this may affect the luminosities of individual objects, but does not affect our general conclusions. For the intermediate luminosity classes IV and II, we use the dwarf and supergiant relations from Table 1, respectively.

We present the resulting Hertzsprung–Russell diagram (HRD) of the BLOeM sample in Fig. 10, together with evolutionary tracks and isochrones for SMC metallicity stars from the extended grid of Schootemeijer et al. (2019). As described in Appendix B of Hastings et al. (2021), these models have efficient semi-convection ($\alpha_{\rm sc}$ = 10) and mass-dependent overshooting ($\alpha_{\rm ov}$ linearly increases from 0.1 at 1.66 $M_\odot$ to 0.3 at 20 $M_\odot$, and remains constant at 0.3 for higher masses). Apart from $\alpha_{\rm sc}$ and $\alpha_{\rm ov}$, this grid has the same physics assumptions as

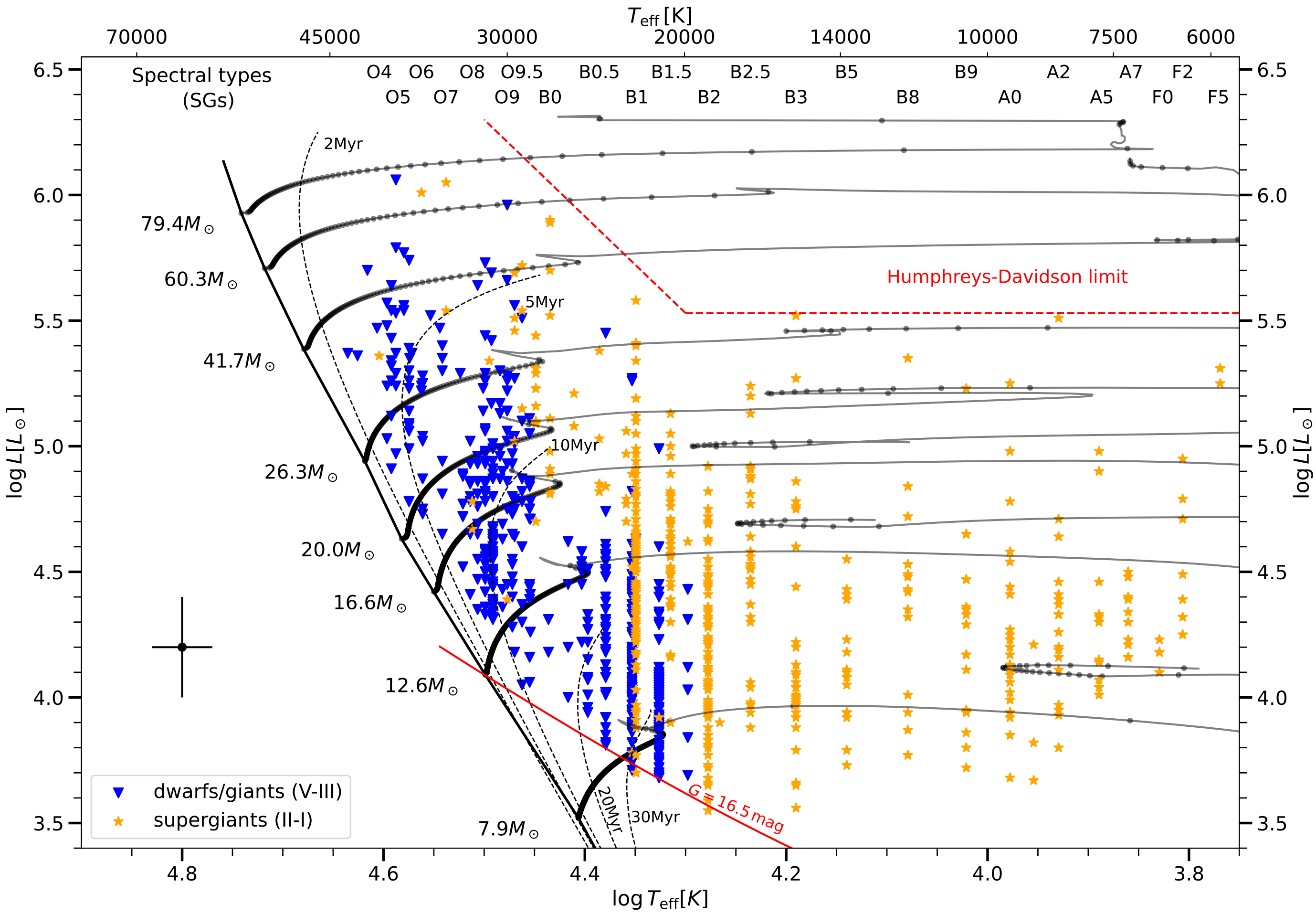

Fig. 10: Approximate location of the BLOeM stars in the HRD of the BLOeM sample based on spectral-type calibrations described in Sect. 5.4, colour-coded for dwarfs and giants (V-III) and supergiants (II-I) with blue triangles and orange stars, respectively. An estimate of the typical error (subject to calibration error, uncertain reddening, and potential binary contamination) is shown in the bottom left corner. We use the same tracks plotted in Fig. 2, but include more initial masses (shown in labels). The $M_{\rm ini} = 7.9\,M_\odot$ track was used to select the BLOeM sample from the *Gaia* catalogue. Black dots along the track are spaced by 0.05 Myr. Also plotted are the ZAMS and isochrones at 2, 5, 10, 20, and 30 Myr. The labels at the top (split into two rows for clarity) show the spectral types corresponding to the temperature scale for supergiants only (adopted from Table 1). The magnitude cut at $G = 16.5$ mag and the H–D limit (identified visually) are also marked.

Brott et al. (2011). We adopt the dwarf temperature calibration for subgiants, and the giant temperature calibration for bright giants. The BLOeM sample includes dwarfs and subgiants in the mass range 10–70 $M_\odot$, plus a few giants and supergiants down to ≈7–8 $M_\odot$. The three sgB[e] objects (BLOeM 2-116, BLOeM 3-012, and BLOeM 4-055) are excluded from the HRD, as standard calibrations cannot be used on them.

The errors on $\log L$ and $T_{\rm eff}$ can only be roughly estimated. The spectral types can be roughly estimated to within one spectral bin, corresponding to $\Delta \log T_{\rm eff}[{\rm K}] \approx 0.02 - 0.04$; this is larger than typical calibration errors. However, the impact of binary contamination is not possible to quantify without further analysis; we set the error in Fig. 10 to 0.03 dex. Similarly, errors on bolometric correction can be estimated from neighbouring spectral-type bins. Depending on the spectral type, they typically range between $\Delta BC = 0.2 - 0.4$, corresponding roughly to $\Delta \log L/L_\odot = 0.1$ dex. Added to this are potential sources contaminating the K_s magnitudes (e.g. infrared excess), binary contamination, and reddening. To remain conservative, we adopt an uncertainty of $\Delta \log L = 0.2$ dex in Fig. 10.

The HRD reveals the span of parameters covered by our sample in terms of initial mass and age. Qualitatively, it is similar to that presented by Humphreys & McElroy (1984), though the BLOeM sample goes substantially deeper in magnitude ($\Delta V \approx 2.5$ mag). This HRD suggests that the sample probes the range $8 \lesssim M_{\rm ini} \lesssim 80\,M_\odot$, though only a minority of targets exceed initial masses of $\gtrsim 30\,M_\odot$. In terms of age, a visual comparison with isochrones implies that the BLOeM sample probes stars as young as ≈ 2 Myr, extending to ages of the order of 20 Myr or more. The lack of very massive stars in the SMC has been noted in the past (e.g. Ramachandran et al. 2019; Schootemeijer et al. 2021), and could be related to a peak of star formation ≈ 10 − 40 Myr ago (Antoniou et al. 2010; Rubele et al. 2015; Schootemeijer et al. 2021). The Humphreys–Davidson (H-D) limit (Humphreys & Davidson 1979; Humphreys & McElroy 1984), which marks the absence of bright stars in the upper-right part of the HRD, is clearly seen above $\log L/L_\odot \approx 5.5$, in agreement with recent evaluations of the H–D limit in the SMC (Ramachandran et al. 2019; Davies et al. 2018; Gilkis et al. 2021; Sabhahit et al. 2021). In Appendix D, we show similar HRDs

Table 1: Adopted spectral type–temperature calibration

Spect. Type	Dwarf $T_{\rm eff}$ kK	Dwarf BC_K mag	Giant $T_{\rm eff}$ kK	Giant BC_K mag	Supergiant $T_{\rm eff}$ kK	Supergiant BC_K mag
O4	46.0	–4.99	41.7	–4.87	40.2	–4.78
O5	41.3	–4.84	39.9	–4.63	38.5	–4.44
O6	39.5	–4.72	38.0	–4.50	36.5	–4.27
O7	38.7	–4.58	36.5	–4.37	34.5	–4.15
O8	36.4	–4.30	35.0	–4.15	32.5	–4.01
O9	33.2	–3.97	31.7	–3.94	30.0	–3.63
O9.5	32.1	–3.82	30.5	–3.75	29.0	–3.48
B0	31.0	–3.74	29.5	–3.61	27.2	–3.29
B0.5	29.6	–3.57	28.5	–3.47	24.3	–2.89
B1	27.3	–3.28	23.9	–2.93	22.3	–2.62
B1.5	26.1	–3.17	22.5	–2.70	20.6	–2.38
B2	24.9	–3.07	21.2	–2.53	18.9	–2.18
B2.5	23.9	–2.95	19.8	–2.34	17.2	–1.78
B3	21.5	–2.59	18.4	–2.05	15.5	–1.45
B5	···		16.7	–1.65	13.8	–1.04
B8	···		···		12.0	–0.62
B9	···		···		10.5	–0.27
A0	···		···		9.5	+0.02
A2	···		···		8.5	+0.30
A5	···		···		7.7	+0.35
A7	···		···		7.2	+0.49
F0	···		···		6.7	+0.62
F2	···		···		6.4	+0.72
F5	···		···		5.9	+0.85

Notes. Based on SMC results from Bouret et al. (2013) and Bouret et al. (2021) for O stars, Dufton et al. (2019) for B0–5 stars, and Evans & Howarth (2003) for cooler supergiants. K_s-band bolometric corrections combine V-band bolometric corrections from Bouret et al. (2013), Bouret et al. (2021), Lanz & Hubeny (2007), Kudritzki et al. (2008) and Cox (2000), and V-K colours from Martins & Plez (2006), Koornneef (1983) and Cox (2000).

for each of the eight SMC fields, which provide an overview of the stellar content in each field.

We note that these estimates are subject to uncertainty given the uncertainties on $\log L$, and could also change depending on the set of evolutionary tracks being used (e.g. Georgy et al. 2013; Choi et al. 2016; Marigo et al. 2017; Keszthelyi et al. 2022). Moreover, an unknown fraction of the sample stars will be affected either by past binary interactions or bright companions, while we only make use of single-star tracks in this first characterisation effort. A full analysis of the mass and age distribution will require treatment of multiplicity (e.g. binary identification, orbital analysis, spectral disentangling), which will be the subject of subsequent papers.

6. Conclusions

This work presents the rationale, target selection, and first characterisation of the sample spectroscopically monitored with FLAMES/VLT in the framework of the Binarity at LOw Metallicity (BLOeM) ESO Large Programme. BLOeM will collect 25 epochs of spectroscopy of 929 massive stars in the low-metallicity conditions of the SMC in the period from October 2023 to September 2025. The sample populates eight fields within the SMC, probing several of its environments, though limited to field stars.

The goals of the survey are to use the time-dependent RVs of all targets to derive the observed and intrinsic binary fraction as a function of stellar mass and age, derive the orbits of all identified binaries, and, through this, establish fundamental properties such as the initial mass function, star formation history, surface abundance pattern, and orbital-parameter distributions of massive stars at low metallicity. Moreover, the survey will enable the identification of unique evolved binaries, such as dormant OB+BH binaries, and provide testbeds for single-star evolution models via dynamical-mass measurements of eclipsing binaries.

The present study is based on 9/25 epochs acquired thus far in the framework of the BLOeM survey during the first semester, with our main goal being to describe the sample selection (Sect. 2), develop a data-reduction pipeline (Sect. 3), perform a spectral classification (Sect. 4), and investigate the mass and age domains probed by the sample (Sect. 5).

The sample spans a wide range of spectral types, extending from O4 for the earliest subtypes to F5 for the latest ones, though it is dominated by B0-2 stars. In total, there are 159 O-type stars, 324 early B-type (B0–B3) dwarfs, subgiants, and giants, 309 early B-type bright giants and supergiants, and 137 late-type supergiants. From spectral-type calibrations and usage of K_s magnitudes, we derived the effective temperatures and luminosities of the targets, assuming they are all single stars. The sample covers the regime $6.5 \lesssim T_{\rm eff} \lesssim 45$ kK and $3.7 \lesssim \log L/L_\odot \lesssim 6.1$. From comparison to evolution tracks and isochrones extended from Schootemeijer et al. (2019), this roughly corresponds to initial masses in the range $8 - 80\,M_\odot$ and ages mainly in the range $\approx 2 - 20$ Myr. The sample corroborates the blue region of the Humphreys-Davidson limit.

We highlight a few peculiar objects in our sample: eight sources are confirmed as X-ray bright, four of which have been classified as HMXBs in the past, and one of which is a promising CWB candidate. Three objects are classified as sgB[e]/LBV-like stars, and two as Be + bloated stripped-star binary candidates. Two candidate magnetic stars, classified as Of?p stars previously, are also included in the sample.

We identify 82stars as OBe stars. As we lack the diagnostic Hα line, this should be considered a lower limit, although usage of low-resolution *Gaia* spectra covering the Hα line only yields a few more candidates, amounting to an OBe fraction of $\approx 11\%$ relative to the non-supergiant OB sample. The Oe fraction among all O stars in the sample is 13%. However, the Be fraction is merely 11%, which is lower than reported in the literature. It is likely that we are biased against Be stars in this sample, because these tend to be redder compared to a 'standard' evolutionary track, which we used to select our sample (see Sect. 5.2). However, the Oe sample is likely unbiased, and so this fraction should represent the Oe fraction in the SMC. Finally, 74 eclipsing binaries are identified, as well as 8 ellipsoidal variables (Sect. 5.3 and Appendix C). We are currently carrying out a systematic analysis of the first batch of data for RV variability for the various subsamples of the study.

Acknowledgements. The research leading to these results has received funding from the European Research Council (ERC) under the European Union's Horizon 2020 research and innovation programme (grant agreement numbers 772225: MULTIPLES). PAC and JMB are supported by the Science and Technology Facilities Council research grant ST/V000853/1 (PI. V. Dhillon). DMB gratefully acknowledges support from UK Research and Innovation (UKRI) in the form of a Frontier Research grant under the UK government's ERC Horizon Europe funding guarantee (SYMPHONY; PI Bowman; grant number: EP/Y031059/1), and a Royal Society University Research Fellowship (PI Bowman; grant number: URF\R1\231631). ZK acknowledges support from JSPS Kakenhi Grant-in-Aid for Scientific Research (23K19071). IM acknowledges support from the Australian Research Council (ARC) Centre of Excellence for Gravitational Wave Discovery (OzGrav), through project number CE230100016. AACS, VR, RRL, and MBP are funded by the Deutsche Forschungsgemeinschaft (DFG, German Research Foundation) in the form of an Emmy Noether Research Group – Project-ID 445674056 (SA4064/1-1, PI Sander). GGT and JJ are supported by the German Deutsche Forschungsgemeinschaft (DFG) under Project-ID 496854903 (SA4064/2-1, PI Sander) VR, GGT, and AACS further acknowledge support from the Federal Ministry of Education and Research (BMBF) and the Baden-Württemberg Ministry of Science as part of the Excellence Strategy of the German Federal and State Governments. ECS acknowledges financial support by the Federal Ministry for Economic Affairs and Climate Action (BMWK) via the German Aerospace Center (Deutsches Zentrum für Luft- und Raumfahrt, DLR) grant 50 OR 2306 (PI: Ramachandran/Sander). This work has received funding from the European Research Council (ERC) under the European Union's Horizon 2020 research and innovation programme (Grant agreement No. 945806) and is supported by the Deutsche Forschungsgemeinschaft (DFG, German Research Foundation) under Germany's Excellence Strategy EXC 2181/1-390900948 (the Heidelberg STRUCTURES Excellence Cluster). LMO is thankful for the funding provided by the DFG grant 443790621. This paper benefited from discussions at the International Space Science Institute (ISSI) in Bern through ISSI International Team project 512 (Multiwavelength View on Massive Stars in the Era of Multimessenger Astronomy). DP acknowledges financial support by the Deutsches Zentrum für Luft und Raumfahrt (DLR) grant FKZ 50OR2005. JIV acknowledges the European Research Council for support from the ERC Advanced grant ERC-2021-ADG101054731. JSV is supported by STFC (Science and Technology Facilities Council) funding under grant number ST/V000233/1. GH, SS-D, SRB and AH acknowledge support from the State Research Agency (AEI) of the Spanish Ministry of Science and Innovation (MICIN) and the European Regional Development Fund, FEDER under grants PID2021-122397NB-C21 and CEX2019-000920-S. SRB also acknowledges financial support by NextGeneration EU/PRTR and MIU (UNI/551/2021) through grant Margarita Salas-ULL. DFR is thankful for the support of the CAPES-Br and FAPERJ/DSC-10 (SEI-260003/001630/2023). F.N., and L.R.P. acknowledge support by grants PID2019-105552RB-C41 and PID2022-137779OB-C41 funded by MCIN/AEI/10.13039/501100011033 by "ERDF A way of making Europe". MG acknowledges financial support from the grants PID2021-125485NB-C22, CEX2019-000918-M funded by MCIN/AEI/10.13039/501100011033 (State Agency for Research of the Spanish Ministry of Science and Innovation) and SGR-2021-01069 (AGAUR). GM acknowledges funding support from the European Research Council (ERC) under the European Union's Horizon 2020 research and innovation programme (Grant agreement No. 772086). JMA acknowledges support from the Spanish Government Ministerio de Ciencia e Innovación and Agencia Estatal de Investigación (10.13 039/501 100 011 033) through grant PID2022-136 640 NB-C22 and from the Consejo Superior de Investigaciones Científicas (CSIC) through grant 2022-AEP 005. MP is supported by the BEKKER fellowship BPN/BEK/2022/1/00106 from the Polish National Agency for Academic Exchange. KS is funded by the National Science Center (NCN), Poland, under grant number OPUS 2021/41/B/ST9/00757. JM acknowledges support from a Royal Society–Science Foundation Ireland University Research Fellowship. SJ acknowledges support from the FWO PhD fellowship under project 11E1721N. FB acknowledges the support of the European Research Council (ERC) Horizon Europe under grant agreement number 101044048.

References

Abbott, B. P., Abbott, R., Abbott, T. D., et al. 2016, Phys. Rev. Lett., 116, 061102
Abdul-Masih, M., Banyard, G., Bodensteiner, J., et al. 2020, Nature, 580, E11
Abt, H. A. 1983, ARA&A, 21, 343
Almeida, L. A., Sana, H., Taylor, W., et al. 2017, A&A, 598, A84
Antoniou, V., Zezas, A., Hatzidimitriou, D., & Kalogera, V. 2010, ApJ, 716, L140
Ardeberg, A. & Maurice, E. 1977, A&AS, 30, 261
Atri, P., Miller-Jones, J. C. A., Bahramian, A., et al. 2019, MNRAS, 489, 3116
Azzopardi, M. & Vigneau, J. 1979, A&AS, 35, 353
Azzopardi, M. & Vigneau, J. 1982, A&AS, 50, 291
Banagiri, S., Doctor, Z., Kalogera, V., Kimball, C., & Andrews, J. J. 2023, ApJ, 959, 106
Banyard, G., Sana, H., Mahy, L., et al. 2022, A&A, 658, A69
Barkat, Z., Rakavy, G., & Sack, N. 1967, Phys. Rev. Lett., 18, 379
Bodensteiner, J., Sana, H., Wang, C., et al. 2021, A&A, 652, A70
Bodensteiner, J., Shenar, T., & Sana, H. 2020, A&A, 641, A42
Bonanos, A. Z., Lennon, D. J., Köhlinger, F., et al. 2010, AJ, 140, 416
Bordier, E., de Wit, W. J., Frost, A. J., et al. 2024, A&A, 681, A85
Bouret, J. C., Lanz, T., Martins, F., et al. 2013, A&A, 555, A1
Bouret, J. C., Martins, F., Hillier, D. J., et al. 2021, A&A, 647, A134
Bowman, D. 2024, Astronomy and Geophysics, 65, 2.20
Bowman, D. M., Burssens, S., Pedersen, M. G., et al. 2019, Nature Astronomy, 3, 760
Breivik, K., Chatterjee, S., & Larson, S. L. 2017, ApJ, 850, L13
Britavskiy, N., Simón-Díaz, S., Holgado, G., et al. 2023, A&A, 672, A22
Broekgaarden, F. S., Berger, E., Neijssel, C. J., et al. 2021, MNRAS, 508, 5028
Brott, I., de Mink, S. E., Cantiello, M., et al. 2011, A&A, 530, A115
Chakrabarti, S., Simon, J. D., Craig, P. A., et al. 2023, AJ, 166, 6
Chen, T.-W., Smartt, S. J., Yates, R. M., et al. 2017, MNRAS, 470, 3566
Choi, J., Dotter, A., Conroy, C., et al. 2016, ApJ, 823, 102
Cioni, M. R., Clementini, G., Girardi, L., et al. 2011, The Messenger, 144, 25
Clark, J. S., Bartlett, E. S., Coe, M. J., et al. 2013, A&A, 560, A10
Coe, M. J. & Kirk, J. 2015, MNRAS, 452, 969
Corcoran, M. F., Stevens, I. R., Pollock, A. M. T., et al. 1996, ApJ, 464, 434
Corral-Santana, J. M., Casares, J., Muñoz-Darias, T., et al. 2016, A&A, 587, A61
Cox, A. N. 2000, Allen's astrophysical quantities
Davies, B., Crowther, P. A., & Beasor, E. R. 2018, MNRAS, 478, 3138
De Angeli, F., Weiler, M., Montegriffo, P., et al. 2023, A&A, 674, A2
de Mink, S. E., Langer, N., Izzard, R. G., Sana, H., & de Koter, A. 2013, ApJ, 764, 166
de Mink, S. E. & Mandel, I. 2016, MNRAS, 460, 3545
de Mink, S. E., Sana, H., Langer, N., Izzard, R. G., & Schneider, F. R. N. 2014, ApJ, 782, 7
Dotter, A. 2016, ApJS, 222, 8
Drout, M. R., Götberg, Y., Ludwig, B. A., et al. 2023, Science, 382, 1287
Dufton, P. L., Evans, C. J., Hunter, I., Lennon, D. J., & Schneider, F. R. N. 2019, A&A, 626, A50
Dunstall, P. R., Dufton, P. L., Sana, H., et al. 2015, A&A, 580, A93
El-Badry, K. 2024, The Open Journal of Astrophysics, 7, 38
El-Badry, K. & Quataert, E. 2021, MNRAS, 502, 3436
El-Badry, K., Rix, H.-W., Cendes, Y., et al. 2023a, MNRAS, 521, 4323
El-Badry, K., Rix, H.-W., Quataert, E., et al. 2023b, MNRAS, 518, 1057
Evans, C. J., Castro, N., Gonzalez, O. A., et al. 2019, A&A, 622, A129
Evans, C. J. & Howarth, I. D. 2003, MNRAS, 345, 1223
Evans, C. J., Howarth, I. D., Irwin, M. J., Burnley, A. W., & Harries, T. J. 2004, MNRAS, 353, 601
Evans, C. J., Lennon, D. J., Smartt, S. J., & Trundle, C. 2006, A&A, 456, 623
Evans, C. J., Taylor, W. D., Hénault-Brunet, V., et al. 2011, A&A, 530, A108
Evans, I. N., Primini, F. A., Glotfelty, K. J., et al. 2010, ApJS, 189, 37
Farmer, R., Renzo, M., de Mink, S. E., Marchant, P., & Justham, S. 2019, ApJ, 887, 53
Ferrario, L., Pringle, J. E., Tout, C. A., & Wickramasinghe, D. T. 2009, MNRAS, 400, L71
Foellmi, C., Moffat, A. F. J., & Guerrero, M. A. 2003, MNRAS, 338, 360
Frost, A. J., Bodensteiner, J., Rivinius, T., et al. 2022, A&A, 659, L3
Frost, A. J., Sana, H., Mahy, L., et al. 2024, Science, 384, 214
Fryer, C. L., Woosley, S. E., & Heger, A. 2001, ApJ, 550, 372
Gaia Collaboration, Panuzzo, P., Mazeh, T., et al. 2024, A&A, 686, L2
Gaia Collaboration, Vallenari, A., Brown, A. G. A., et al. 2023, A&A, 674, A1
Gal-Yam, A. 2012, Science, 337, 927
Garmany, C. D., Conti, P. S., & Massey, P. 1987, AJ, 93, 1070
Georgy, C., Ekström, S., Eggenberger, P., et al. 2013, A&A, 558, A103
Giacobbo, N., Mapelli, M., & Spera, M. 2018, MNRAS, 474, 2959
Giesers, B., Dreizler, S., Husser, T.-O., et al. 2018, MNRAS, 475, L15
Gilkis, A., Shenar, T., Ramachandran, V., et al. 2021, MNRAS, 503, 1884
Götberg, Y., de Mink, S. E., Groh, J. H., et al. 2018, A&A, 615, A78
Graczyk, D., Pietrzyński, G., Thompson, I. B., et al. 2020, ApJ, 904, 13
Graham, J. F. & Fruchter, A. S. 2017, ApJ, 834, 170
Graus, A. S., Lamb, J. B., & Oey, M. S. 2012, ApJ, 759, 10
Gray, R. O. & Corbally, Christopher, J. 2009, Stellar Spectral Classification (Princeton University Press)
Grunhut, J. H., Wade, G. A., Neiner, C., et al. 2017, MNRAS, 465, 2432
Guo, Y., Li, J., Xiong, J., et al. 2022, Research in Astronomy and Astrophysics, 22, 025009
Haberl, F. & Sturm, R. 2016, A&A, 586, A81
Hainich, R., Pasemann, D., Todt, H., et al. 2015, A&A, 581, A21
Harmanec, P. 1988, Bulletin of the Astronomical Institutes of Czechoslovakia, 39, 329
Hastings, B., Langer, N., Wang, C., Schootemeijer, A., & Milone, A. P. 2021, A&A, 653, A144
Hilditch, R. W., Howarth, I. D., & Harries, T. J. 2005, MNRAS, 357, 304
Hubeny, I. & Lanz, T. 1995, ApJ, 439, 875
Humphreys, R. M. 1983, ApJ, 265, 176
Humphreys, R. M. & Davidson, K. 1979, ApJ, 232, 409
Humphreys, R. M., Kudritzki, R. P., & Groth, H. G. 1991, A&A, 245, 593
Humphreys, R. M. & McElroy, D. B. 1984, ApJ, 284, 565
Hunter, I., Dufton, P. L., Smartt, S. J., et al. 2007, A&A, 466, 277
Irrgang, A., Geier, S., Kreuzer, S., Pelisoli, I., & Heber, U. 2020, A&A, 633, L5
Janssens, S., Shenar, T., Sana, H., et al. 2022, A&A, 658, A129
Janssens, S., Shenar, T., Sana, H., & Marchant, P. 2023, A&A, 670, A79
Jermyn, A. S., Bauer, E. B., Schwab, J., et al. 2023, ApJS, 265, 15

Keszthelyi, Z., de Koter, A., Götberg, Y., et al. 2022, MNRAS, 517, 2028
Kiminki, D. C. & Kobulnicky, H. A. 2012, ApJ, 751, 4
Klencki, J., Moe, M., Gladysz, W., et al. 2018, A&A, 619, A77
Kobulnicky, H. A. & Fryer, C. L. 2007, ApJ, 670, 747
Koornneef, J. 1983, A&A, 128, 84
Kraus, M. 2019, Galaxies, 7, 83
Kroupa, P. 2001, MNRAS, 322, 231
Kudritzki, R.-P., Urbaneja, M. A., Bresolin, F., et al. 2008, ApJ, 681, 269
Kummer, F., Toonen, S., & de Koter, A. 2023, A&A, 678, A60
Lamb, J. B., Oey, M. S., Graus, A. S., Adams, F. C., & Segura-Cox, D. M. 2013, ApJ, 763, 101
Lamb, J. B., Oey, M. S., Segura-Cox, D. M., et al. 2016, ApJ, 817, 113
Lamers, H. J. G. L. M., Zickgraf, F.-J., de Winter, D., Houziaux, L., & Zorec, J. 1998, A&A, 340, 117
Langer, N. 2012, ARA&A, 50, 107
Langer, N., Baade, D., Bodensteiner, J., et al. 2020, A&A, 633, A40
Langer, N., Norman, C. A., de Koter, A., et al. 2007, A&A, 475, L19
Lanz, T. & Hubeny, I. 2003, ApJS, 146, 417
Lanz, T. & Hubeny, I. 2007, ApJS, 169, 83
Laycock, S., Zezas, A., Hong, J., Drake, J. J., & Antoniou, V. 2010, ApJ, 716, 1217
Lennon, D. J. 1997, A&A, 317, 871
Lorenzo, M., Garcia, M., Najarro, F., et al. 2022, MNRAS, 516, 4164
Machida, M. N. 2008, ApJ, 682, L1
Mahy, L., Almeida, L. A., Sana, H., et al. 2020a, A&A, 634, A119
Mahy, L., Sana, H., Abdul-Masih, M., et al. 2020b, A&A, 634, A118
Mahy, L., Sana, H., Shenar, T., et al. 2022, A&A, 664, A159
Maíz Apellániz, J., Sota, A., Arias, J. I., et al. 2016, ApJS, 224, 4
Mandel, I. & Broekgaarden, F. S. 2022, Living Reviews in Relativity, 25, 1
Mandel, I. & Farmer, A. 2022, Phys. Rep., 955, 1
Maravelias, G., Zezas, A., Antoniou, V., & Hatzidimitriou, D. 2014, MNRAS, 438, 2005
Marchant, P. & Bodensteiner, J. 2023, arXiv e-prints, arXiv:2311.01865
Marchant, P., Langer, N., Podsiadlowski, P., Tauris, T. M., & Moriya, T. J. 2016, A&A, 588, A50
Marigo, P., Girardi, L., Bressan, A., et al. 2017, ApJ, 835, 77
Marín Pina, D., Rastello, S., Gieles, M., et al. 2024, A&A, 688, L2
Marks, M., Kroupa, P., Dabringhausen, J., & Pawlowski, M. S. 2012, MNRAS, 422, 2246
Martayan, C., Frémat, Y., Hubert, A. M., et al. 2007, A&A, 462, 683
Martins, F. & Plez, B. 2006, A&A, 457, 637
Martins, F., Schaerer, D., & Hillier, D. J. 2005, A&A, 436, 1049
Mashian, N. & Loeb, A. 2017, MNRAS, 470, 2611
Mason, B. D., Hartkopf, W. I., Gies, D. R., Henry, T. J., & Helsel, J. W. 2009, AJ, 137, 3358
Massey, P. 2002, ApJS, 141, 81
Massey, P., Bresolin, F., Kudritzki, R. P., Puls, J., & Pauldrach, A. W. A. 2004, ApJ, 608, 1001
Massey, P., Lang, C. C., Degioia-Eastwood, K., & Garmany, C. D. 1995, ApJ, 438, 188
Massey, P., Waterhouse, E., & DeGioia-Eastwood, K. 2000, AJ, 119, 2214
Massey, P., Zangari, A. M., Morrell, N. I., et al. 2009, ApJ, 692, 618
McQuinn, K. B. W., Skillman, E. D., Dolphin, A., et al. 2015, ApJ, 812, 158
Mennickent, R. E., Cidale, L., Pietrzyński, G., Gieren, W., & Sabogal, B. 2006, A&A, 457, 949
Millward, C. G. & Walker, G. A. H. 1985, ApJS, 57, 63
Mirabel, I. F. & Rodrigues, I. 2003, Science, 300, 1119
Modjaz, M., Kewley, L., Kirshner, R. P., et al. 2008, AJ, 135, 1136
Moe, M. & Di Stefano, R. 2013, ApJ, 778, 95
Moe, M., Kratter, K. M., & Badenes, C. 2019, ApJ, 875, 61
Mokiem, M. R., de Koter, A., Evans, C. J., et al. 2006, A&A, 456, 1131
Morrell, N., Ostrov, P., Massey, P., & Gamen, R. 2003, MNRAS, 341, 583
Nazé, Y., Corcoran, M. F., Koenigsberger, G., & Moffat, A. F. J. 2007, ApJ, 658, L25
Nazé, Y., Manfroid, J., Stevens, I. R., Corcoran, M. F., & Flores, A. 2004, ApJ, 608, 208
Negueruela, I., Simón-Díaz, S., de Burgos, A., Casasbuenas, A., & Beck, P. G. 2024, arXiv e-prints, arXiv:2407.04163
Neugent, K. F., Levesque, E. M., Massey, P., Morrell, N. I., & Drout, M. R. 2020, ApJ, 900, 118
Neugent, K. F., Massey, P., & Morrell, N. 2018, ApJ, 863, 181
Neugent, K. F., Massey, P., Skiff, B., et al. 2010, ApJ, 719, 1784
Offner, S. S. R., Moe, M., Kratter, K. M., et al. 2023, in Astronomical Society of the Pacific Conference Series, Vol. 534, Protostars and Planets VII, ed. S. Inutsuka, Y. Aikawa, T. Muto, K. Tomida, & M. Tamura, 275
Oskinova, L. M. 2005, MNRAS, 361, 679
Oskinova, L. M., Sun, W., Evans, C. J., et al. 2013, ApJ, 765, 73
Paczyński, B. 1967, Acta Astron., 17, 355
Pasquali, A., Nota, A., Langer, N., Schulte-Ladbeck, R. E., & Clampin, M. 2000, AJ, 119, 1352
Pasquini, L., Avila, G., Blecha, A., et al. 2002, The Messenger, 110, 1
Patrick, L. R., Lennon, D. J., Britavskiy, N., et al. 2019, A&A, 624, A129
Paul, K. T., Subramaniam, A., Mathew, B., Mennickent, R. E., & Sabogal, B. 2012, MNRAS, 421, 3622
Pauli, D., Langer, N., Aguilera-Dena, D. R., Wang, C., & Marchant, P. 2022a, A&A, 667, A58
Pauli, D., Oskinova, L. M., Hamann, W. R., et al. 2022b, A&A, 659, A9
Pawlak, M., Soszyński, I., Udalski, A., et al. 2016, Acta Astron., 66, 421
Paxton, B., Bildsten, L., Dotter, A., et al. 2011, ApJS, 192, 3
Paxton, B., Cantiello, M., Arras, P., et al. 2013, ApJS, 208, 4
Paxton, B., Marchant, P., Schwab, J., et al. 2015, ApJS, 220, 15
Paxton, B., Schwab, J., Bauer, E. B., et al. 2018, ApJS, 234, 34
Paxton, B., Smolec, R., Schwab, J., et al. 2019, ApJS, 243, 10
Podsiadlowski, P., Morris, T. S., & Ivanova, N. 2006, in Astronomical Society of the Pacific Conference Series, Vol. 355, Stars with the B[e] Phenomenon, ed. M. Kraus & A. S. Miroshnichenko, 259
Pols, O., Cote, J., Waters, L. B. F. M., & Heise, J. 1991, A&A, 241, 419
Portegies Zwart, S. F. & Verbunt, F. 1996, A&A, 309, 179
Price-Whelan, A. M., Hogg, D. W., Rix, H.-W., et al. 2020, ApJ, 895, 2
Prinja, R. K. 1987, MNRAS, 228, 173
Quimby, R. M., Kulkarni, S. R., Kasliwal, M. M., et al. 2011, Nature, 474, 487
Ramachandran, V., Hamann, W. R., Oskinova, L. M., et al. 2019, A&A, 625, A104
Rastello, S., Iorio, G., Mapelli, M., et al. 2023, MNRAS, 526, 740
Renzo, M. & Götberg, Y. 2021, ApJ, 923, 277
Renzo, M., Zapartas, E., de Mink, S. E., et al. 2019, A&A, 624, A66
Ricker, G. R., Winn, J. N., Vanderspek, R., et al. 2015, Journal of Astronomical Telescopes, Instruments, and Systems, 1, 014003
Rivinius, T., Carciofi, A. C., & Martayan, C. 2013, A&A Rev., 21, 69
Rubele, S., Girardi, L., Kerber, L., et al. 2015, MNRAS, 449, 639
Sabhahit, G. N., Vink, J. S., Higgins, E. R., & Sander, A. A. C. 2021, MNRAS, 506, 4473
Saigo, K., Matsumoto, T., & Umemura, M. 2004, ApJ, 615, L65
Sana, H., de Koter, A., de Mink, S. E., et al. 2013, A&A, 550, A107
Sana, H., de Mink, S. E., de Koter, A., et al. 2012, Science, 337, 444
Sana, H., Le Bouquin, J. B., Lacour, S., et al. 2014, ApJS, 215, 15
Sana, H., Rauw, G., Nazé, Y., Gosset, E., & Vreux, J. M. 2006, MNRAS, 372, 661
Sanduleak, N. 1968, AJ, 73, 246
Schneider, F. R. N., Ohlmann, S. T., Podsiadlowski, P., et al. 2019, Nature, 574, 211
Schootemeijer, A., Langer, N., Grin, N. J., & Wang, C. 2019, A&A, 625, A132
Schootemeijer, A., Langer, N., Lennon, D., et al. 2021, A&A, 646, A106
Schootemeijer, A., Lennon, D. J., Garcia, M., et al. 2022, A&A, 667, A100
Schootemeijer, A., Shenar, T., Langer, N., et al. 2024, arXiv e-prints, arXiv:2406.01420
Shahaf, S., Bashi, D., Mazeh, T., et al. 2023, MNRAS, 518, 2991
Sheets, H. A., Bolatto, A. D., van Loon, J. T., et al. 2013, ApJ, 771, 111
Shenar, T., Bodensteiner, J., Abdul-Masih, M., et al. 2020, A&A, 639, L6
Shenar, T., Hainich, R., Todt, H., et al. 2016, A&A, 591, A22
Shenar, T., Sana, H., Mahy, L., et al. 2022a, Nature Astronomy, 6, 1085
Shenar, T., Sana, H., Mahy, L., et al. 2022b, A&A, 665, A148
Shenar, T., Wade, G. A., Marchant, P., et al. 2023, Science, 381, 761
Shore, S. N., Sanduleak, N., & Allen, D. A. 1987, A&A, 176, 59
Skillman, E. D., Kennicutt, R. C., & Hodge, P. W. 1989, ApJ, 347, 875
Smith Neubig, M. M. & Bruhweiler, F. C. 1999, AJ, 117, 2856
Sota, A., Maíz Apellániz, J., Walborn, N. R., et al. 2011, ApJS, 193, 24
Stegmann, J., Antonini, F., & Moe, M. 2022, MNRAS, 516, 1406
Sturm, R., Haberl, F., Pietsch, W., et al. 2013, A&A, 558, A3
Tauris, T. M., Kramer, M., Freire, P. C. C., et al. 2017, ApJ, 846, 170
Telford, O. G., McQuinn, K. B. W., Chisholm, J., & Berg, D. A. 2023, ApJ, 943, 65
Testor, G. 2001, A&A, 372, 667
Testor, G. & Lortet, M. C. 1987, A&A, 178, 25
Torres, G., Andersen, J., & Giménez, A. 2010, A&A Rev., 18, 67
Traulsen, I., Schwope, A. D., Lamer, G., et al. 2020, A&A, 641, A137
Udalski, A. 2003, Acta Astron., 53, 291
Udalski, A., Szymański, M. K., & Szymański, G. 2015, Acta Astron., 65, 1
van Son, L. A. C., de Mink, S. E., Renzo, M., et al. 2022, ApJ, 940, 184
Vigna-Gómez, A., Willcox, R., Tamborra, I., et al. 2024, Phys. Rev. Lett., 132, 191403
Villaseñor, J. I., Taylor, W. D., Evans, C. J., et al. 2021, MNRAS, 507, 5348
Vink, J. S., Mehner, A., Crowther, P. A., et al. 2023, A&A, 675, A154
Walborn, N. R. 1972, AJ, 77, 312
Walborn, N. R. 1983, ApJ, 265, 716
Walborn, N. R. & Fitzpatrick, E. L. 1990, PASP, 102, 379
Walborn, N. R., Fullerton, A. W., Crowther, P. A., et al. 2002, ApJS, 141, 443
Walborn, N. R., Lennon, D. J., Heap, S. R., et al. 2000, PASP, 112, 1243
Walborn, N. R., Sana, H., Simón-Díaz, S., et al. 2014, A&A, 564, A40
Wang, C., Langer, N., Schootemeijer, A., et al. 2020, ApJ, 888, L12

Wang, L., Gies, D. R., & Peters, G. J. 2017, ApJ, 843, 60
Wang, S., Liu, J., Qiu, Y., et al. 2016, ApJS, 224, 40
Webb, N. A., Coriat, M., Traulsen, I., et al. 2020, A&A, 641, A136
Weiler, M., Carrasco, J. M., Fabricius, C., & Jordi, C. 2023, A&A, 671, A52
Woosley, S. E. 2017, ApJ, 836, 244
Woosley, S. E. & Heger, A. 2006, ApJ, 637, 914
Wu, S., Everson, R. W., Schneider, F. R. N., Podsiadlowski, P., & Ramirez-Ruiz, E. 2020, ApJ, 901, 44
Yang, M., Bonanos, A. Z., Jiang, B.-W., et al. 2019, A&A, 629, A91
Yoon, S. C. & Langer, N. 2005, A&A, 443, 643
Zasche, P., Wolf, M., Vraštil, J., et al. 2014, A&A, 572, A71
Zickgraf, F. J., Kovacs, J., Wolf, B., et al. 1996, A&A, 309, 505
Zivick, P., Kallivayalil, N., van der Marel, R. P., et al. 2018, ApJ, 864, 55

[1] The School of Physics and Astronomy, Tel Aviv University, Tel Aviv 6997801, Israel;
e-mail: tshenar@tau.ac.il
[2] ESO - European Southern Observatory, Karl-Schwarzschild-Strasse 2, 85748 Garching bei München, Germany
[3] Institute of Astronomy, KU Leuven, Celestijnenlaan 200D, 3001 Leuven, Belgium
[4] Department of Physics & Astronomy, Hounsfield Road, University of Sheffield, Sheffield, S3 7RH, United Kingdom
[5] Instituto de Astrofísica de Canarias, C. Vía Láctea, s/n, 38205 La Laguna, Santa Cruz de Tenerife, Spain
[6] Universidad de La Laguna, Dpto. Astrofísica, Av. Astrofśico Francisco Sánchez, 38206 La Laguna, Santa Cruz de Tenerife, Spain
[7] Escola de CiÃłncias e Tecnologia, Universidade Federal do Rio Grande do Norte, Natal, RN 59072-970, Brazil
[8] Zentrum für Astronomie der Universität Heidelberg, Astronomisches Rechen-Institut, Mönchhofstr. 12-14, 69120 Heidelberg, Germany
[9] School of Mathematics, Statistics and Physics, Newcastle University, Newcastle upon Tyne, NE1 7RU, UK
[10] Heidelberger Institut für Theoretische Studien, Schloss-Wolfsbrunnenweg 35, 69118 Heidelberg, Germany
[11] Universität Heidelberg, Department of Physics and Astronomy, Im Neuenheimer Feld 226, 69120 Heidelberg, Germany
[12] Royal Observatory of Belgium, Avenue Circulaire/Ringlaan 3, B-1180 Brussels, Belgium
[13] Anton Pannekoek Institute for Astronomy, University of Amsterdam, Science Park 904, 1098 XH Amsterdam, the Netherlands
[14] Max-Planck-Institute for Astrophysics, Karl-Schwarzschild-Strasse 1, 85748 Garching, Germany
[15] European Space Agency (ESA), ESA Office, Space Telescope Science Institute, 3700 San Martin Drive, Baltimore, MD 21218, USA
[16] ICREA, Pg. Lluís Companys 23, E08010 Barcelona, Spain
[17] Institut de Ciències del Cosmos (ICCUB), Universitat de Barcelona (IEEC-UB), Martí Franquès 1, E08028 Barcelona, Spain
[18] Institute of Astronomy, University of Cambridge, Madingley Road, Cambridge CB3 0HA, United Kingdom
[19] Argelander-Institut für Astronomie, Universität Bonn, Auf dem Hügel 71, 53121 Bonn, Germany
[20] Institute of Science and Technology Austria (ISTA), Am Campus 1, 3400 Klosterneuburg, Austria
[21] Space Telescope Science Institute, 3700 San Martin Drive, Baltimore, MD 21218, USA
[22] Department of Astronomy and Physics, Saint Mary's University, 923 Robie Street, Halifax, B3H 3C3, Canada
[23] Gemini Observatory/NSF's NOIRLab, Casilla 603, La Serena, Chile
[24] Center for Computational Astrophysics, Division of Science, National Astronomical Observatory of Japan, 2-21-1, Osawa, Mitaka, Tokyo 181-8588, Japan
[25] Astronomical Institute, Academy of Sciences of the Czech Republic, Fričova 298, CZ-251 65 Ondřejov, Czech Republic
[26] Department of Astronomy and Astrophysics, University of Toronto, 50 St. George Street, Toronto, Ontario, M5S 3H4, Canada
[27] Dublin Institute for Advanced Studies, DIAS Dunsink Observatory, Dunsink Lane, Dublin 15, Ireland
[28] Centro de Astrobiología (CSIC-INTA), campus ESAC, camino bajo del castillo s/n, 28 692 Villanueva de la Cañada, Spain
[29] School of Physics and Astronomy, Monash University, Clayton VIC 3800, Australia
[30] ARC Centre of Excellence for Gravitational-wave Discovery (OzGrav), Melbourne, Australia
[31] IAASARS, National Observatory of Athens, GR-15236, Penteli, Greece
[32] Institute of Astrophysics, FORTH, GR-71110, Heraklion, Greece
[33] Centro de Astrobiología (CSIC-INTA), Ctra. Torrejón a Ajalvir km 4, 28850 Torrejón de Ardoz, Spain
[34] Institut für Physik und Astronomie, Universität Potsdam, Karl-Liebknecht-Str. 24/25, 14476 Potsdam, Germany
[35] McWilliams Center for Cosmology & Astrophysics, Department of Physics, Carnegie Mellon University, Pittsburgh, PA 15213, USA
[36] Lund Observatory, Division of Astrophysics, Department of Physics, Lund University, Box 43, SE-221 00, Lund, Sweden
[37] Department of Astronomy & Steward Observatory, 933 N. Cherry Ave., Tucson, AZ 85721, USA
[38] Observatório Nacional, R. Gen. José Cristino, 77 - Vasco da Gama, Rio de Janeiro - RJ, 20921-400, Brazil
[39] Institute of Astronomy, Faculty of Physics, Astronomy and Informatics, Nicolaus Copernicus University, Grudziadzka 5, 87-100 Torun, Poland
[40] Department of Particle Physics and Astrophysics, Weizmann Institute of Science, Rehovot 7610001, Israel
[41] Lennard-Jones Laboratories, Keele University, ST5 5BG, UK
[42] Center for Computational Astrophysics, Flatiron Institute, New York, NY 10010, USA
[43] Max-Planck-Institut für Astronomie, Königstuhl 17, D-69117 Heidelberg, Germany
[44] Armagh Observatory, College Hill, Armagh, BT61 9DG, Northern Ireland, UK

Appendix A: Epoch dates and spectral types

Table A.1 provides the field centres and MJD values of the mid-exposures of the combined two sub-exposures per field and epoch. Table A.2 provides *Gaia* DR3 IDs, common aliases, K_s magnitudes from the VISTA/VMC catalogue (Cioni et al. 2011), previous spectral-type classifications, newly derived spectral types, flags for Hα-emitters in low-resolution *Gaia* spectra (Sect. 5.2), and additional comments. Newly derived spectral types are based on the BLOeM dataset unless otherwise stated in the comments.

Table A.1: Field centres and epoch dates for the eight fields.

	Field 1	Field 2	Field 3	Field 4	Field 5	Field 6	Field 7	Field 8
RA centre [h:m:s]	01:02:53.8	00:52:01.0	00:48:20.2	00:59:41.8	01:05:56.2	01:15:08.2	00:59:51.4	00:52:44.2
DEC centre [d:':"]	-72:05:26.1	-72:41:26.1	-73:16:14.1	-72:11:26.1	-72:19:50.1	-73:15:02.1	-72:37:50.1	-72:15:02.1
Epoch 1 [MJD]	60219.10	60242.07	60242.10	60242.12	60242.15	60261.16	60246.12	60246.14
Epoch 2 [MJD]	60220.26	60247.19	60247.21	60247.24	60247.26	60267.20	60248.17	60261.18
Epoch 3 [MJD]	60242.05	60256.20	60256.24	60254.35	60256.22	60280.02	60256.18	60267.06
Epoch 4 [MJD]	60245.02	60261.09	60261.11	60256.27	60261.03	60282.12	60261.07	60268.11
Epoch 5 [MJD]	60248.15	60267.15	60262.13	60261.14	60262.11	60285.09	60267.04	60280.12
Epoch 6 [MJD]	60252.21	60281.10	60267.09	60267.12	60267.17	60286.22	60268.13	60280.14
Epoch 7 [MJD]	60256.29	60285.16	60270.03	60281.05	60270.05	60288.14	60280.16	60282.10
Epoch 8 [MJD]	60261.05	60289.05	60281.08	60285.18	60280.04	60290.05	60286.19	60285.11
Epoch 9 [MJD]	60285.20	60290.09	60285.13	60289.07	60281.12	60291.09	60288.16	60288.19

Table A.2: Provided from left to right are BLOeM IDs, Gaia DR IDs, common aliases, K_s magnitudes from the VISTA catalogue (Cioni et al. 2011), spectral types from the literature (references are provided at the end of the table), newly derived spectral types, Hα emitters based on low-resolution *Gaia* spectroscopy (see Sect. 5.2), and additional comments.

ID	Gaia DR3 ID	Alias	K_s [mag]	SpT (old)	SpT (new)	Hα emit.	Comment
1-001	4690503998385774848	AzV 76F	13.69	B8 [Azz79]	B9 Iab	no	-
1-002	4690519082313236608	[M2002] SMC 49825	15.85	B0.2 III [Lam16]	B0 IV:	no	-
1-003	4690519151032663296	-	15.52	-	B2.5 II:	no	-
1-004	4690501146531455744	Sk 92, AzV 260	13.57	B1.5 Iab [Len97]	B1 Ib	no	-
1-005	4690505510214025472	[M2002] SMC 50031	15.45	B0 [She13]	B1 II	no	-
1-006	4690520010026062336	OGLE SMC725.15.018759	15.12	-	O9.5 V + early B	no	SB2, EB [Paw13]
1-007	4690506781524350336	-	16.31	-	B1.5: II:	no	-
1-008	4690501180887206656	Sk 93, AzV 263	12.79	B9 Ia [Len97]	B9 Iab	no	-
1-009	4690520387983090432	Sk 94, AzV 264	12.78	B1 Ia [Len97]	B1 Ia	no	-
1-010	4690505883854563840	-	15.27	-	B1.5 III:	no	-
1-011	4690506712804881792	OGLE SMC108.3 21525	14.50	-	B1.5 II	no	EB [Paw13]
1-012	4690507022042458624	AzV 267	15.65	O8 Vn [Mas02]	O7.5 Vn	no	LC from [Mas02]
1-013	4690506747164575872	-	16.66	-	B1.5 III:	no	-
1-014	4690520074427341184	-	15.20	-	B1 II	no	-
1-015	4690505986961967872	-	15.74	-	B0.2 III	no	-
1-016	4690506914646214912	Sk 99, AzV 273	11.78	A0 I [Neu10]	A2 Ib	no	-
1-017	4690507193841111296	-	15.71	-	B1 II:	no	-
1-018	4690506025610129152	LHA 115-S 34, AzV 276	14.32	B0e [Azz75]	B2 II: e	yes	-
1-019	4690501558844407936	AzV 277	14.47	B1-2 (II) [Eva04]	B2.5 Ib	no	-
1-020	4690519047953407232	AzV 279	14.77	B0 III [Gar87]	B0 III	no	-
1-021	4690519425910500352	AzV 280	14.16	B pec [Gar87]	B1 Ib	no	-
1-022	4690519700788344064	-	17.07	-	B1 III	no	-
1-023	4690502452197510272	AzV 282	15.42	O7 V [Eva04]	O7.5V(n)	no	LC from [Eva04]
1-024	4690506437926915840	2dFS 1609	15.76	O7 II(f) [Eva04]	O8 II(f)	no	LC from [Eva04]
1-025	4690502452197478528	Sk 101, AzV 287	13.61	O9.5 I [Wal83]	O9.2 Ib(n)	no	-
1-026	4690519455996745216	-	15.09	-	B1 Ib	no	-
1-027	4690501661923520768	AzV 296	15.04	O8.5 V((f)) [Mas04]	O7.5 V((f))n	no	LC from [Mas04]
1-028	4690519769509887488	RMC 23, AzV 297	12.21	B8 Ia [Len97]	B8 Iab/Ia	no	-
1-029	4690519803867505024	-	15.35	-	B2 II	no	-
1-030	4690506266128220160	-	17.06	-	B1 II	no	-
1-031	4690507670561677696	RMC 24, AzV 298	12.33	A0 I [Neu18]	A0 Iab	no	-
1-032	4690506541006084224	2dFS 5105	15.96	B0 (V) [Eva04]	B1.5 III:	no	-
1-033	4690502860220750208	AzV 300	15.18	B0 IIw [Gar87]	O9.5 V:n	no	-
1-034	4690519803867499648	AzV 301	14.98	B1 V [Mas95]	B1 II	no	-
1-035	4690507709237145856	[M2002] SMC 53417	15.39	-	B1.5 III-II	no	-
1-036	4690519593389669632	RMC 25, AzV 303	13.26	B1.5 Iab [Len97]	B1.5 Ib	no	-
1-037	4690506300487960576	OGLE SMC113.6 5437	16.20	-	B1.5 III	no	EB [Paw13]
1-038	4690513653473762176	-	14.15	-	B2.5 Ib	no	-
1-039	4690503306873686912	Dachs SMC 2-2	12.40	A3 I [Neu10]	A2 II/Ib	no	-
1-040	4690525438865707904	LIN 393	13.23	-	O9.7 III:n e	yes	-
1-041	4690512485242560000	[M2002] SMC 54325	15.03	-	O9.7: V:n + O9.7:	no	SB2
1-042	4690512485242543104	-	13.83	-	B2 Ib	no	-
1-043	4690526641456527360	AzV 311	15.24	O7-9 [She13]	O9.7 III: + O9.7	no	SB2, EB [Paw13]
1-044	4690512485242552960	[M2002] SMC 54432	15.75	-	B1 II	no	-
1-045	4690501971160817792	AzV 312	14.47	B0 (III) [Eva04]	B0.5 II	no	-
1-046	4687499475466452864	-	15.95	-	B1 III	no	-
1-047	4690512279084139392	-	15.10	-	B1 III-II	no	-
1-048	4690513687833493760	AzV 313	15.10	B1 [Azz75]	B2 III-II	no	-
1-049	4690503375593898624	-	14.67	-	B1.5 II: + early B	no	SB2
1-050	4690503036312684544	2dFS 1707	12.64	F0 [Eva04]	A7 Ib	no	-
1-051	4690502280398446720	RMC 27, Sk 106, AzV 315	10.56	A0 Ia [Len97]	A0 Ia	no	-
1-052	4690512588321738496	-	15.31	-	B1 II neb	no	-
1-053	4690502280398443776	AzV 318	14.09	B2 I [Gar87]	B1 Ib	no	-
1-054	4690512584031941504	[M2002] SMC 54931	14.92	-	B0 II	no	-
1-055	4690513516034604032	-	15.57	-	B1.5 III-II	no	-
1-056	4690508980549304704	AzV 321, 2dFS 1720	14.30	O9.5 Ib [Eva04]	O9.5 Ibn	no	LC from [Eva04]
1-057	4690513344235943040	-	15.08	-	B1.5 II:	no	-
1-058	4690512313443855360	LIN 404	13.31	-	O9.5 II: pe	yes	-
1-059	4690508151597375616	[M2002] SMC 55168	15.86	-	B0 IV	no	-
1-060	4690508907539818112	OGLE J010302.31-720836.1	14.12	-	B1.5 Ib	no	-
1-061	4690512244724379264	OGLE SMC-SC9 175326	14.30	B1-2 (II) [Eva04]	B1.5 Ib:	no	-
1-062	4690507881037706112	Dachs SMC 2-8, AzV 324	13.09	B4 Iab: [Smi97]	B8 Iab	no	-
1-063	4690509289786901504	Cl* NGC 371 KAG V12	16.94	-	B1.5 II: e?	no	-
1-064	4690508087196130304	2dFS 1734	14.66	B9 (II) [Eva04]	B9 Ib	no	-
1-065	4687505389671548672	AzV 90F	12.45	F0 Ib [Neu10]	A7 Ib	no	-
1-066	4690512691400904448	RMC 28, AzV 327	13.81	O9.5 II-Ibw [Wal00]	O9.7 II-Ib	no	-
1-067	4690508946189561728	[M2002] SMC 55556	15.48	-	B0.7 III	no	-
1-068	4690527088132999552	[M2002] SMC 55948	14.72	OBe? [She13]	O9.7 III:	no	-
1-069	4690514134509862528	[M2002] SMC 55952	15.15	B0.2 V [Lam16]	B0.7 III	no	-
1-070	4690512347803574400	[MWD2000] h53-40	14.83	B2 I [Mas00]	B1.5 II neb	no	-
1-071	4687505320952170880	-	16.17	-	B0.5 III	no	-
1-072	4690509324146632704	MOA J010321.3-720538	14.27	O6 V +O4-5 III(f) [Mor03]	O5 V(n) + O6.5(n)	no	SB2, EB [Paw13]
1-073	4690526057340871040	[MA93] 1373	14.68	-	B1 II: e	yes	-
1-074	4690509117967865088	-	16.54	-	B1 II	no	-
1-075	4690526057340870272	AzV 330	13.02	Be [Mas95]	O9.2 II:n pe	yes	-
1-076	4690509049268759808	[MWD2000] h53-60	14.54	O8 III [Mas00]	O9 III:	no	-
1-077	4690512450882740480	RMC 30, AzV 331	12.57	A2 I [Mas00]	A2 II/Ib	no	-
1-078	4690513859631967616	-	15.05	-	O9.7 III:	no	-

1-079	4690512828839860096	[MA93] 1380	13.31	-	O9.2 III:(n) pe neb	yes	-
1-080	4690509358506360320	[MWD2000] h53-91	14.78	O8.5 V [Mas00]	O8: V: + (early B + early B) neb	no	SB2, EB [Paw13]
1-081	4690509427225802624	-	16.95	-	B1.5: III: neb	no	-
1-082	4690525988621394816	[M2002] SMC 56680	15.57	-	B1.5 III-II	no	-
1-083	4690512760120397312	[MWD2000] h53-101	14.84	-	B0.5: V: neb + early B	no	SB2
1-084	4687505527110195072	[M2002] SMC 56785	15.44	-	B1 II	no	-
1-085	4687503946562429184	Dachs SMC 2-14, AzV 84F	12.46	A7 II [Eva04]	A7 Ib/ab	no	-
1-086	4687505454063447936	[M2002] SMC 56834	15.44	O7-9 [She13]	B0 IV:	no	-
1-087	4690509732152391680	[M2002] SMC 56942	15.07	-	B1 II:	no	-
1-088	4690508258994548352	[M2002] SMC 57134	15.53	-	B1.5 III + early B	no	SB2
1-089	4690514340668263552	[M2002] SMC 57144	14.47	-	B1 II	no	-
1-090	4687505252232336512	OGLE SMC-SC10 28913	14.40	B9 (II) [Eva04]	A1 Ib	no	-
1-091	4690512794480131072	[MWD2000] h53-137	14.20	O8.5 III [Mas00]	O9.5 III: + O9.2 neb	no	SB2
1-092	4690513997070898944	[M2002] SMC 57269	15.29	-	B2 II	no	-
1-093	4690509766512143232	AzV 339a	11.94	F5 [Azz82]	A7 Ib	no	-
1-094	4687505217872848000	OGLE SMC-SC10 28919	15.68	B1-3 (III) [Eva04]	B1.5 II:	no	-
1-095	4690508632639753984	RMC 33, AzV 349	12.82	B0 IIIw [Gar87]	B1 Ia	no	-
1-096	4690509495924424960	-	16.60	-	B1 II	no	-
1-097	4690509942621639680	RMC 35, AzV 342	13.30	B2.5 Iab [Len97]	B2.5 Ib	no	-
1-098	4690512966278545792	-	14.76	-	B1 Ib	no	-
1-099	4690508671311394816	-	15.78	-	B2: II:	no	-
1-100	4690508740030862208	[M2002] SMC 58016	14.86	-	B1 II	no	-
1-101	4690508671311389824	[M2002] SMC 58132	15.78	-	B1.5 III-II	no	-
1-102	4690509599024293376	AzV 345a	14.29	O7 III [Gar87]	O6 III(n)	no	-
1-103	4690508774390594944	[MWD2000] h53-197	14.78	B1 I [Mas00]	B1 II:	no	-
1-104	4690514409387557376	[M2002] SMC 58803	15.46	-	O9 V:	no	-
1-105	4687504874275456896	-	16.42	-	B2: II	no	-
1-106	4687505801988031232	LHA 115-S 41, AzV 351	13.23	B1-2 (Ib)e [Eva04]	B1.5 e	yes	-
1-107	4690508808750315776	-	16.49	-	B0.2 III-II	no	-
1-108	4687504977354372864	-	15.49	-	B1 II:	no	-
1-109	4690510286219053312	AzV 356	14.03	B0 Iw [Gar87]	B1.5 Ib	no	-
1-110	4690510286219047936	AzV 358a	14.53	B0 I [Azz79]	B1 Ib	no	-
1-111	4687507584364583040	RMC 36, Sk 114, AzV 362	11.34	B3 Ia [Len97]	B3 Ia	no	-
1-112	4687507245097014144	RMC 37, AzV 367	10.88	B9 Ia$^+$ [Len97]	B9 Ia	yes	-
1-113	4690511626248698368	AzV 364	14.39	B2 IIIe [Men06]	B1 II e	yes	-
1-114	4690510492377435776	Sk 118, AzV 369	9.71	F4 Ia [Ard77]	F5:	no	-
1-115	4690510419368517760	OGLE SMC113.6 39585	15.27	-	B1 II:	no	EB [Paw13]
1-116	4687507554335030656	OGLE SMC-SC10 106172	15.20	B0.5 (IV) [Eva04]	B1 II	no	-
2-001	4688959562535054976	-	16.55	-	O9.2 V:	no	-
2-002	4688959356376632960	-	16.43	-	B2 II	no	-
2-003	4688981823353120896	2dFS 745	14.94	B1-2 (II) [Eva04]	B1 II	no	-
2-004	4688965575504047744	2dFS 5036	15.65	B1-5 (III) [Eva04]	B3 II:	no	-
2-005	4688983614358317184	AzV 67	14.17	O9 III [Eva04]	O8.5 II:(n)	no	-
2-006	4688981857676434816	-	15.40	-	B1.5 III	no	-
2-007	4688978383366817280	Sk 35, AzV 70	12.88	O9.5 Ib [Wal02]	O9.5 II-I	no	-
2-008	4688982235684518016	OGLE SMC719.12.035620	13.84	O9 III: [Lam13]	O9 II:	no	-
2-009	4688977463965651712	[M2002] SMC 16769	16.00	-	O9.7 IV(n)	no	-
2-010	4688964506004003840	-	15.23	-	B1.5 III-II	no	-
2-011	4688977837586212608	-	16.24	-	B1 II:	no	-
2-012	4688979250671773184	-	13.87	-	A0 Ib	no	-
2-013	4688982343048079488	-	15.59	-	B1 II	no	-
2-014	4688964613419753984	-	15.65	-	B1 II	no	-
2-015	4688978219879759360	-	15.54	-	B2.5 II:	no	-
2-016	4688964334254663168	AzV 80	13.77	O4-6n(f)p [Wal00]	O6 III:nn(f)p neb	no	(f)p from [Wal00]
2-017	4688982652297652352	-	14.12	-	B2 II e	yes	-
2-018	4688966090888390784	LIN 157, AzV 82	14.70	B2e [Azz75]	O6.5 III: e?	yes	-
2-019	4688964918322093312	-	15.13	-	O9.7 V:	no	-
2-020	4688966125248119808	AzV 83	13.99	O7 Iaf$^+$ [Wal00]	O7 Iaf$^+$	no	f$^+$ from [Wal00]
2-021	4688964922657391744	LIN 163	14.08	-	B2.5: II: e	yes	-
2-022	4688978254239473408	-	13.34	-	A0 Ib	no	-
2-023	4688978048081059712	-	15.26	-	B2.5 III	no	-
2-024	4688977979361634816	OGLE SMC-SC5 316725	15.15	O9 + O9 [Har03]	O9.7: V + O9.7	no	SB2, EB [Paw13]
2-025	4688978048081047296	-	15.45	-	B3 II:	no	-
2-026	4688965777314555264	OGLE SMC101.1 39365	14.85	-	B2 II + early B	no	SB2, EB [Paw13]
2-027	4688961624122202624	-	17.00	-	B1.5 III neb	no	-
2-028	4688977979361594880	AzV 87	14.31	B0 IIw [Gar87]	B1.5 Ib	no	-
2-029	4688961654195517952	2dFS 5047	15.42	O9.5 V [Eva04]	O9.7 V neb	no	LC from [Eva04]
2-030	4688978082440780672	[M2002] SMC 19070	15.57	-	B2 II	no	-
2-031	4688966189635061760	Dachs SMC 1-5, AzV 93	14.53	B1 Ib [Mas95]	B1 II	no	-
2-032	4688964853937446912	-	15.05	-	B1 II	no	-
2-033	4688961452323508736	-	16.99	-	B1 III-II	no	-
2-034	4688961383604048768	-	15.63	-	B1 II	no	-
2-035	4688965060095843072	AzV 95	14.15	O7 III((f)) [Wal00]	O7.5 III((f))	no	((f)) from [Wal00]
2-036	4688960627689838976	-	15.98	-	B2 II:	no	-
2-037	4688961761561107456	AzV 99	13.17	B2.5 Iab [Len97]	B2.5 Ib	no	-
2-038	4688967735823484800	-	14.80	-	B1.5 II	no	-
2-039	4688961864640239488	AzV 103	13.84	B0.7 Ib [Len97]	B1 II-Ib	no	-
2-040	4688984026675105280	-	14.74	-	B2 II	no	-
2-041	4688960657713202304	-	16.75	-	B2 II	no	-
2-042	4688960765128725760	-	15.49	-	B2 IV:	no	-
2-043	4688961795920796928	[M2002] SMC 20706	13.68	-	B1 Iab	no	-
2-044	4688967465277409408	-	16.08	-	B2: II	no	-
2-045	4688960765128723584	-	16.26	-	B2 III:	no	-

2-046	4688967396557954432	-	14.94	-	B1 II	no	-
2-047	4688979594268679296	AzV 106	14.85	B1 II [Lam16]	B1 Ib	no	-
2-048	4688981003018180992	2dFS 821	15.63	O9 V [Eva04]	O9.2 V	no	-
2-049	4688984404616099200	-	16.33	-	B1.5: III	no	-
2-050	4688979972225779968	AzV 107, 2dFS 822	12.52	F0 [Eva04]	A5 Ib	no	-
2-051	4688960421531447296	OGLE J005146.64-725121.3	16.58	B1 [Zas14]	B2.5 IV:	no	EB [Paw13]
2-052	4688967705795512448	AzV 109	14.66	O9.5 + B0.5 [Har03]	B0.5 V: + B0-0.7	no	SB2, EB [Paw13]
2-053	4688960485917320448	-	16.11	-	B2 III	no	-
2-054	4688966292708802304	Sk 49, AzV 110	11.72	A3 Ia [Neu10]	A0 Ia	no	-
2-055	4688984061034529408	AzV 102	14.26	O9.5-B0 IV-V [Coe15]	O9.7 V:n e	no	-
2-056	4688981106097035008	AzV 111	14.07	B0 II [Gar87]	B2 II: e	no	-
2-057	4688980831219164416	2dFS 832	14.49	B0 (III) [Eva04]	B0.7 II	no	-
2-058	4688963303411565056	Dachs SMC 1-9, AzV 32F	12.22	A3 I [Neu10]	A5 Ib	no	-
2-059	4688967602716295168	AzV 114	15.39	O8 V [Eva04]	O7.5 V(n) neb	no	LC from [Eva04]
2-060	4688963307749203072	-	14.55	-	B1.5 Ib	no	-
2-061	4688961894666576768	[MA93] 536	14.77	B1 [She13]	B2 II: e	no	-
2-062	4688963410828391680	[M2002] SMC 22729, 2dFS 850	15.15	B0-3 (III) [Eva04]	B1 III-II	no	-
2-063	4688963204681907328	[MA93] 555	14.73	-	B2 III e	yes	-
2-064	4688966537564476288	MOA J005219.2-724151	15.31	B0.2 + B1 [Har03]	B1.5: V-III + early B	no	SB2, EB [Paw13]
2-065	4688967568356557440	Dachs SMC 1-11, AzV 121	9.56	F5 Ia [Hum83]	F5:	no	-
2-066	4688966739421000448	[M2002] 23352	14.18	B0-2 [Pau12]	O9.7 III:nnn pe+	yes	-
2-067	4685959235845498240	AzV 123	13.24	B8 [Azz75]	B8 Ib	no	-
2-068	4688980414561766016	2dFS 5057	12.79	B9 (Iab) [Eva04]	B9 Iab	no	-
2-069	4688963887532390528	2dFS 875	15.44	O9 V [Eva04]	O9 V	no	EB [Paw13]
2-070	4688962414395649792	[MA93] 584	13.88	B1-2 (II) [Eva04]	B1 II e	no	-
2-071	4688968049392847488	2dFS 5058	14.86	B1-3 (III)e? [Eva04]	B1.5 II: e	no	-
2-072	4685959373284393728	2dFS 880	13.53	A2 II [Eva04]	A2 II/Ib	no	-
2-073	4688963548266999808	Dachs SMC 1-16, AzV 131	12.34	A0 [Azz75]	B9 Ia	no	-
2-074	4688968049392837248	2dFS 881	15.12	B1-5 (II) [Eva04]	B3 II:	no	-
2-075	4688968358630475136	AzV 133	14.48	O6.5 V((f)) [Eva04]	O6 Vn((f))	no	((f)) from [Eva04]
2-076	4688966881161489280	[M2002] SMC 24500	15.30	-	B1 Ib	no	-
2-077	4688963926224354816	-	15.25	-	B1 II	no	-
2-078	4688963651346132224	Dachs SMC 1-17	14.71	-	B0 II	no	-
2-079	4688963548266951808	[M2002] SMC 24767	15.26	-	O4 V: + early B	no	SB2
2-080	4688962517474878720	-	13.00	-	A2 II/Ib	no	-
2-081	4688968461709335040	[M2002] SMC 24895	14.13	B0-3 [Pau12]	B2 II e	yes	-
2-082	4685960021758355584	AzV 138	13.98	O9 III-Vpe [Lam16]	O9.2 III pe	no	-
2-083	4688963582626684544	Sk 53, AzV 137	12.64	B2 Iab [Len97]	B2.5 Ia	no	-
2-084	4688962448755796608	-	15.33	-	B2 II:	no	-
2-085	4688963582627047424	-	15.87	-	O9 V	no	-
2-086	4688962757993027328	[M2002] SMC 25142	15.45	-	O8 V(n)	no	-
2-087	4688967323503140992	-	15.04	-	O9.5 III	no	-
2-088	4688968461709333632	2dFS 898	13.16	A5 II [Eva04]	A5 Ib	no	-
2-089	4688968118111968512	OGLE SMC-SC6 167473	15.27	-	B2 II	no	EB [Paw13]
2-090	4688966984219996288	[M2002] SMC 25387	14.98	B0 [She13]	O7.5 Vn	no	-
2-091	4688967052939420672	Dachs SMC 1-21	14.32	-	O8.5 V	no	-
2-092	4688967289176997504	Dachs SMC 1-22	12.17	-	B8 Iab	no	-
2-093	4688967362197739392	HD 5291, RMC 11, Sk 56	10.58	B8 Ia^{+} [Len97]	B8 Ia	no	-
2-094	4688964029303180416	[M2002] SMC 25741	15.27	-	B0.5 III-II	no	-
2-095	4688963960583732736	-	16.20	-	B0 IV	no	-
2-096	4688962483115141248	[M2002] SMC 25866	14.97	-	O9.5 III:	no	-
2-097	4689003680451206272	LIN 230, AzV 141, 2dFS 915	14.27	B5 (II) [Eva04]	B5 II: e	yes	-
2-098	4688991585819715712	2dFS 5066	14.99	O6 V((f)) [Eva04]	O6.5 V((f))	no	LC from [Eva04]
2-099	4688991585819679104	-	16.30	-	B0 IV neb	no	-
2-100	4688962929791640064	-	15.43	-	B0 V	no	-
2-101	4688991585819641088	-	13.53	-	B9 Ib	no	-
2-102	4688990555027643904	AzV 143, 2dFS 932	14.54	B0 (III) [Eva04]	B0 II:	no	-
2-103	4688987256492902528	[M2002] SMC 27080	15.32	-	B0.7 V: + B0:	no	SB2
2-104	4688987252155037568	2dFS 936	14.68	O6.5f?p [Eva04]	O5.5f?pe	yes	f?p from [Eva04]
2-105	4688991688898752896	AzV 39F	13.57	A0 [Azz79]	A2 II/Ib	no	-
2-106	4688990589387328384	AzV 145	13.99	B1 [Azz75]	B0.7 II	no	-
2-107	4685960129198503936	-	14.99	-	B1.5 III-II	no	-
2-108	4685983665623961216	-	14.89	-	B5 II	no	-
2-109	4688990692466513408	2dFS 5071	15.00	B1-5 (II) [Eva04]	B2 II e	no	-
2-110	4688986431859207296	AzV 148	14.97	O8.5 V [Mas02]	B0 II	no	-
2-111	4685983699984262912	[MA93] 715	14.67	-	B2 II: e	yes	-
2-112	4688987389594710272	OGLE SMC-SC6 447961	14.57	-	B2 II:	no	EB [Paw16]
2-113	4685983420730442624	Sk 57, AzV 151	12.36	B2.5 Ia [Len97]	B2.5 Ia	no	-
2-114	4688986569298097792	-	14.58	-	B1.5 II	no	-
2-115	4688990658106753280	AzV 153	13.71	B8 [Azz75]	B5 Ib	no	-
2-116	4688986534938381184	LHA 115-S 18, AzV 154	11.11	B[e] [Lam16]	sgB[e]	yes	-
3-001	4685853682687097088	Sk 6, AzV 9	13.20	B0 III [Smi97]	B2.5 Ib	no	-
3-002	4685853609694629888	-	15.83	-	O6 V:nn	no	-
3-003	4685854056331151232	2dFS 5005	15.74	B1-5 (II) [Eva04]	B1.5 III	no	-
3-004	4685849696957595136	-	16.65	-	O9.7 IV:	no	-
3-005	4685849319000715904	-	16.30	-	B1 III	no	-
3-006	4685849623922204160	-	13.65	-	B5: + early A Ia	no	SB2
3-007	4685848597446171904	-	12.37	-	A5 Ib	no	-
3-008	4685836880771632512	-	16.18	-	O7.5 V:(n) neb	no	-
3-009	4685850036241667840	-	14.52	-	B5 II	no	-
3-010	4685836876461619328	-	15.54	-	O9.7 V: neb	no	-
3-011	4685854369881566848	LIN 84	14.39	-	B0.5 III: e	yes	-
3-012	4685854571724688768	HA 115-S 6, RMC 4, Sk 11, AzV 16	11.02	B0[e] [Zic96]	sgB[e]	yes	-
3-013	4685848666165653504	-	13.82	-	A0 Ib	no	-

3-014	4685848734885047680	[M2002] SMC 7782	14.86	O7.5 V [Lam13]	O8 Vn	no	-
3-015	4685850139318317312	-	16.73	-	B2 III	no	-
3-016	4685849044122619264	[SBV2013] B11	16.82	-	B2 III e	no	-
3-017	4685836571534016128	[M2002] SMC 7909	14.44	-	B0.7 II	no	-
3-018	4685836635962991104	LIN 88	13.84	-	B1.5: II: e	yes	EB [Paw13]
3-019	4685948481244298112	2dFS 5010	15.04	O8.5 V [Eva04]	O9.2 V	no	LC from [Eva04]
3-020	4685849112841980928	[M2002] SMC 8017	15.42	-	B0 III	no	-
3-021	4685835536431612288	-	14.82	-	B1.5 II	no	-
3-022	4685948412524815616	OGLE SMC-SC4 120783	14.65	-	B2 II neb	no	-
3-023	4685849078482253440	-	15.17	-	B3 II	no	-
3-024	4685850177993655424	-	14.88	-	B5 II	no	-
3-025	4685850242400168960	[MA93] 167	14.50	-	B2 II e	yes	-
3-026	4685947038135411200	-	15.06	-	B1.5 II-III	no	-
3-027	4685948515603957376	LIN 91	13.44	B0-2 [Pau12]	B1.5 II e	yes	-
3-028	4685835575101684608	[M2002] SMC 8609	14.52	B0 III [Lam16]	B0.5 II	no	-
3-029	4685944117556288640	[M2002] SMC 8649	14.34	-	B1.5 Ib	no	-
3-030	4685947141214597376	BBB SMC 289, AzV 21	14.80	B1 [Azz75]	B1 II	no	-
3-031	4685836708972891648	[MA93] 177	14.14	-	B0: III: + OB e	yes	SB2, EB [Paw13]
3-032	4685836708972886400	-	14.56	-	B1.5 II	no	-
3-033	4685948275085868928	-	15.50	-	O9.5 IV:n neb	no	-
3-034	4685943773959001984	[M2002] SMC 8909	14.72	-	B0 III	no	-
3-035	4685835884339216512	-	16.34	-	B2 II e	no	-
3-036	4685947519171645952	2dFS 5014	15.28	B1-3 (II) [Eva04]	B0.7 III-II neb	no	-
3-037	4685835884339219456	Sk 17, AzV 23	11.96	B3 Ia [Len97]	B3 Ia	no	-
3-038	4685930614175426560	-	13.16	-	A0 Ia	no	-
3-039	4685944151915964928	AzV 25	13.25	B5 [Azz75]	B3 Ib	no	-
3-040	4685942949325301120	-	14.00	-	B2 II: e	yes	-
3-041	4685944147624292224	-	13.25	-	B8 Ib	no	-
3-042	4685947553531340800	BBB SMC 266, Sk 18, AzV 26	12.94	O6 I(f) [Mas04]	O6 I(f) + O7.5	no	SB2, LC from [Mas04]
3-043	4685943121123943680	Sk 19, AzV 27	11.63	B8 I [Neu10]	A2 Iab	no	-
3-044	4685929750832616320	AzV 28, 2dFS 668	13.88	B1-2 (II) [Eva04]	B1 Ib	no	-
3-045	4685944250703291520	-	13.44	-	A0 Ib	no	-
3-046	4685947209934051200	[M2002] SMC 9532	14.45	-	O8.5 V(n) neb	no	SB
3-047	4685944250646464768	[M2002] SMC 9534	14.27	-	B1 II	no	-
3-048	4685926491006945536	-	15.29	-	B0.5 III	no	-
3-049	4685926147408274304	[M2002] SMC 9647	15.08	-	O4 I(n)	no	-
3-050	4685943121123938048	OGLE SMC720.28.039935	15.36	-	B1.5 III	no	EB [Paw16]
3-051	4685942777526639744	[MA93] 203	14.81	-	O5.5: V neb	no	EB [Paw13]
3-052	4685942777526626432	[M2002] SMC 9845	15.16	-	O7 V: + O7.5 neb	no	SB2
3-053	4685943082442898432	LIN 106	14.87	O8 V [Tes01]	O7.5 V(n) neb	no	-
3-054	4685929926980635136	OGLE SMC720.28.000244	15.05	-	O7 V(n) neb	no	EB [Paw13]
3-055	4685944285006166144	[M2002] SMC 10202	15.42	-	B0.5 IV	no	-
3-056	4685947652249342080	OGLE SMC-ECL- 1376	14.46	-	B1.5 Ib neb	no	EB [Paw13]
3-057	4685926181767968000	[M2002] SMC 10209	15.54	-	B1 II	no	-
3-058	4685926559725017600	AzV 34	13.11	B2: [Azz75]	A0 Iab	no	-
3-059	4685947897128639744	-	14.38	-	B1 II	no	-
3-060	4685925146630858240	[M2002] SMC 10505	15.31	O7-9 [She13]	O6 Vn:	no	
3-061	4685943254211136000	AzV 28F	13.00	B5 [Azz79]	B3 Ib	no	-
3-062	4685948064629440768	Sk 22	14.01	OB: [San68]	O9.7 II e	no	-
3-063	4685947622250808832	[M2002] SMC 10818	14.70	-	O9.2 II(n)	no	-
3-064	4685926353526652160	-	14.99	-	B3 II	no	-
3-065	4685943254211144832	[M2002] SMC 10947	14.66	-	B0.7 II neb	no	-
3-066	4685926319206869632	-	14.95	-	O7 III:	no	-
3-067	4685948000207808384	OGLE SMC-SC4 175149	15.09	-	B0.2 IV	no	EB [Paw13]
3-068	4685930334952220416	-	13.75	-	B5 Ib	no	-
3-069	4685931468820884864	-	14.97	-	B1.5 II: neb	no	-
3-070	4685926662804412800	-	15.36	-	B1 II	no	-
3-071	4685925563292648576	[M2002] SMC 11294	16.17	-	B0 V	no	-
3-072	4685943288573729920	2dFS 5021	15.36	B1-5 (II) [Eva04]	B1 III	no	EB [Paw13]
3-073	4685943219851406208	OGLE SMC-SC5 26508	13.20	-	B3 Ib	no	EB [Paw13]
3-074	4685943670879523840	[SBV2013] B37	15.19	B1 [She13]	B1 III-II	no	-
3-075	4685925872530280192	AzV 44	14.45	B0 IIww [Gar87]	O6.5 V:nnn	no	EB [Paw13], SB2?
3-076	4685925872530300544	-	16.10	-	O8 Vn	no	-
3-077	4685947828409081088	[MA93] 256	14.32	B0-2 [Pau12]	B1 II e	yes	-
3-078	4685925666371896576	AzV 47	14.16	O8 III((f)) [Wal00]	O8 III((f))	no	LC from [Wal00]
3-079	4685925936902711424	[M2002] SMC 12022	15.28	-	B1.5 III + B2.5:	no	SB2
3-080	4685931232650460032	-	15.36	-	B1 III-II	no	-
3-081	4685946282220487424	[MA93] 265	14.34	-	O6 III: neb	no	-
3-082	4685926800243109760	OGLE SMC100.8 45085	14.60	-	B1 II + B1.5:	no	SB2
3-083	4685943636519760512	-	13.71	-	A0 Ib	no	-
3-084	4685931335729612288	[M2002] SMC 12787	14.54	-	B0 Ib:	no	-
3-085	4685926009969170816	AzV 49	13.54	A0 [Azz75]	B9 Iab	no	-
3-086	4685931267010164480	-	14.76	-	B1 III: + B2.5:	no	SB2
3-087	4685944839111584256	OGLE J004915.62-731210.4	12.57	-	A2 II/Ib	no	-
3-088	4685945968691683456	-	13.12	-	A2 II	no	-
3-089	4685926933335252992	-	16.50	-	B2 III:	no	-
3-090	4685932744479939584	-	13.76	-	B0.2 Ia	no	-
3-091	4685927212559921536	-	15.20	-	B1 III-II	no	-
3-092	4685933053717525632	-	14.44	-	B5 II	no	-
3-093	4685932843197054208	-	16.62	-	B1 II:	no	-
3-094	4685945247096928256	[M2002] SMC 13774	16.17	O7 [She13]	O8: V(n)	no	-
3-095	4685925833826106368	[M2002] SMC 13986	15.10	-	B2 II: e	no	-
3-096	4685928410806791936	-	14.18	-	B2.5 II	no	-

3-097	4685928415151555712	2dFS 5031	14.55	B1-3 (II) [Eva04]	B2.5 II	no	-
3-098	4685931679327948800	[M2002] SMC 14324	14.25	O6 V((f))e [Lam16]	O6 V((f))n e	no	LC from [Lam16]
3-099	4685928724389105536	AzV 55	13.24	B5 [Azz75]	B9 Iab	no	-
3-100	4685928449511258112	-	15.22	-	B3 II	no	-
3-101	4685928445163783552	OGLE SMC100.8 52871	14.82	O9 + O9 [Hil05]	O9.7 V: + O9.7	no	SB2, EB [Paw13]
3-102	4685932052995296768	-	14.65	-	B8 II-Ib	no	-
3-103	4685932126004485376	-	15.16	-	B1 II-Ib	no	-
3-104	4685933191156274432	BBB SMC 126, AzV 59	13.27	A0 [Azz75]	B8 Iab	no	-
3-105	4685927620532759808	OGLE SMC-SC5 95214	15.19	B0 (IV) [Eva04]	B0.2 III-II	no	-
3-106	4685945010910000640	AzV 63	13.34	A0 [Azz75]	B5 Ib	no	-
3-107	4685880277148119040	AzV 64	14.32	B1 [Azz75]	O9.7 II:(n) e?	yes	-
3-108	4685927727956781568	-	-	-	B0 III	no	-
3-109	4685931816766886656	AzV 66	14.10	B0. 5V [Mas95]	B0.2 Ib	no	-
3-110	4685933569113371904	-	14.28	-	B8 II-Ib	no	-
3-111	4685931812407476864	-	13.96	-	B1 Ib	no	-
3-112	4685931816766868224	OGLE SMC100.2 30	14.78	-	O6.5 V-III	no	EB [Paw13]
3-113	4685927453078935680	-	14.77	-	B2 II:	no	-
3-114	4685928793108545152	ISO-MCMS J005013.7-731710	12.00	-	F2:	no	-
3-115	4685928861827989120	OGLE SMC100.2 35	14.66	-	B1 II	no	EB [Paw13]
3-116	4685928071554123264	-	15.04	-	B3 II	no	-
4-001	4689018661298288000	[BLK2010] flames1004	13.04	A2 Ib [Duf19]	A1 Ib	no	-
4-002	4689016049958328576	AzV 191, Cl* NGC 346 ELS 4	13.21	Be(B1:) [Eva06]	B1.5: e	yes	-
4-003	4689019073615200768	2dFS 1252	15.69	B0.5 III [Duf19]	B1 II	no	-
4-004	4689067585206690176	-	15.40	-	B5 II:	no	-
4-005	4689016049958297600	2dFS 1259,Cl* NGC 346 ELS 20	15.41	B1 V+early B [Eva06]	B1 III-II	no	SB2 [Eva06]
4-006	4689002851458876800	AzV 197	10.58	F0 I [Neu10]	F2:	no	SB2?
4-007	4689014709928718464	[BLK2010] flames1028	15.16	B2.5 III [Duf19]	B1.5 III	no	-
4-008	4689019589011024128	AzV 68F, Cl* NGC 346 ELS 2	12.99	A2: Iab [Eva06]	A0 Ib	no	-
4-009	4689014778648125824	Cl* NGC 346 ELS 52	15.50	B1.5 V [Eva06]	B2 III	no	SB1 [Eva06], EB [Paw13]
4-010	4689016221756877184	AzV 201	12.99	B1e [Duf19]	B1 e +	yes	-
4-011	4689014808648096896	OGLE SMC-SC8 107285	15.48	B0 III [Duf19]	B1 II	no	-
4-012	4689020722882360192	Cl* NGC 346 ELS 84, 2dFS 1296	16.46	B1 V [Eva06]	B2 III	no	-
4-013	4689019245413731840	Cl* NGC 346 MPG 11, ELS 43	15.87	B0 V [Eva06]	B0 IV	no	-
4-014	4689016221756858624	Cl* NGC 346 MPG 12, ELS 26	15.33	B0 IV (Nstr) [Eva06]	B0 III	no	-
4-015	4689019898248677888	AzV 202, Cl* NGC 346 ELS 12	14.94	B1 Ib [Eva06]	B1 II-Ib	no	-
4-016	4689020825961546496	[BLK2010] flames1046	15.38	B0.5 V [Duf19]	B0.7 III	no	-
4-017	4689002787095701248	[BLK2010] flames1041	14.58	B2 III-II [Duf19]	B1.5 Ib	no	-
4-018	4689002787095693568	[BLK2010] flames1067	16.13	O9 V [Duf19]	O9.5 IV	no	-
4-019	4689002718376234112	OGLE SMC-SC8 104191	15.20	B1 III [Duf19]	B1 II	no	-
4-020	4689003027613801216	Sk 73, AzV 210	12.78	B1.5 Ia [Len97]	B1 Iab-Ib	no	RV variable [Duf19]
4-021	4689015294044085248	[SBV2013] B135	15.47	O7-9 [She13]	O9.2 V	no	-
4-022	4689015500202439296	LIN 336, Cl* NGC 346 MPG 184	14.73	B2-3e [Duf19]	B2.5 II: e	yes	-
4-023	4689015225324629120	OGLE SMC-SC8 110238	15.50	B2.5 III-II [Duf19]	B2 II:	no	-
4-024	4689003126336982272	OGLE SMC-SC8 107276	15.22	B1.5 II [Duf19]	B1 II	no	-
4-025	4689001721943896192	-	15.38	-	B1 III	no	-
4-026	4689015328403760128	Cl* NGC 346 MPG 217, ELS 18	14.60	O9.5 IIIe [Eva06]	O9.5 III pe	no	LC from [Eva06]
4-027	4689001721943908096	-	16.90	-	B2 II	no	-
4-028	4689001653225111680	OGLE SMC-SC8 104178	15.71	B1-3 (III) [Eva04]	B2 II	no	-
4-029	4689020070047305472	Cl* NGC 346 ELS 38	15.73	B1 V [Eva06]	B1.5 IV	no	EB [Paw13]
4-030	4689015259684292608	AzV 214, Cl* NGC 346 MPG 293	13.34	B1 Ia [Duf19]	B1 Ia	no	-
4-031	4689016462274935296	Cl* NGC 346 MPG 304, ELS 93	16.16	B0 V [Eva06]	B0 V neb	no	-
4-032	4689003508650071040	[BLK2010] flames1023	14.53	B0 V [Duf19]	O9.7 III:	no	EB SB1 [Duf19, Paw13]
4-033	4689016840231937792	Cl* NGC 346 ELS 27	15.60	B0.5 V [Eva06]	B0.7 III neb	no	-
4-034	4689015736378946688	LIN 345, Cl* NGC 346 MPG 482	14.28	B0.5e [Duf19]	B2 II pe neb	yes	-
4-035	4689016771512472960	Cl* NGC 346 ELS 24	14.90	B2:(Be-Fe) [Eva06]	B3 II: e	yes	-
4-036	4689002409138503040	AzV 219	15.10	B1 III [Duf19]	B1.5 II	no	SB1 [Duf19]
4-037	4689015667659473920	Cl* NGC 346 NMC 13, MPG 549	13.14	O9.5 V [Duf19]	O9.7 IV neb	no	-
4-038	4689002134260639232	-	16.08	-	B1.5 III-II	no	-
4-039	4690521006458654464	AzV 220	15.03	O6.5f?p [Wal00]	O6.5f?pe	yes	f?p from [Wal00]
4-040	4689015736378951936	Cl* NGC 346 ELS 33	13.12	O8 V [Eva06]	O7 V(n) neb	no	-
4-041	4689015465788811008	Cl* NGC 346 MPG 602	15.19	O6.5 V((f)) [Duf19]	O6.5 V: neb	-	-
4-042	4688999041884354944	AzV 222	13.45	B3 [Mas00]	B2.5 Ib	no	-
4-043	4689015397123159424	Cl* NGC 346 MPG 637, ELS 29	15.37	B0 V [Eva06]	O9.5 V neb	no	SB1 [Eva06]
4-044	4689002237339841792	[BLK2010] flames1176	16.85	B1.5 V [Duf19]	B1.5 III neb	no	-
4-045	4690521109537837440	AzV 224, Cl* NGC 346 ELS 8	14.73	B1e [Eva06]	B1 Iab	no	-
4-046	4688998835725922176	[MA93] 1135, 2dFS 1375	14.15	B1-5 (II)e? [Eva04]	B2 II:	yes	-
4-047	4690518085880908544	Cl* NGC 346 ELS 37	15.62	B3 III [Eva06]	B2 II	no	-
4-048	4689003371211130624	Cl* NGC 346 ELS 21, 2dFS 5099	15.33	B1 III [Eva06]	B1 II	no	-
4-049	4689002443498253440	AzV 226, Cl* NGC 346 ELS 10	15.02	O7 IIIn((f)) [Eva 06]	O7 IIIn((f))	no	((f)) from [Eva06]
4-050	4690521487494893952	Cl* NGC 346 ELS 103	16.91	B0.5 V [Eva06]	B1 II:	no	-
4-051	4688999140607234944	-	14.94	-	B1 II	no	-
4-052	4690521040818521600	Cl* NGC 346 ELS 32	15.73	B0.5 V [Eva06]	B1.5 III:	no	-
4-053	4690504857379258496	Cl* NGC 346 MPG 770	15.20	B0 V [Duf19]	B0 V neb	no	-
4-054	4688998938805087232	AzV 231	14.08	A0 [Azz75]	B9 Ib	no	-
4-055	4690522273449262592	LHA 115-S 29, RMC 15, Sk 79	12.10	B 7I[e] [Gra12]	sgB[e]	yes	-
4-056	4690517742283562624	[BLK2010] flames1059	16.02	B0 V [Duf19]	B0 V: neb	no	SB1 [Duf19], EB [Paw13]
4-057	4690504582501410432	Cl* NGC 346 ELS 46	16.06	O7 Vn [Eva06]	O6.5 Vnn neb	no	-
4-058	4690516677131714432	Sk 80, AzV 232	12.70	O7 Iaf$^+$ [Wal77]	O7 Iaf$^+$	no	f^+ from [Wal77], Binary [Eva06]
4-059	4690503689148323328	2dFS 5100, Cl* NGC 346 ELS 18	15.22	B0.5 Vn [Eva06]	B1: III: + early B	no	SB2 [Eva06], EB [Paw13]
4-060	4690516711491448960	Cl* NGC 346 MPG 802	14.45	B8 Ib [Duf19]	B8 II-Ib neb	no	-
4-061	4689002271699550720	OGLE SMC-SC8 157867	16.08	B2(shell) [Duf19]	B2 II	no	-
4-062	4688998973164819200	-	16.27	-	B2: III: + B2:	no	SB2
4-063	4690504582501405696	[M2002] SMC 46892	12.00	A5 V [Neu10]	A7 Ib	no	-

4-064	4688999248042623744	-	16.38	-	B2 IV:	no	-
4-065	4690517089448534272	[BLK2010] flames1021	15.01	B2 II [Duf19]	B2 II: neb	no	-
4-066	4690518223319786624	Sk 81, AzV 234	13.19	B3 Iab [Duf19]	B2.5 Ib	no	-
4-067	4690518154600349184	2dFS 1418, Cl* NGC 346 ELS 35	15.62	B1 V [Eva06]	B2 II:	no	SB2 [Eva06], EB [Paw13]
4-068	4690518154600325760	[BLK2010] flames1029	15.30	B2.5 III [Duf19]	B2 II:	no	EB [Paw13]
4-069	4690517879722483328	-	17.05	-	B1 II neb	no	-
4-070	4690516745851186048	Cl* NGC 346 MPG 842	16.95	B1 V [Duf19]	B2 II neb	no	-
4-071	4690504926098661504	[MA93] 1167, Cl* NGC 346 ELS 9	14.18	B0e [Eva06]	O9.7 II: e? neb	no	-
4-072	4690500184455105536	RMC 16, Sk 83, AzV 237	12.32	B9 Ia [Eva04]	B9 Ia	no	-
4-073	4690504994818102016	Cl* NGC 346 ELS 25, MPG 848	15.45	O9 V [Eva06]	O9.2 V neb	no	SB1 [Eva06]
4-074	4690518532557434496	Cl* NGC 346 ELS 31	15.74	O8 Vz [Eva06]	O9 V	no	-
4-075	4690504651220842880	Cl* NGC 346 MPG 859, 2dFS 5102	13.25	A2 Ib [Duf19]	A0 Ib	no	-
4-076	4690503792227414400	AzV 238	14.24	O9 III [Duf19]	O9.7 III	no	SB1 [Duf19]
4-077	4690517055088782848	[BLK2010] flames1014	14.88	B3 Ib + mid A? [Duf19]	B3 Ib neb	no	SB2? [Duf19], EB [Paw13]
4-078	4690503826587160832	RMC 18, Sk 85, AzV 242	12.35	B1 Ia [Len97]	B1 Ia	no	-
4-079	4690521762372716160	-	13.10	-	A0 Ib	no	-
4-080	4690503929666296960	MOA J010015.9-721244	14.81	O8 + O9 [Hil05]	O9.7 + (O8-8.5 + B)	no	SB2 [Duf19] EB [Paw13]
4-081	4690503860946856832	[BLK2010] flames1091	16.28	B0.5: + B0.5: [Duf19]	B0.2: V	no	SB2 [Duf19]
4-082	4690517256934074624	[BLK2010] flames1114	16.64	O9 V [Duf19]	O9.5 IV:(n) neb	no	-
4-083	4690500317576535040	[M2002] SMC 48657	15.05	-	B1 II:	no	-
4-084	4690522002890799488	Sk 86, AzV 250	12.57	A0 :I [San68]	A0 Iab	no	-
4-085	4690505097897766144	Sk 87, AzV 252	13.27	B2.5 Iab [Len97]	B2.5 Ib	no	-
4-086	4690504341983110272	OGLE SMC-SC9 41748	13.90	A0 (Ib) [Eva04]	A2 II/Iab	no	-
4-087	4690504341983098368	-	15.76	-	B1 II:	no	-
4-088	4690500734210820352	-	16.26	-	B0.5: IV:	no	-
4-089	4690500665491363456	-	15.85	-	O9 V	no	-
4-090	4690503998385814272	OGLE SMC-SC9 41745	15.31	B1-3 (II) [Eva04]	B1 II	no	-
4-091	4690505475854319360	-	13.44	-	B8 Ib/Iab	no	-
4-092	4690518429478167680	-	16.52	-	B2 III	no	-
4-093	4690517604844488832	-	15.36	-	B1 III:	no	-
4-094	4690517329966645632	-	15.39	-	B1 III	no	-
4-095	4690505578937619712	OGLE SMC-SC9 47454	16.17	B1 + B1-2 [Hil05]	B2 III:	no	EB [Paw13]
4-096	4690504170184413952	[MA93] 1233	14.86	B0-5 (II) [Eva04]	B1.5 II:	yes	-
4-097	4690504204544113152	-	16.24	-	B2 III:	no	-
4-098	4690500802930242816	OGLE J010103.75-721544.4	14.18	-	B2.5 II:	no	-
4-099	4690500802930226432	[M2002] SMC 50390	15.38	-	B0.5 III	no	-
4-100	4690506712804884352	OGLE SMC-SC9 44811	16.01	B1-2 (III) [Eva04]	B1 III	no	-
4-101	4690499978296571392	OGLE SMC-SC9 38950	15.30	B1-2 (II) [Eva04]	B1.5 II:	no	-
4-102	4690500871649654656	OGLE SMC-SC9 41776	16.16	B0-5 (IV) [Eva04]	O7.5 V:n	no	-
4-103	4690500047016009728	AzV 80F	12.20	A3 V [Neu18]	A5 Ib	no	-
4-104	4690518841795059840	-	15.15	-	B1.5 II:	no	-
4-105	4690501180887186944	Sk 96, AzV 268, 2dFS 1550	13.56	B2.5 Iab [Len97]	B2: Ib:	no	-
4-106	4690507125121661696	-	16.43	-	B2-2.5 III	no	-
4-107	4690506747164583424	-	15.87	-	B1 II	no	-
4-108	4690505986933925888	-	15.99	-	B1.5 III:	no	-
4-109	4690502417837769344	-	16.18	-	B0.7 III	no	-
4-110	4690505819451697920	-	15.83	-	O7 V:(n)	no	-
4-111	4690518979233951104	OGLE SMC113.6 22632	15.98	-	B3: II	no	EB [Paw13]
4-112	4690501623246789376	AzV 83F, 2dFS 1607	14.88	B5 (II) [Eva04]	B5 II	no	-
4-113	4690502761435017984	OGLE SMC-SC9 131970	15.33	B1-3 (III) [Eva04]	B2.5 II pe	no	-
4-114	4690501352685999616	AzV 291	14.92	B1 [Azz75]	B5 II	no	-
4-115	4690503208111546496	-	16.47	-	B2 III:	no	-
4-116	4690506266128219904	-	16.39	-	B1.5 III:	no	-
5-001	4687500991624952064	OGLE SMC-SC10 24428	15.05	O9 Ve [Lam16]	O9.7 Vn + B	no	SB2, LC from [Lam16]
5-002	4687504324519462528	OGLE SMC113.7 34708	15.94	-	B2 IV	no	EB [Paw13]
5-003	4687504358879209088	-	16.81	-	B2.5 III	no	-
5-004	4687499922153760256	-	15.95	-	B2.5 III-II	no	-
5-005	4687504182822540416	SV* HV 1954	12.16	-	F2:	no	-
5-006	4687487763123080704	-	15.94	-	B2 II:	no	-
5-007	4687499685954929664	AzV 346	14.34	B1-5 (II) [Eva04]	B2.5 II	no	-
5-008	4687501537095707264	-	15.99	-	B1 II:	no	-
5-009	4687500063912170112	OGLE SMC-SC10 63718	15.38	B2.5 (III) [Eva04]	B2.5 II	no	-
5-010	4687501468343335808	-	15.33	-	B3 II	no	-
5-011	4687487660043860096	-	16.10	-	B2 III:	no	-
5-012	4687499720314663296	Dachs SMC 2-33	12.91	-	A2 II/Ib	no	-
5-013	4687487625684130688	OGLE SMC-SC10 61625	16.25	B3 (III) [Eva04]	B2 III	no	EB [Paw13]
5-014	4687487900566335744	Dachs SMC 2-34,AzV 352,2dFS 1898	12.65	A0 (Iab) [Eva04]	A0 Ib	no	-
5-015	4687505733268579968	-	15.92	-	B2 III:	no	-
5-016	4687486556213576960	AzV 354, 2dFS 1904	15.18	B1-3 (II) [Eva04]	B1.5 II	no	-
5-017	4687501678819589888	OGLE J010437.78-721352.7	16.18	-	B0 IV	no	-
5-018	4687505763370767104	-	14.62	-	B3 II	no	-
5-019	4687501678819562880	-	16.20	-	B2 III	no	-
5-020	4687486526172590720	LIN 435, AzV 359, 2dFS 1922	14.17	B0-3 (II)e [Eva04]	B1.5 II e	yes	-
5-021	4687487999358589824	Dachs SMC 2-41,AzV 360,2dFS 1923	15.04	B0.5 (IV) [Eva04]	B1 II	no	-
5-022	4687500579308038016	2dFS 1925	15.15	B0-5 (II) [Eva04]	B3 II	no	-
5-023	4687487247726980864	AzV 363	14.88	B0.5 III [Mas00]	B1.5 III e	yes	-
5-024	4687483502515662336	AzV 365, 2dFS 1934	15.02	B0 (IV) [Eva04]	B0.5 III	no	-
5-025	4687488102403240320	-	16.93	-	B1 III	no	-
5-026	4687500304430157312	AzV 368, 2dFS 1939	15.20	B0-3 (II) [Eva04]	B1 II	no	-
5-027	4687487282086698240	AzV 370	15.46	B0 V: [Cra82]	B1.5 III:	no	-
5-028	4687501640142199936	-	16.66	-	B0 V	no	-
5-029	4687487213367243392	Dachs SMC 2-44, 2dFS 1949	12.35	A5 II [Eva04]	A7 Ib	no	-
5-030	4687501365297007232	OGLE SMC-ECL- 7623	15.69	-	B1.5 III:	no	EB [Paw13]
5-031	4687487007208845056	LIN 440	14.19	-	B2.5: II:e + early AIa	yes	SB2

5-032	4687500270070426496	2dFS 1967	15.77	B1-3 (III) [Eva04]	B2.5 II	no	-
5-033	4687487385165885568	-	16.82	-	B1 III	no	-
5-034	4687486938489379328	LIN 444, 2dFS 1977	14.82	B1-5 (II) [Eva04]	B1.5 II: e	yes	-
5-035	4687482780961207424	[MA93] 1525, 2dFS 1982	14.06	B0-5 (II) [Eva04]	B1.5 II: e	no	-
5-036	4687482884040407936	2dFS 1997	14.32	A0 (Ib) [Eva04]	B9 Ib	no	-
5-037	4687487144647743616	OGLE SMC-ECL- 7650	15.65	-	B0.5 V: + early B	no	SB2, EB [Paw13]
5-038	4687483738714882304	[M2002] SMC 61844	15.18	-	B1.5 III-II	no	-
5-039	4687487419525570816	-	16.03	-	B1.5 III	no	-
5-040	4687489927786395776	AzV 381	14.86	B0 IIw [Gar87]	B1 II	no	EB [Paw13]
5-041	4687482815320929152	AzV 383, 2dFS 2018	14.71	B1-5 (Ib) [Eva04]	B1 II	no	-
5-042	4687482609162518784	2dFS 2023	15.50	O9.5 III [Eva04]	O9.7 III(n)	no	-
5-043	4687482712241716608	nan	14.64	B1-2 (II) [Eva04]	B1.5 II	no	-
5-044	4687488896994307712	-	15.60	O9.5 V [Lam13]	O9.5 IV	no	-
5-045	4687501884978067584	AzV 387	14.62	O9.5 III [Eva04]	O9.2 III + early B	no	SB2, LC from [Eva04], EB [Paw13]
5-046	4687483777393718400	LHA 115-S 44	13.56	B2 Ib [Dac70]	B1.5 II: e	yes	-
5-047	4687502228575362688	[MA93] 1545, 2dFS 2055	14.96	B1-5 (II) [Eva04]	B2.5 III: e	yes	-
5-048	4687482952759849728	LIN 446	13.87	B0-3 [Pau12]	O9.7 V(n)	no	-
5-049	4687435708116998400	OGLE SMC110.4 12773	16.53	-	B0 IV	no	EB [Paw13]
5-050	4687501953697501568	AzV 389	14.33	B0 IIw [Gar87]	O9.7 V: + early B	no	SB2
5-051	4687501884978054784	-	17.11	-	B0.2 III	no	-
5-052	4687488862634574848	AzV 104F	13.09	B8 [Azz79]	B9 Iab	no	-
5-053	4687485319263467520	2dFS 2068	16.24	B0-5 (III) [Eva04]	B3 II:	no	-
5-054	4687488587757077504	2dFS 2069	13.25	A3 II [Eva04]	A5 Ib	no	-
5-055	4687482746601417216	2dFS 2070	14.02	A0 (Ib) [Eva04]	A1 II/Ib	no	-
5-056	4687501988057218688	2dFS 2074	15.42	B2.5 (III) [Eva04]	B2 II	no	-
5-057	4687488656476146432	2dFS 2077	15.27	B0-5 (III) [Eva04]	B1 III: + early B	no	SB2
5-058	4687490168304521344	2dFS 2085	15.91	B1-5 (II) [Eva04]	B1 III-II	no	-
5-059	4687484498948014464	-	16.45	-	B0.2 IV	no	-
5-060	4687502572172727808	2dFS 2086	14.93	B1-3 (II) [Eva04]	B1.5 II	no	-
5-061	4687489790347907328	-	16.93	-	B2 III:	no	-
5-062	4687502640892163456	2dFS 2090	15.74	B0.5 (V) [Eva04]	B1.5 + early B	no	SB2, EB [Paw13]
5-063	4687488690835887360	2dFS 2098	15.73	B0 (V) [Eva04]	B0 V: + early B	no	SB2
5-064	4687485564099788544	AzV 394, 2dFS 2097	14.04	B1-5 (Iab) [Eva04]	B1.5 II	no	-
5-065	4687502366014559232	AzV 396	14.96	B0 III [Mas04]	B0 IV	no	-
5-066	4687489824707171456	LHA 115-S 47, AzV 397	13.56	B1-2 (II) [Eva04]	B2 II: e+	yes	-
5-067	4687485387976612736	Sk 126, AzV 399	12.21	A0 I [Hum83]	A0 Iab	no	-
5-068	4687489000073470720	-	16.14	-	B1 III-II	no	-
5-069	4687502400374028928	LIN 455, AzV 400, 2dFS 2127	14.03	B2.5 (II) [Eva04]	B3 II e	yes	-
5-070	4687484636386901760	-	15.93	-	B2 III:	no	-
5-071	4687437254305162880	HA 115-S 49, AzV 402, 2dFS 2139	13.54	O9.7 Ib [Eva04]	O8.5: Ib + OB pe	yes	SB2, LC from [Eva04]
5-072	4687484361509061504	[M2002] SMC 63718	14.74	-	B1 II	no	-
5-073	4687490305743468416	2dFS 2148	15.72	B1-5 (II)e? [Eva04]	B2 II:	no	-
5-074	4687502331654573056	2dFS 2151	15.89	B0.5 (V) [Eva04]	B0.5 IV	no	-
5-075	4687502434733747440	SV* HV 2016	15.58	B0.5+B2 [Har03]	B2 II:	no	EB [Paw13], SB2?
5-076	4687502709611614336	-	16.97	-	B1.5 III:	no	-
5-077	4687485491055825536	Sk 128, AzV 404, 2dFS 2174	12.47	B2.5 Iab [Len97]	B2.5 Ia	no	-
5-078	4687502434733761280	-	15.48	-	B1.5 III:	no	-
5-079	4687490305743456000	-	16.53	-	B2 III:	no	-
5-080	4687485873337367936	-	16.09	-	B2 III:	no	-
5-081	4687502537812927744	-	17.02	-	B0.5 III	no	-
5-082	4687489206231868800	-	17.12	-	B1.5 III	no	-
5-083	4687489584188971392	[M2002] SMC 64573	16.47	-	B1 II	no	-
5-084	4687484773825841408	2dFS 2211	15.47	B1-3 (III) [Eva04]	B2 II:	no	-
5-085	4687489579873557120	-	16.30	-	B0.2 III	no	-
5-086	4687486182574932352	2dFS 2215	14.47	B9 (Ib) [Eva04]	B9 Ib	no	-
5-087	4687489240591624832	2dFS 2216	15.56	B2 (II) [Eva04]	B1 II	no	-
5-088	4687489579867156864	-	15.33	-	B1.5 III-II	no	-
5-089	4687437494823799168	-	16.07	-	B2 III: e	yes	-
5-090	4687513910877142528	AzV 411, 2dFS 2238	14.53	O9 III [Eva04]	O9.5 III	no	-
5-091	4687437426103845376	AzV 412, 2dFS 2243	13.11	B8 (Iab) [Eva04]	B8 Ib	no	-
5-092	4687437529183051136	2dFS 2249	14.04	B0-5 (II) [Eva04]	B1 II: pe	no	-
5-093	4687437907140147712	2dFS 2257	14.98	B1-5 (II) [Eva04]	B1 II	no	-
5-094	4687485976416952832	LIN 468, AzV 413	14.74	Be [Gar85]	B1 e	yes	-
5-095	4687436700232929536	[M2002] SMC 65523	15.95	-	B1.5 III:	no	-
5-096	4687437834104778624	[MA93] 1620, 2dFS 2265	15.06	B1-3 (II) [Eva04]	B1.5 III-II	yes	-
5-097	4687513876517417856	2dFS 2266	16.02	OC7 II(f) [Eva04]	O8 II(f)	no	LC from [Eva04]
5-098	4687437632262257024	AzV 414	13.13	B8 [Azz75]	B9 Ia	no	-
5-099	4687512845725520640	2dFS 2281	16.24	O9.5 III [Eva04]	O9.7 III	no	LC from [Eva04]
5-100	4687514048316067968	2dFS 2283	15.42	B0.5 (IV) [Eva04]	B0 V	no	EB [Paw13]
5-101	4687437563542778880	-	12.98	-	A5 Ib	no	-
5-102	4687508413319210368	AzV 417, 2dFS 2289	12.63	F5 [Eva04]	F0:	no	-
5-103	4687509753348904832	AzV 418	15.04	B2: [Azz75]	B3 II	no	-
5-104	4687512948804514176	AzV 419	13.54	B2 [Azz75]	B2.5 Ia	yes	-
5-105	4687509749039520768	Sk 131, AzV 420	13.76	B0.5 Ia [Len97]	B0.7 II	no	-
5-106	4687508344599737216	AzV 421, 2dFS 2299	15.14	B2 (II) [Eva04]	B2 II	no	-
5-107	4687512880085044608	LIN 469, AzV 422, 2dFS 2316	14.30	B1-5 (II)e [Eva04]	B2.5 II + early A	yes	SB2
5-108	4687437597895960448	2dFS 2317	16.42	B0 (V) [Eva04]	O9.7 IV:	no	-
5-109	4687513567279735552	2dFS 2340	12.19	F0 ([Eva04]	A7 Iab	no	-
5-110	4687513361121326080	-	16.82	-	B1 III	no	-
5-111	4687508825635978752	OGLE SMC-SC11 89163	16.50	-	B2 III:	no	EB [Paw13]
5-112	4687461099956943744	2dFS 2350	14.46	B8 (II) [Eva04]	A0 Ib	no	-
5-113	4687508550758084864	-	14.24	-	B1 II	no	-
5-114	4687508585117812736	AzV 432	14.43	B0 [Azz75]	B1.5 II	no	-

5-115	4687460481482120832	LHA 115-S 54, AzV 436, 2dFS 2413	13.40	B0 (II)e [Eva04]	O9.5: V: pe	yes	-
5-116	4687461649712663296	-	16.24	-	B2 II	no	-
6-001	4687162582543422080	[MA93] 1760	14.53	B0 Ve [Lam13]	B0.5 III: e	yes	-
6-002	4687161929708394752	Dachs SMC 3-1, AzV 122F, 2dFS 2876	12.47	A0 (Iab) [Eva04]	A2 Ib	no	-
6-003	4687161654830500480	2MASS J01124381-7318457, 2dFS 2877	15.91	B2 (III) [Eva04]	B1.5 III-II	no	-
6-004	4687161860988920960	2MASS J01124660-7317497, 2dFS 2883	15.66	B2 (III) [Eva04]	B2 III:	no	-
6-005	4687161895348646400	Sk 151, AzV 471, 2dFS 2905	13.87	O9.5 I [Lam16]	O9.7 II-Ib(n)	no	-
6-006	4687158592506675328	Dachs SMC 3-4, AzV 473	11.20	F8 I [Neu10]	F2:	no	-
6-007	4687157286836619520	2MASS J01132216-7324067, 2dFS 2937	15.24	B3 (II) [Eva04]	B5 II	no	-
6-008	4687159868124113152	HD 7583, RMC 45, Sk 152, AzV 475	9.62	A0 Ia-0 [Fea60]	A2 Ia	no	-
6-009	4687163235378435328	Dachs SMC 3-9	12.89	A3 V: [Dac70]	A2 II/Ib	no	-
6-010	4687158768612502528	OGLE SMC116.7 9681	16.73	-	B2 IV:	no	EB [Paw13]
6-011	4687160280440948608	-	15.36	-	B2 III: e neb	no	-
6-012	4687160280440940672	-	15.88	-	B1 III neb	no	-
6-013	4687160207423517312	WBBe NGC 456 2	14.65	O6-7 V [Tes87]	O7.5 V: + O9.5 neb	no	SB2
6-014	4687160211708489088	-	15.18	-	O9.5 V(n) neb	no	-
6-015	4686408111398825728	[BKB2004b] 182	11.74	F0 I [Neu18]	F2:	no	-
6-016	4687160246081207680	OGLE SMC116.6 11072	15.40	-	B0.5: IV neb	no	EB [Paw13]
6-017	4687165125163949952	Sk 153, AzV 477, 2dFS 2980	13.50	B2 (Ib) [Eva04]	B1 Ib	no	-
6-018	4687176979273664512	2dFS 2983	16.97	B0-5 (IV) [Eva04]	B2 IV-III	no	-
6-019	4687160246081200256	LIN 503	15.06	-	O9.7 V neb	no	-
6-020	4687164128731574400	2MASS J01141596-7311537, 2dFS 2995	15.73	B2.5 (III) [Eva04]	B2.5 III	no	-
6-021	4687164060012111616	2MASS J01141722-7313014, 2dFS 2998	15.93	O9.5 III [Eva04]	B0 V-IV	no	-
6-022	4687183159725860736	-	17.00	-	B2 III-II	no	-
6-023	4687160727117511168	OGLE SMC116.3 37	15.96	-	O9.2 V	no	EB [Paw13]
6-024	4687164055705068288	Sk 154, AzV 478	11.09	A2-3 I [Hum91]	A5 Iab	no	-
6-025	4687163853853686144	GSC 09142-00856, 2dFS 3006	15.27	O8.5 V [Eva04]	O9.2 V	no	EB [Paw13]
6-026	4687159593246187136	-	16.58	-	B1 III neb	no	-
6-027	4687164919005535616	2dFS 3010	15.90	B1-3 (III) [Eva04]	B1.5 III	no	-
6-028	4687159558886453760	-	16.29	-	B0 V neb	no	-
6-029	4687160486599363712	2dFS 3023	16.87	O9.5 III [Eva04]	B0 III neb	no	-
6-030	4687163819493940992	-	16.46	-	B0 IV:	no	-
6-031	4687159661965655552	OGLE SMC733.30.000053	15.48	-	O8.5 V: neb	no	EB [Paw16]
6-032	4687159455807235072	-	16.35	-	O9 V:(n) neb	no	-
6-033	4687159657667699712	[MA93] 1794	15.21	-	O4.5 V: neb	no	-
6-034	4686408313260119552	2dFS 3036	15.23	B1-3 (III) [Eva04]	B2 III-II e	yes	EB [Paw13]
6-035	4687171206837590272	[M2002] SMC 75626	15.81	O9 III-V [Lam16]	B0 IV	no	-
6-036	4686408691230920448	-	15.25	-	B0 V neb	no	-
6-037	4687159387087763968	-	16.35	-	B2 III: neb	no	-
6-038	4686408764233799168	OGLE SMC-ECL- 5820	16.60	-	B2 IV: neb	no	EB [Paw13]
6-039	4686408764233794816	-	16.69	-	B2 III: neb	no	-
6-040	4687159421447500160	-	16.64	-	B1.5 III: neb	no	-
6-041	4686408729874075008	2dFS 3066	16.70	B1-2 (IV) [Eva04]	B1.5 III:	no	
6-042	4686408729874061952	AzV 482, 2dFS 3077	15.05	B1-3 (II) [Eva04]	B0.5 III	no	-
6-043	4686407389844312704	-	16.01	-	B2 III	no	-
6-044	4686414674108779008	-	16.13	-	B1.5 IV-III neb	-	-
6-045	4687170966319428992	2dFS 3082	15.43	B1-2 (III) [Eva04]	B1 III-II	no	-
6-046	4687169935527321088	2dFS 3083	16.83	B0.5 (V) [Eva04]	B1 III	no	-
6-047	4687170141685733376	2dFS 3086	16.23	B1-3 (III) [Eva04]	B1.5 III	no	-
6-048	4686414399230889600	-	16.75	-	B0.5 III neb	no	-
6-049	4687170588362310912	2dFS 3088	16.74	B1-5 (III)	B2 III:	no	EB [Paw13]
6-050	4686414708468514688	[M2002] SMC 76150	15.35	-	B1 III	no	-
6-051	4687169862500848256	2dFS 3092	15.93	B0.5 (V) [Eva04]	B0.5 IV	no	-
6-052	4687165709279578368	OM 3, 2dFS 3094	12.25	A3 II [Eva94]	A2 II/Ib	no	-
6-053	4687170588362312192	2dFS 3095	17.04	B0-5 (IV) [Eva04]	B2 III:	no	-
6-054	4686414429294260608	-	15.27	-	B0.5 IV	no	-
6-055	4687166843150898304	2dFS 3102	16.79	B1-5 (III) [Eva04]	B2 III:	no	-
6-056	4687165709279571968	2dFS 3103	16.04	B0 (V) [Eva04]	B0.5 III	no	-
6-057	4686414330511426048	-	16.06	-	B0.5 V	no	-
6-058	4687170244764966912	-	16.42	-	B1 III	no	-
6-059	4687170244764958336	-	16.14	-	B2 III:	no	-
6-060	4687165503121154944	2dFS 3106	16.32	O9 V [Eva04]	O9.7 IV	no	-
6-061	4687166843150894208	2dFS 3107	15.09	B0 (IV) [Eva04]	B0 V	no	EB [Paw13]
6-062	4686413505877718784	2dFS 3108	16.19	B1-3 (III) [Eva04]	B2 III-IV	no	EB [Paw13]
6-063	4686413230999833856	2dFS 3109	16.51	B0-5 (IV) [Eva04]	B2 III:	no	-
6-064	4687166636992467328	[M2002] SMC 76350	15.98	-	B0 V	no	-
6-065	4686414364871151360	-	16.84	-	B1.5 III:	no	-
6-066	4687165812358767104	2dFS 3117	16.43	B0 (V) [Eva04]	B0.7 IV	no	-
6-067	4686413230999834496	AzV 484, 2dFS 3118	14.82	O9.5 III [Eva04]	O9.7 III	no	-
6-068	4686414742828249472	2dFS 3120	15.77	B0 (V) [Eva04]	B0.2 IV:	no	-
6-069	4686413608956928640	2dFS 3121	16.43	B0-3 (IV) [Eva04]	B1 II	no	-
6-070	4686414364871146624	2dFS 3130	14.77	B1-2 (II) [Eva04]	B1: II	no	EB [Paw13]
6-071	4686414467950361344	-	15.52	-	B1.5 III:	no	-
6-072	4686413540237697408	2dFS 3134	14.59	B3 (II) [Eva04]	B3 II	no	-
6-073	4686413540237697152	-	16.66	-	B2 III-II	no	-
6-074	4686414532373479680	-	16.46	-	B1.5 III neb	no	-
6-075	4686413712036121088	-	16.07	-	B0.7: V	no	-
6-076	4686414467950355072	Sk 158, AzV 487	13.18	BC0 Ia [Len97]	B0 Ib	no	-
6-077	4686413712036117376	-	16.49	-	B2 III:	no	-
6-078	4687165915437998848	2dFS 3150	16.72	B0-5 (IV) [Eva04]	B2 II	no	-
6-079	4686413712029003904	2dFS 3152	16.05	B1-3 (III) [Eva04]	B0.5 III	no	-
6-080	4686413437158238208	Sk 159, AzV 488	12.22	B0.5 Iaw [Wal83]	B0 Ia	no	-
6-081	4686414566732495872	2dFS 3165	16.37	B0-3 (IV) [Eva04]	B1.5 IV: + B1.5 IV:	no	SB2 [Julia]

6-082	4686413677676380672	-	17.05	-	B1.5 IV-III	no	-
6-083	4687165949797725696	-	16.57	-	B1 III:	no	-
6-084	4687167152388524032	2dFS 3170	14.35	O9.5 Ib [Eva04]	O9.7 I:(n)	no	-
6-085	4686413402798497920	-	16.87	-	B1.5 IV	no	-
6-086	4687166323447798016	-	16.07	-	B1.5 III:	no	-
6-087	4687172271989430912	2dFS 3187	16.22	B1-3 (III) [Eva04]	B1.5 III-II	no	-
6-088	4686413398501396736	2dFS 3188	16.30	B1-5 (III) [Eva04]	B1.5 III-II	no	-
6-089	4686413849475073920	2dFS 3191	16.33	B0-3 (IV) [Eva04]	B0 V:	no	-
6-090	4687167186748236544	2dFS 3192	16.33	B1-3 (IV) [Eva04]	B2 III	no	-
6-091	4686415361303520512	[M2002] SMC 76980	15.88	-	O9.5 IV:	no	-
6-092	4687168870375394944	2dFS 3193	16.30	B1-3 (III) [Eva04]	B1 III	no	EB [Paw13]
6-093	4686413810818254464	2dFS 3199	14.58	O9 V [Eva04]	O8.5 V	no	-
6-094	4686413879538156544	2dFS 3202	16.70	B1-5 (III) [Eva04]	B2 III:	no	-
6-095	4686410550940229888	-	13.82	-	A0 Ib	no	-
6-096	4686414193072434944	2dFS 3208	16.86	B1-5 (IV) [Eva04]	B2 IV	no	-
6-097	4687172100190744448	-	14.89	-	B8 II-Ib	no	-
6-098	4686410787161979008	-	15.81	-	O8.5 V:	no	-
6-099	4686414261791903360	2dFS 3213	17.00	B2 (IV) [Eva04]	B2 II	no	-
6-100	4687168629857232000	[M2002] SMC 77248	15.42	B0 [She13]	B1 II	no	-
6-101	4687167873943001600	2dFS 3216	16.18	B0 (V) [Eva04]	B0 V	no	-
6-102	4686416873131995776	2dFS 3217	16.26	B1-5 (III) [Eva04]	B2 II	no	-
6-103	4687167873943006208	-	16.59	-	B1 III:	no	-
6-104	4687168732936450048	2dFS 3222	16.58	O9.5 V [Eva04]	B0 IV	no	-
6-105	4686410997616777984	2dFS 3225	14.70	O6.5 V [Eva04]	O6 V:n	no	-
6-106	4687167908302747136	AzV 489	15.35	O8.5 V [Mas95]	O9.7 V	no	-
6-107	4686416907491729664	-	16.21	-	O8.5 V:	no	-
6-108	4686410688379157888	-	13.05	-	A0 Iab	no	-
6-109	4687167633424856320	OGLE SMC-ECL- 7941	16.54	nan	B2 III:	no	EB [Paw16]
6-110	4686416941851468160	2dFS 3248	16.05	B1-3 (III) [Eva04]	B1.5 III:	no	-
6-111	4686416941851466880	Sk 161, AzV 492, 2dFS 3252	13.12	B0.5 I [Lam13]	B0.5 Ib	no	-
6-112	4686412475085517440	-	16.42	-	B1 III-II	no	-
6-113	4686415430023013760	AzV 493	13.78	Ope pec [Lam16]	Onnpe	no	-
6-114	4686416976211204992	2dFS 3267	16.84	B1-5 (III) [Eva04]	B2 IV-III	no	-
6-115	4686415842339856256	2dFS 3269	15.40	B0-3 (III) [Eva04]	B2 III-II	no	EB [Paw13]
6-116	4686417148009897344	2dFS 3274	12.80	A7 II [Eva04]	A7 Iab	no	-
7-001	4685992530438263808	AzV 186, CL* NGC 330 ELS 13	14.52	O8.5 III((f)) [Mas95]	O8.5 III((f))	no	LC from [Mas95]
7-002	4685991224768443392	-	15.30	-	B3 II:	no	-
7-003	4685988196744734080	-	16.51	-	B1.5 III-II	no	-
7-004	4685987857514223744	AzV 195	13.51	A0 [Azz75]	A0 Iab	no	-
7-005	4685988132392086016	-	16.04	-	B2 III-II	no	-
7-006	4688995468472128128	2dFS 1268	15.17	B2 (II) [Eva04]	B1 II	no	-
7-007	4685987960593409024	[MA93] 1042	15.06	-	B1 II neb	no	-
7-008	4685992663601032576	TIC 181882730	15.06	-	B2 II:	yes	-
7-009	4685987960593372928	-	16.68	-	B1.5 III neb	no	-
7-010	4685991838904940928	[VA82] II-8	15.84	-	B1 III	no	-
7-011	4688995640270760960	Cl* NGC 330 ELS 53	16.07	B0.5 V [Eva04]	B1 III	no	-
7-012	4685991632807805312	-	14.61	-	B5 II	-	-
7-013	4685988544708868864	LIN 329, 2dFS 1283	14.33	B1-3 (II) [Eva04]	B1.5 III e	yes	-
7-014	4685988265464182528	-	16.36	-	B1 III	no	-
7-015	4685986792362398976	2dFS 1288	14.88	B1-2 (II) [Eva04]	B1 II	no	-
7-016	4685991602725468800	-	16.18	-	B1 III:	no	-
7-017	4685991602725840128	-	13.46	-	A2 Ib	no	-
7-018	4685987513916795776	[M2002] SMC 42648	15.15	O9 [She13]	B0 IV	no	-
7-019	4685986792362380928	[M2002] SMC 42686	15.64	-	B1.5: II	no	-
7-020	4685988304190737536	-	15.27	-	O7.5 V: neb	no	-
7-021	4685987165948226432	-	16.55	-	B1.5 III	no	-
7-022	4685988647787974784	-	15.89	-	B1 II:	no	-
7-023	4685991705804639360	OGLE SMC-SC8 90998	16.14	nan	B1.5 III-II	no	EB [Paw13]
7-024	4685993183273028224	-	16.04	-	O9.7 V:n	no	-
7-025	4685987475279399936	-	15.46	-	O7.5 V:n neb	no	-
7-026	4685987479557047808	-	16.23	-	B1 II	no	-
7-027	4685975350565410048	2dFS 1313	15.33	B0 (IV) [Eva04]	O9.7 Vn	no	-
7-028	4685987651355702528	-	16.08	-	B1 III:	no	-
7-029	4685975453644517248	GEN# +6.20138214, [VA82] II-14	15.32	-	B2 II	no	-
7-030	4685975110047325568	-	16.57	-	B0.5: V	no	-
7-031	4685994695101439360	-	15.93	-	B1.5 III	no	-
7-032	4685975488004257920	OGLE SMC105.3 89	16.39	-	B2 III:	no	EB [Paw13]
7-033	4685975110047300352	[M2002] SMC 44302	15.43	-	B0.7 III	no	-
7-034	4685993217632942720	[M2002] SMC 44634	16.02	-	B0 V	no	-
7-035	4685975213126487424	AzV 212, 2dFS 1348	15.15	B0.5 (IV) [Eva04]	B1 II:	no	-
7-036	4685987410837520256	[VA82] II-16	15.96	-	B1.5 III-II	no	-
7-037	4685974457212254336	OGLE J005854.41-724352.3	15.52	-	B1.5 III: e	no	-
7-038	4685975213126426368	OGLE J005855.40-724300.8	14.76	-	B0 II: e	yes	-
7-039	4685974388492830080	-	16.19	-	B1 IV:	no	-
7-040	4685988888306231936	-	15.90	-	B1.5 III-II	no	-
7-041	4685994454583299840	-	15.59	B1 Ve [Mas95]	B2 II:	no	-
7-042	4685974491571903744	-	16.52	-	B1.5 III-II	no	-
7-043	4685993423791257984	Sk 77, AzV 221	13.67	B0 Ia [Gar87]	B1.5 Ib	no	-
7-044	4685988819586784896	AzV 223	14.33	O9.5 II [Mas09]	O9.7 III	no	-
7-045	4685993419427102848	-	17.01	-	B2 III: e	no	-
7-046	4685993733028817664	AzV 225, 2dFS 1376	14.14	B8 (Ib) [Eva04]	B5 II	no	-
7-047	4685975625443431808	AzV 228, 2dFS 1384	14.49	B0.5 (III) [Eva04]	B0.2 III: pe	yes	-
7-048	4685990056537133824	-	15.92	-	B2 III	no	-
7-049	4685975964679436672	[M2002] SMC 46115	15.05	-	B0.2 III	no	-

7-050	4685994110985897472	-	16.88	-	B2 III:	no	-
7-051	4685990434494050048	[M2002] SMC 46241	15.33	B1 V [Lam16]	B1 II: e	no	-
7-052	4685976759314509824	-	16.05	-	B1.5 III-II	no	-
7-053	4685972597426070016	-	16.47	-	B0 IV	no	-
7-054	4685975694162792448	2dFS 1392	16.03	B1-2 (IV) [Eva04]	B2 III:	no	EB [Paw13]
7-055	4685972322546968448	-	16.63	-	B0 V	no	-
7-056	4685971566632674304	-	16.96	-	B1.5 III	no	-
7-057	4685972391266444800	OGLE SMC-SC8 129157	14.90	-	B0 V	no	EB [Paw13]
7-058	4685975934680882304	AzV 233	15.18	B1 V [Mas95]	B1 II:	no	-
7-059	4685972670505925888	-	14.90	-	B3 II	no	-
7-060	4685972601786502784	-	16.04	-	B2 III:	no	EB [Paw13]
7-061	4685976926752244480	-	16.57	-	B2: II:	no	-
7-062	4685972631870071808	-	16.01	-	B2 IV	no	-
7-063	4685972636146192128	OGLE SMC-SC8 132562	15.25	O9.5 III [Eva04]	O9.5 III(n)	no	LC from [Eva04]
7-064	4685972636146149504	RMC 17, Sk 82, AzV 235	12.25	B0 Ia [Wal83]	B0 Ia	yes	-
7-065	4685975762891732096	AzV 236	15.27	B0 III [Mas95]	B1 II	no	EB [Paw13]
7-066	4685976067758705280	2dFS 1430	16.38	B0.5 (V) [Eva04]	B1 II	no	-
7-067	4685993904827461504	AzV 74F, 2dFS 1434	13.39	A0 (Ib) [Eva04]	A0 Ib	no	-
7-068	4685993904827455616	-	12.59	-	A5 Ib	no	-
7-069	4685971639713881344	Sk 84, AzV 243	14.50	O6 V [Mok06]	O6.5 V	no	LC from [Mok06]
7-070	4685989850378489472	-	16.46	-	B1.5 III:	no	-
7-071	4685976209558662016	AzV 249, 2dFS 1458	14.22	B0 (III) [Eva04]	B0 II: + B0	no	SB2
7-072	4685990709381204864	AzV 251	15.39	O7 Vn [Cra82]	O8 Vnn	no	-
7-073	4685989816018758272	-	15.34	-	B2 II:	no	-
7-074	4685976656235152640	2dFS 1471	15.17	B0-5 (III) [Eva04]	B2 III:	no	-
7-075	4685976621875402368	-	12.99	-	B8 Ib	no	-
7-076	4687491886297246336	AzV 256, 2dFS 1497	15.33	B0 (IV) [Eva04]	O9.7 I(n)	yes	-
7-077	4687491126099277696	2dFS 1503	16.29	B1-5 (III) [Eva04]	B2 II:	no	-
7-078	4687491886293188608	AzV 258	13.46	O9 e [Azz75]	B0.2 e	yes	-
7-079	4685976346997537536	-	16.13	-	B2 III:	no	-
7-080	4685976621876337664	-	16.36	-	B1.5 III:	no	-
7-081	4685924803028734080	OGLE SMC-SC9 10098	16.10	O9 + B0 [Hil05]	O9.7 Vnn	no	EB [Paw13]
7-082	4687491164738701056	AzV 261, 2dFS 1527	13.75	B2 (Ib)e [Eva04]	B2 e+	yes	-
7-083	4687490958580285440	2dFS 1528	15.69	B0-5 (III) [Eva04]	B2 II:	no	-
7-084	4687477558279928320	AzV 262, 2dFS 1532	13.49	O9.7 Iab [Eva04]	O9.7 Iab	no	-
7-085	4687478692151243776	-	16.30	-	B1.5 III-II	no	-
7-086	4687479070108329216	-	16.54	-	B2 II	no	-
7-087	4687477661359126144	2dFS 1543	15.74	B0-5 (III) [Eva04]	B1.5 III-II	no	-
7-088	4685971948951359488	AzV 265, 2dFS 1544	14.66	B2.5 (II) [Eva04]	B2.5 II	no	-
7-089	4687478863949904384	-	16.01	-	B1.5 III-II	no	-
7-090	4687477588328496128	-	16.32	-	B2 III:	no	-
7-091	4687479173187523584	Sk 97, AzV 269	10.90	A 5I [San68]	A5 Iab	no	-
7-092	4687478863949902336	-	15.91	-	B2 II	no	-
7-093	4687477592639651072	[MA93] 1254, 2dFS 1555	14.68	B1-5 (II) [Eva04]	B2 II e	yes	-
7-094	4687477970596745344	[MA93] 1255	15.45	-	O9.7 V(n)	yes	-
7-095	4687473435111194240	2dFS 1557	16.32	B1-5 (III) [Eva04]	B1.5 III:	no	-
7-096	4687490924220536576	-	15.95	-	B2 II:	no	-
7-097	4687474568982696960	-	12.80	-	A7 Ib	no	-
7-098	4687490924220548736	-	15.27	-	B2 II:	no	-
7-099	4687477764438325376	2dFS 1561	14.92	B0.5 (IV) [Eva04]	B1 II	yes	-
7-100	4687479104468055552	-	16.67	-	B2 II	no	-
7-101	4687426156109067008	-	16.32	-	B2 III:	no	-
7-102	4687477798798048640	[M2002] SMC 51419	16.07	O9 III [Lam16]	B0 V-IV	no	-
7-103	4687473641269604352	AzV 278	14.92	B0 [Azz75]	B1 II	no	-
7-104	4687473366391708288	OGLE J010140.61-724251.5	16.72	-	B1.5 III:	no	-
7-105	4687474397183820800	-	16.89	-	B1 II	no	-
7-106	4687478451632815104	-	12.90	-	B8 Ib	no	-
7-107	4687475084378539136	-	16.56	-	B1.5 III-II	no	-
7-108	4687426087389568768	AzV 283	14.02	B3 [Azz75]	B2.5 Ia	no	-
7-109	4687426396627189760	-	16.59	-	B2 III:	no	-
7-110	4687426396627182080	-	16.52	-	B1.5 III:	no	-
7-111	4687478138084449536	Sk 103, AzV 289	12.74	B0 Ia [Wal83]	B0 Ia	no	SB1
7-112	4687478142395205888	[M2002] SMC 52555	14.17	-	B1 Ib	no	-
7-113	4687475187457720448	2dFS 1620	14.81	B1-5 (II) [Eva04]	B3 II	no	-
7-114	4687475118738255616	-	15.74	-	B2 II e	no	-
7-115	4687478245474401024	2dFS 1635	15.99	O9.5 III [Eva04]	B0 IV	no	-
7-116	4687474942629350272	OGLE SMC110.6 17837	16.02	-	B3 II: + B1.5 V:	no	SB2, EB [Paw13]
8-001	4689054670286883968	Sk 37, AzV 72, 2dFS 765	12.98	B8 (Iab) [Eva04]	B8 Ib	no	-
8-002	4689049894283437696	-	15.99	-	B2 II	no	-
8-003	4689051131233907840	-	16.51	-	B2 III-II	no	-
8-004	4689038177610689664	-	16.48	-	B2 III	no	-
8-005	4689054876445285760	AzV 84, 2dFS 786	15.38	B0.5 (IV) [Eva04]	B0.7 III	no	-
8-006	4689037181200454656	AzV 92	13.88	B3 [Azz75]	B2.5 II-Ib	no	-
8-007	4689032778796455808	-	15.48	-	B2 III:	no	-
8-008	4689054945164735616	Sk 46, AzV 96	12.97	B1.5 Ia [Len97]	B1 Iab	no	-
8-009	4689055009551389440	[MA93] 462	14.85	-	A5: I: + B3: Ib:	yes	SB2
8-010	4689033539046230400	Sk 45, AzV 98	11.23	A0 Ia [Len97]	A0 Ia	no	-
8-011	4689038413838504704	-	16.16	-	B2 III-II	no	-
8-012	4689050890715677952	-	16.17	-	B2 II:	no	-
8-013	4689038418150993920	-	16.02	-	B2 II	no	-
8-014	4689034221906397184	-	16.74	-	B1.5 III-II	no	-
8-015	4689075217413489408	2dFS 825	15.75	B0.5 (V) [Eva04]	B0 V	no	-
8-016	4689075213077405824	-	16.92	-	B2 IV:	no	-

8-017	4689050577143317888	-	15.99	-	B2 III-II	no	-
8-018	4689075492291367936	-	16.38	-	B2 II:	no	-
8-019	4689074392779777280	-	16.36	-	B1.5 III:	no	-
8-020	4689037662215249792	OGLE SMC101.4 21947	15.82	O7 Vz [Lam13]	O8 V	no	EB [Paw13]
8-021	4689032851851488000	AzV 113	13.78	O7: V [Eva04]	O7 V-IIInnn pe	yes	-
8-022	4689062298150064640	AzV 115, 2dFS 837	14.01	B0.5 (II) [Eva04]	B0.5 II	no	-
8-023	4689033229778815360	-	16.48	-	B1.5 III:	no	-
8-024	4689037456056174592	-	16.34	-	O9.5 V:(n) neb	no	-
8-025	4689033023650128256	OGLE SMC101.4 8338	16.22	-	B1.5 III	no	EB [Paw13]
8-026	4689037456056165376	2dFS 840	15.62	B1-5 (II) [Eva04]	B2.5 II neb	no	-
8-027	4689075625394544512	-	16.36	-	B1 III:	no	-
8-028	4689075183074291072	Sk 50, AzV 116, 2dFS 843	14.00	B0 (II) [Eva04]	O9.7 II-Ib(n)	no	-
8-029	4689033023650129536	-	16.51	-	B1 IV:	no	EB [Paw13]
8-030	4689032954930686720	-	15.53	-	O6.5 Vn	no	-
8-031	4689075354852418176	-	15.80	-	O9.5 V	no	-
8-032	4689061954552698112	-	15.76	-	B1 III-II	no	-
8-033	4689032950664343552	-	16.29	-	B2 III:	-	-
8-034	4689074358420039680	2dFS 854	15.29	B0 (IV) [Eva04]	B0.2 III	no	-
8-035	4689074461499247744	LHA 115-S 15, Sk 51, AzV 118	12.49	B0 III [Pri87]	O9.7 III: e	yes	-
8-036	4689074461499243648	-	17.09	-	B1 III:	no	-
8-037	4688985985180031744	-	15.80	-	B2 II	no	-
8-038	4689074530194683520	OGLE SMC102.1 11822	16.51	-	B2 III-II	no	EB [Paw13]
8-039	4689062435588998400	-	15.82	-	B0 V	no	-
8-040	4689062435588992640	-	16.56	-	B2 IV	no	-
8-041	4689056525713977472	-	15.31	-	B1.5 III-II	no	-
8-042	4689009521606825856	2dFS 873	13.32	A3 II [Eva04]	A5 Ib	no	-
8-043	4689057934463327616	LIN 207	14.71	B1e [Lam16]	B2 II: e+	yes	-
8-044	4689062160711095808	LIN 209, AzV 128	14.85	O7 V [Mas95]	O7 Vn + O7 V	no	SB2
8-045	4689009521606804736	[M2002] SMC 24096	15.62	B0 V [Lam16]	B0.2 IV	no	-
8-046	4689056766232136064	AzV 129	14.60	B1 [Azz75]	B1.5 II	no	-
8-047	4689009452887349504	-	16.21	-	B2 IV	no	-
8-048	4689056456994593408	-	15.18	-	B3 II	no	-
8-049	4689062195070825216	-	16.31	-	B1.5 III:	no	-
8-050	4689062126351355776	[M2002] SMC 24631	16.09	-	O9.7 IV	no	-
8-051	4689057968822902912	-	16.56	-	B1.5 III	no	-
8-052	4689062195070824320	2dFS 888	15.58	O8.5 V [Eva04]	O9.2 V	no	-
8-053	4689074598938187776	AzV 135, 2dFS 889	14.79	O8 III [Eva04]	O9 III	no	-
8-054	4689058071902092928	2dFS 890	16.04	B0-5 (III) [Eva04]	B2 II	no	-
8-055	4689057693945011072	2dFS 892	16.01	B1-5 (III) [Eva04]	B2 III-II	no	-
8-056	4689074598938189568	-	15.99	-	A2: I: + B3:	no	SB2
8-057	4689058071902087808	-	16.11	-	B2 III:	no	-
8-058	4689056869311331840	OGLE SMC101.4 8384	16.39	-	B2 III:	no	EB [Paw13]
8-059	4689061748394242944	LIN 225	14.98	-	B2 II: e	no	-
8-060	4689008177223333888	[MA93] 645, 2dFS 910	15.17	B1-5 (II) [Eva04]	B2 II:	no	-
8-061	4689056903671040512	[MFH2007] SMC5-78415	14.12	B8 II-III [Mar07]	B9 Ib	no	-
8-062	4689056697512629376	MACHO 207.16147.27	16.02	B2 IV [Mar07]	B2 III:	no	-
8-063	4689008559534153856	AzV 36F	13.65	B3 [Azz79]	B3 Ib	no	-
8-064	4689056628793468928	[M2002] SMC 26108	15.15	B2 III [Mar07]	B3 II e	yes	-
8-065	4689062916625049216	2dFS 918	15.68	B0 (V) [Eva04]	B1 III-II	no	-
8-066	4689058174981307392	-	15.14	-	B2 II:	no	-
8-067	4689009620370577024	AzV 142	12.00	A5 I [Neu10]	A7 Ib	no	-
8-068	4689058415499454080	-	16.40	-	B1.5 III:	no	-
8-069	4689061507875858560	-	16.30	-	B1.5 III:	no	-
8-070	4689058484219114496	2dFS 924	16.14	B0.5 (V) [Eva04]	B0.5 IV	no	-
8-071	4689009349808102016	-	16.52	-	B1.5 III:	no	-
8-072	4689057346006300544	TYC 9138-1910-1	10.98	F0 I [Neu10]	F2:	no	-
8-073	4689061812778239488	-	16.16	-	O9.7 V(n)	no	-
8-074	4689061507875864064	2dFS 926	16.04	B0-5 (III) [Eva04]	B2 III-II	no	-
8-075	4689061817113476608	-	14.86	-	B1.5 III-II	no	-
8-076	4689009796484689792	-	12.99	-	A5 Ib	no	-
8-077	4689061817113484416	[MFH2007] SMC5-82923	14.47	B3 III [Mar07]	B5 II	no	-
8-078	4689010067007622656	[MFH2007] SMC5-74471	14.49	B2 III [Mar07]	B2 II:	yes	-
8-079	4689058415499441280	-	16.15	-	B1 III	no	-
8-080	4689058209341023104	OGLE SMC101.4 29381	16.08	-	B2 III:	no	EB [Paw13]
8-081	4689057109829464448	[MFH2007] SMC5-22612	16.54	B2 IV [Mar07]	B2 III:	no	-
8-082	4689061920192649984	AzV 38F, 2dFS 938	13.06	B9 (Iab) [Eva04]	B9 Iab	no	-
8-083	4689058243700777088	-	12.82	-	F0:	no	-
8-084	4689010101367347456	-	16.08	-	B2 IV	no	-
8-085	4689057041109984128	-	14.79	-	B1 II	no	-
8-086	4689008903131074176	-	12.22	-	A7 Ib	no	-
8-087	4689061576595320064	-	16.24	-	O9.7 V(n)	no	SB
8-088	4689058548602468352	-	16.50	-	B0 IV	no	-
8-089	4689064497172976896	-	12.35	-	F2:	no	-
8-090	4689057487786300288	2dFS 950	15.30	B1-5 (II) [Eva04]	B1 II	no	EB [Paw13]
8-091	4689008937490759040	-	13.62	-	A0 II	no	-
8-092	4689057453426569984	[M2002] SMC 28153	15.64	-	O9.2 V(n)	no	-
8-093	4689063122783487872	-	15.95	-	B1.5 III:	no	-
8-094	4689059824248453888	AzV 41F	13.27	B5 [Azz79]	B3 Ib	no	-
8-095	4689060099126312192	-	16.71	-	B2 III:	no	-
8-096	4689057453426553728	-	12.68	-	A7 Ib	no	-
8-097	4689058999614762368	-	12.62	-	F0:	no	-
8-098	4689058656017416320	2dFS 972	15.10	B1-5 (II) [Eva04]	B3 II	no	-
8-099	4689058724736877824	-	15.90	-	B2 II:	no	-

8-100	4689009070622046336	[MA93] 742	15.17	-	B2 II e	yes	-
8-101	4689008868771226240	-	12.50	-	F0:	no	-
8-102	4689009143649631232	OGLE SMC108.8 33982	16.01	-	O9.7 V	no	EB [Paw13]
8-103	4689058965255025280	[MFH2007] SMC5-5045	16.17	B2 IV [Mar07]	B2 III	no	-
8-104	4689011445751390848	2dFS 983	15.90	B0.5: (V) [Eva04]	B1.5 III:	no	-
8-105	4689009070575136512	OGLE SMC-ECL- 2967	15.02		B0.5 III	no	EB [Paw13]
8-106	4689059029649262464	[MFH2007] SMC5-38564	16.59	O9 V [Mar07]	O9.7 Vnn	no	-
8-107	4689011651909783424	AzV 156	14.05	A0 [Azz75]	A0 Ib	no	-
8-108	4689059892967905920	2dFS 985	14.93	B0.5 (IV) [Eva04]	B0.5 V	no	-
8-109	4689011754988965888	LHA 115-S 20, AzV 157	13.40	B0e [Azz75]	B0 III: pe	yes	-
8-110	4689011445751392000	OGLE SMC108.8 34068	16.38	-	B1 III: + B1 III:	no	SB2, EB. [Paw13]
8-111	4689010346239909888	-	16.92	-	B2 III	no	-
8-112	4689011411391693440	[M2002] SMC 30095	16.26	-	B1.5 III:	no	-
8-113	4689058690377131520	AzV 159	12.54	F2 [Azz75]	A5 Ib	no	-
8-114	4689011411391652992	-	16.45	-	B2.5 III:	no	-
8-115	4689058793456333824	-	16.02	-	B1 II	no	-
8-116	4689058892200836096	-	12.73	-	A2 Ib	no	-
8-117	4689011583190270720	-	14.98	-	B1.5 III-II	no	-

Ard77: Ardeberg & Maurice (1977); Azz79: Azzopardi & Vigneau (1979); Azz82: Azzopardi & Vigneau (1982); Coe15: Coe & Kirk (2015); Eva04: Evans et al. (2004); Eva06: Evans et al. (2006); Gar87: Garmany et al. (1987); Gra12: Graus et al. (2012); Hil05: Hilditch et al. (2005); Hum83: Humphreys (1983); Hum91: Humphreys et al. (1991); Lam13: Lamb et al. (2013); Mar07: Martayan et al. (2007); Mas95: Massey et al. (1995); Mas00: Massey et al. (2000); Mas02: Massey (2002); Mas04: Massey et al. (2004); Mas09: Massey et al. (2009); Men06: Mennickent et al. (2006); Mok06: Mokiem et al. (2006); Mor03: Morrell et al. (2003); Neu10: Neugent et al. (2010); Neu18: Neugent et al. (2018); Pau12: Paul et al. (2012); Paw16: Pawlak et al. (2016); Pri87: Prinja (1987); San68: Sanduleak (1968); She13: Sheets et al. (2013); Smi97: Smith Neubig & Bruhweiler (1999); Tes87: Testor & Lortet (1987); Tes01: Testor (2001); Wal83: Walborn (1983); Wal00: Walborn et al. (2000); Wal02: Walborn et al. (2002); Zas14: Zasche et al. (2014); Zic96: Zickgraf et al. (1996);

Appendix B: DSS images for nebular contamination

In order to get a better handle on which stars are affected by nebular contamination, and which objects show intrinsic emission like in the case of classical OeBe stars, we investigated wide-field Digitized Sky Survey (DSS) 2-red images. We retrieved 25' x 25' cutouts for each of the fields and overplotted all BLOeM sources in order to investigate their local surroundings. We inspected the spectra of all sources that show overdensitites in DSS 2-red, in particular all objects classified as emission-line stars, to better distinguish between nebular contamination and classical OeBe stars. We designated with 'neb' all objects located inside a nebulosity visible in DSS 2-red and show narrow emission lines, mainly in the Hγ line.

In Figs. B.1 and B.2 we show the DSS 2-red cutouts for each of the eight fields. Here, we overplot all BLOeM sources, in particular emission-line stars classified as OeBe stars, and mark stars that are affected by nebular contamination. Some fields, for example Field 1, 4 or 6, have large nebulosities in the fields of view and many sources are affected by nebular contamination. Other fields, like fields 5, 7 or 8, are barely or not affected at all. Few objects are classical OeBe stars and additionally show nebular contamination in their spectra.

Appendix C: Cross-matches with additional catalogues

Appendix C.1: ESO archive

We cross-matched the BLOeM catalogue with spectroscopic databases in the ESO archive, defining a search radius of 3" per target. We retrieve a total of 1,988 spectra for 202 stars out of the 929 in our sample. These spectra were acquired with various instruments of the VLT. These data will be used to improve the quantitative spectroscopy in subsequent papers.

Appendix C.2: Hubble UV Legacy Library of Young Stars as Essential Standards (ULLYSES)

ULLYSES is a legacy survey of the *Hubble* Space Telescope (HST), which includes the acquisition of high-resolution UV spectra for 128 massive stars in the SMC[7]. The programme also includes a follow-up with the X-SHOOTER spectrograph of the VLT to obtain a visual and infrared coverage of the targets Vink et al. (2023). A cross-match of the BLOeM sample with the ULLYSES sample, using a search radius of 3", resulted in an overlap of 43 targets. From ULLYSES and XShootU there will be broad wavelength coverage of the UV and visible spectrum of these objects that will also be used to inform the analysis of these targets.

Appendix C.3: X-ray catalogues

The SMC was extensively observed in X-rays. The largest modern X-ray observatories, *XMM-Newton* and *Chandra*, which operate in 0.2-12.0 keV range, conducted surveys of the entire SMC galaxy (Laycock et al. 2010; Sturm et al. 2013). The deep observations of individual fields, such as the SMC Wing and NGC 346 star cluster have also been performed (Nazé et al. 2004; Oskinova et al. 2013). However, despite these efforts X-ray emission of individual 'normal' massive OB stars is below current detection limits. On the other hand, X-ray detections of massive stars in the SMC allow to select binary stars. Specifically, X-ray detections are excellent tracers of CWBs, some of which are significantly more X-ray bright compared to single stars (Corcoran et al. 1996; Sana et al. 2006; Oskinova 2005; Nazé et al. 2007). But best of all, X-ray detections are suited to identify high-mass X-ray binaries (HMXBs), where a compact object is accreting matter of its OB-type companion. HMXBs are X-ray variable, especially so are BeXRBs where the donor stars have OBe spectral type. BeXRBs are transient X-ray sources, and may remain quiescent over long periods of time and could be detected only during outbursts.

To explore X-ray properties of our targets, the BLOeM catalog was cross-correlated with catalogues produced by the *XMM-Newton*, *Chandra*, eROSITA, and ROSAT X-ray telescopes. Only eight BLOeM stars are firmly detected, while the positional uncertainty of one X-ray source (6-116) precludes its firm detection. The detected sources are listed in Table C.1. There are four already known HMXBs among them. Four other X-ray sources may be either CWBs or newly discovered HMXBs. The BLOeM spectroscopy will shed light on their nature, since HMXBs are SB1 systems while CWBs are likely to be SB2. Some sources listed in Table C.1 have different fluxes according to different catalogues. This may reflect true source variability, e.g. in case of BeXRBs. To estimate the X-ray luminosity, we adopted a neutral hydrogen column density $N_{\rm H} = 5 \times 10^{21}\,{\rm cm}^{-2}$ and a power-law spectrum with $\Gamma = 1.7$ for all objects.

Appendix C.4: OGLE photometry

A large number of the BLOeM targets has been monitored by the OGLE photometric survey. Out of the 929 targets, 847 were observed in the OGLE-III (Udalski 2003) and 785 continue to be observed in the OGLE-IV (Udalski et al. 2015). Among them, there are 82 objects identified as binary systems by Pawlak et al. (2016), including 74 eclipsing and 8 ellipsoidal binaries.

Appendix C.5: TESS photometry

All BLOeM targets have been and continue to be periodically observed by the all-sky time-series photometry TESS space mission (Ricker et al. 2015). An initial survey of photometric variability for XShootU targets in the LMC and SMC was performed by Bowman (2024), who found similar stochastic low-frequency (SLF) variability to Galactic OB stars (Bowman et al. 2019). In the future, we will extract light curves for as many BLOeM targets as possible to identify possible eclipsing binaries, stars with rotational modulation, and pulsations. In so doing, this will provide complementary constraints and inform the search for multiplicity for the BLOeM sample.

Appendix D: HRDs separated by field

Figure D.1 shows the HRDs of each of the eight SMC fields observed in the framework of BLOeM (shown in Fig. 2). The differences between the populations are not blatant. Generally, fields 1 – 4 contain a higher number of stars "born as O-type" ($M_{\rm ini} \gtrsim 14\,M_{\odot}$) compared to fields 5 – 8, which could be anticipated given the automated way with which the fields were selected, prioritizing fields with the most massive stars (Sect. 2). Field 5 appears to contain the oldest population among the eight fields.

[7] https://ullyses.stsci.edu/ullyses-targets-smc.html

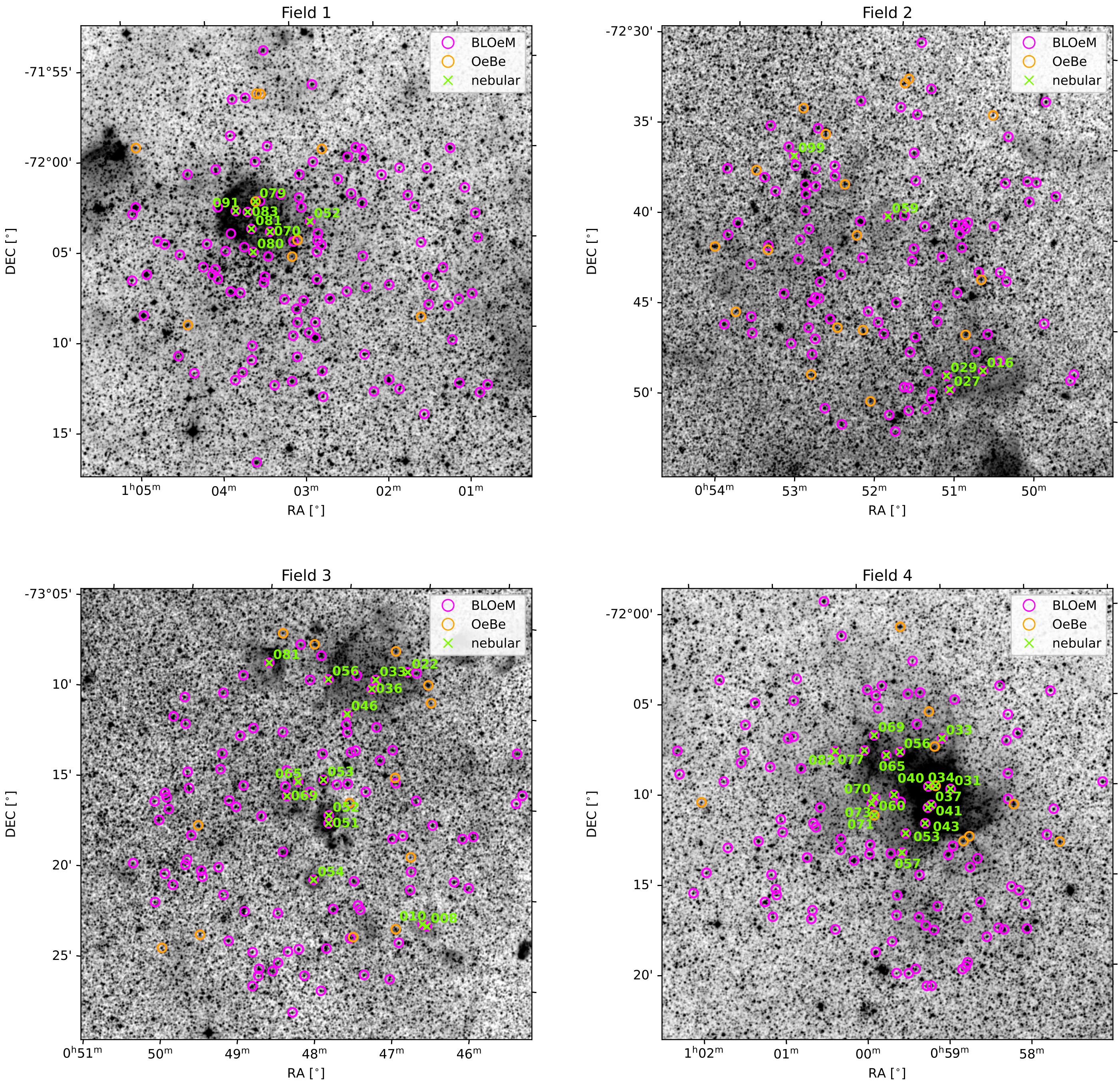

Fig. B.1: BLOeM sources in Field 1–4 overlaid on a DSS 2-red image (pink circles). OeBe stars are marked with orange circles. Stars that show nebular contamination in their spectra are marked with green crosses.

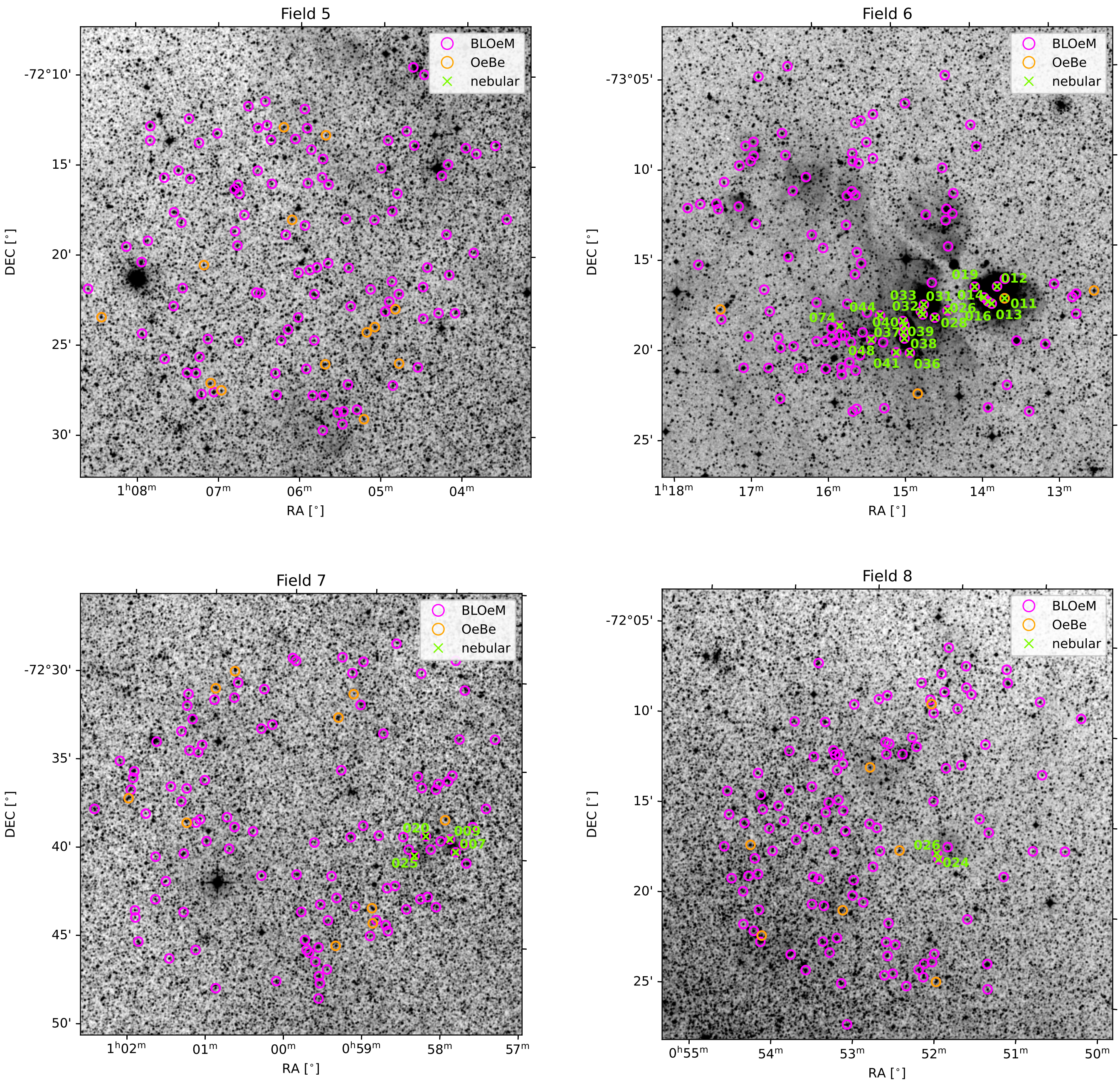

Fig. B.2: Same as Fig. B.1, but for fields 5 – 8.

Table C.1: BLOeM stars detected in X-rays.

BLOeM ID	Alias	Uncertainty X-ray (″)	Separation (″)	F_X [erg cm^{-1} s^{-1}]	Spectral Type	L_X (erg s^{-1})	Catalog	Remarks
3-042	AzV 26	1.9	0.7	$5.2 \pm 1.9 \times 10^{-16}$	O6 I(f)+O7.5	4e32	CSC v.2	CWB (?)
2-055	AzV 102	0.95	0.7	$30 \pm 3 \times 10^{-15}$	O9.7 V:n e	2e34	SMCDFSCXO	HMXB SXP 8.80
		1.0	1.8	$3.6 \pm 2.6 \times 10^{-15}$		3e33	4XMM-DR13s	
		1.3	0.6	1.8×10^{-13}		1e35	CXOGSGSRC	
		2.6	0.2	$29 \pm 4 \times 10^{-15}$		2e34	CSC v.2	
8-029	-	1.9	0.6	$4.3 \pm 1.5 \times 10^{-14}$	B1 IV:	3e34	4XMM-DR13	HMXB (?)
2-082	AzV 138	1.7	0.4	$87 \pm 5 \times 10^{-16}$	O9.2 III pe	6e33	CSC v.2	HMXB
2-116	AzV 154	0.9	2.4	$5.1 \pm 2.9 \times 10^{-15}$	sgB[e]	4e33	4XMM-DR13s	HMXB
		1.4	1.2	$8.4 \pm 4.5 \times 10^{-15}$		6e33	SMCPSCXMM	
			0.6	$14 \pm 6 \times 10^{-16}$		1e33	CSC v.2	
4-026	Cl* NGC 346 MPG 217		0.1	$7.1 \pm 1.5 \times 10^{-16}$	O9.5 IIIpe	5e32	CSC v.2	HMXB
4-113	OGLE SMC-SC9 131970	0.86	1.2	$25 \pm 9 \times 10^{-15}$	B2.5 II pe	2e34	SMCPSCXMM	HMXB
		1.5	1.2	3.6×10^{-14}		3e34	CXOGSGSRC	
			1.7				CSC v.2	
1-102	AzV 345a		0.1	2.07×10^{-16}	O6 III(n)	1e32	CSC v.2	CWB ? HMXB?
6-116	2dFS 3274	1.7	1.4	$9.6 \pm 6.0 \times 10^{-15}$	A7 Iab	7e33	SMCPSCXMM	spurious?
		1.1	2.5	$15 \pm 7 \times 10^{-15}$		1e34	4XMM-DR13s	

Notes. The columns are, in order of appearance: BLOeM identifiers, uncertainties on the X-ray position from the corresponding X-ray catalog, separations between *Gaia* DR3 coordinates and X-ray coordinates, X-ray fluxes, energy ranges from corresponding catalogs, spectral type, the seventh column: estimated X-ray luminosity in the same energy range as flux; the eighth column: catalog name; the ninth column: preliminary identification of a source type. The catalogues are:

CSC v.2 *Chandra* Source Catalog v.2 (Evans et al. 2010)
SMCDFSCXO SMC Deep Fields X-Ray Point Source Catalog (Laycock et al. 2010)
4XMM-DR13s *XMM-Newton* Serendipitous Source Catalog from Stacked Observations(Traulsen et al. 2020)
4XMM-DR13 *XMM-Newton* Serendipitous Source Catalog DR13 (Webb et al. 2020)
CXOGSGSRC *Chandra* ACIS GSG Point-Like X-Ray Source Catalog (Wang et al. 2016)
SMCPSCXMM SMC *XMM-Newton* Point Source Catalog (Sturm et al. 2013)

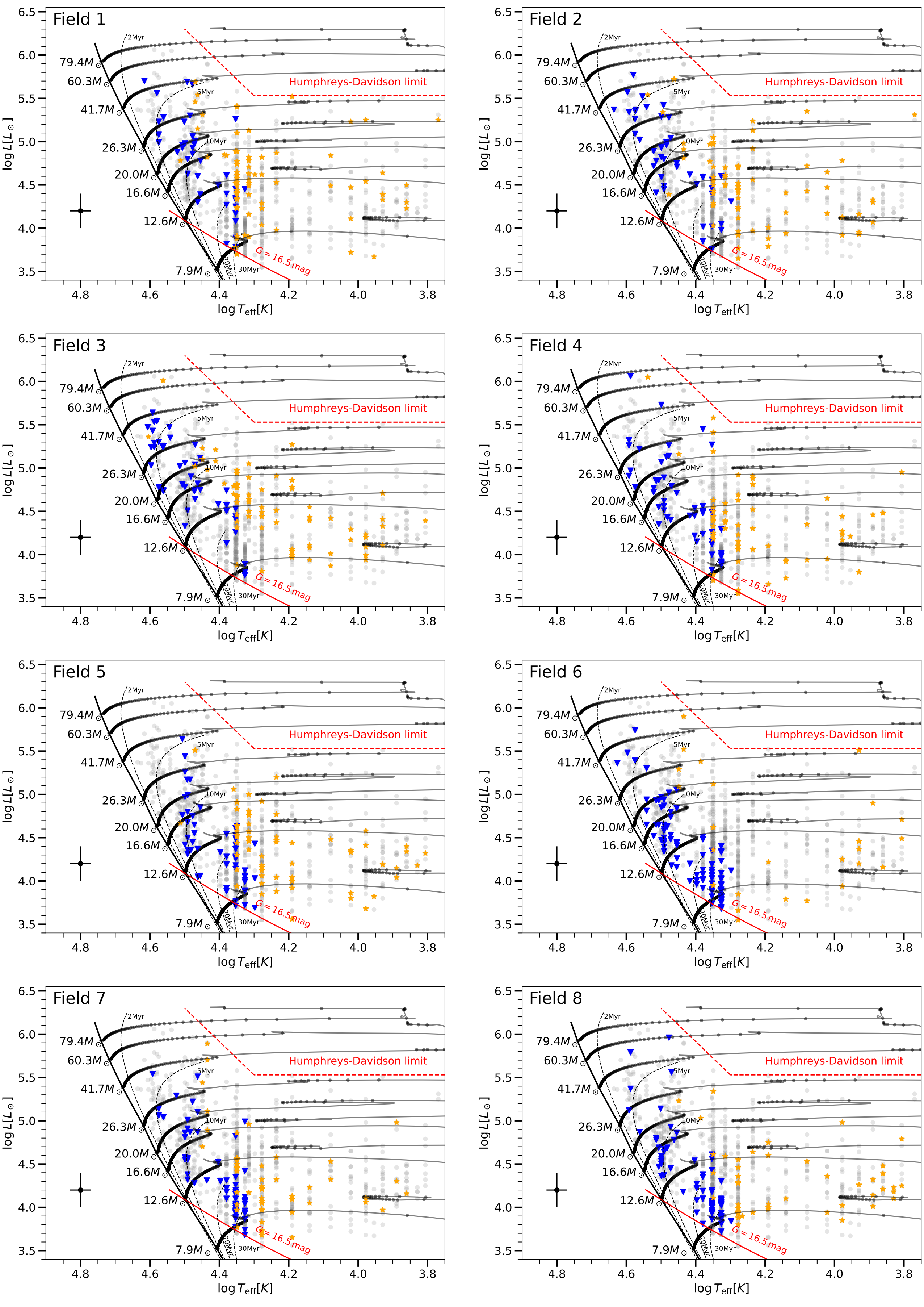

Fig. D.1: Same as Fig. 10, but with the samples of the eight SMC fields shown in Fig. 2 highlighted in colour (colour meaning is the same as in Fig. 10). The entire sample is shown in grey in each panel.